Space-time Control of Stokes Swimmers

Antoine Laurain
Department of Applied Mathematics
University of Duisburg-Essen
Email: antoine.laurain@uni-due.de

Shawn W. Walker
Department of Mathematics
Louisiana State University,
Baton Rouge, LA 70803-4918, U.S.A.
Email: walker@math.lsu.edu

Abstract

We develop a method for the optimal control of a self-deforming swimming body within a Stokesian fluid. By using the time-dependent geometry of the swimming body as a control variable, the swimmer can modify its center position and velocity. Hence, this becomes a free boundary control problem, since the center velocity of the swimmer depends implicitly on its (time-dependent) shape through the solution of the Stokes equations. We also investigate the optimal actuation of a force (thrust) control acting on the swimmer.

We start by defining the mathematical model and objective functional, followed by our variational formulation of the Stokes equations coupled to the swimmer motion. Next, we perform a formal sensitivity analysis and describe an unfitted finite element method for simulating the problem. Basic stability and consistency is established. Numerical experiments, in two dimensions, are shown that validate the model and sensitivity analysis, and exhibit time-irreversible motions that propel the swimmer through the fluid.

Keywords: micro-swimmer, Stokes flow, optimal shape control, control of moving sets

1 Introduction

Self-propelling, or *swimming*, at low Reynolds number is a fluid-dynamical problem with significant biological relevance. In this regime, the dynamics exhibit unique characteristics, as inertia becomes negligible and bodies remain at rest in the absence of driving forces. The motion is governed by the Stokes equations, which describe fluid flow at low Reynolds number. Without inertia, a swimmer's movement through a fluid is entirely dictated by the geometry of its shape changes rather than the timing of these changes, provided the transitions occur slowly. An important characteristic of this motion is described by the scallop theorem [55], which states that at least two elementary deformations are necessary to achieve controlled locomotion in this regime, due to the kinematic reversibility of the Stokes equations. For modeling the swimming of micro-organisms and nano-robots, the low Reynolds numbers regime is appropriate [51]. Some related work in this area is the mathematical modeling and simulation of amoeboid cell swimming in [11], sperm swimming [61], and cell motility [21, 15].

There exist several contributions on the optimal locomotion of self-deforming swimming bodies at low Reynolds number. The seminal paper [54] considers the question of optimal locomotion of

flagellated micro-organisms (e.g. sperm); in order to derive a solution, a simplified model of the fluid was used (resistive force theory). The next major contribution was in [2], which considered the swimming body to be three disconnected spheres moving as a group along a given line. By taking advantage of the analytic solution for Stokes flow around a moving sphere, they were able to "eliminate" the Stokes constraint and reduce the problem of locomotion to a finite dimensional ODE for the center of the swimming body. Then, by the classic theory of optimal control for ODEs, they obtained the optimal stroke profile of the moving spheres. They later followed up on this work in [1] which considers stoke optimization for axisymmetric microswimmers.

More recent contributions employ tools from optimization and control theory. The locomotion induced by boundary deformations has been investigated in [12, 44, 45, 56], where the stationary Stokes equations in an unbounded domain (exterior Stokes problem) are considered. In [12], the authors derive a coupled system of ordinary differential equations (ODEs) and partial differential equations (PDEs) via the Euler-Lagrange equation, utilizing differential geometry tools. They study the controllability of the swimmer and its ability to track arbitrary trajectories. The shape changes are represented through conformal mappings, restricting the problem to two dimensions but allowing infinite degrees of freedom related to the shape changes. In addition, the link between shape deformations and internal forces is examined. In [45], the controllability and time-optimal control for low Reynolds numbers swimmers are established under a small body deformation assumption. The controllability problem consists of proving the existence of a sequence of deformations that steers the swimmer's center of mass from an initial to a final position. The swimmer's motion is decomposed into a rigid component, to be determined, and a component not affecting its mass center and global orientation. This leads to a reduced system of ODEs governing the full dynamics. In [44], it is demonstrated that a swimmer can track any given trajectory through a sequence of shape changes; the analysis takes advantage of spherical harmonics for dealing with the Stokes equations. When shape changes are expressed as a finite combination of elementary deformations without macro shape changes, only four elementary deformations suffice for trajectory tracking. In [46], the swimmer's shape remains fixed, with the ciliary propelling mechanism replaced by time-periodic tangential displacements. The goal is to control the swimmer's position and orientation via boundary displacements. The study shows that only three elementary deformations are necessary to achieve full control of the swimmer. The authors also mention that their results probably hold true for two elementary deformations, but one would need to consider non-symmetric shapes.

As noted in [46], the methodologies developed for fluid-structure systems in unbounded domains are no longer applicable when bounded domains are considered. In this work, we propose a model for self-deforming swimming micro-organisms in a bounded domain. The fluid dynamics are governed by the Stokes equations, while the shape control of the swimmer is achieved using a finite set of radial basis functions. These shape controls influence the system by modifying the fluid velocity at the body's boundary. The swimmer's center position depends implicitly on its evolving shape, leading to a coupled system consisting of the Stokes equations for the fluid velocity and an additional boundary integral equation determining the center position. Since the body shape's center position is defined implicitly, the problem can be interpreted as a free boundary problem, as the fluid domain's shape is unknown. However, unlike classical free boundary problems, here the deformation is prescribed, leaving only a specific subcomponent of the shape unknown. Thus, the forward problem is better described as a "hybrid" or semi-free boundary problem. This means that the shape control framework shares similarities with the control of free boundary problems, such as [31, 33, 36, 37], but with some simplifications due to the partially prescribed shape deformations. In other words, one can show that the center position satisfies an ODE by using the solution operator associated with the Stokes equations posed on the fluid domain $\Omega(t)$ at time t.

We take an optimal control approach, where we minimize a cost function for the tracking of the

body's center velocity. The main task is to perform the sensitivity analysis of the cost function with respect to the boundary shape deformations and a force (or "thrust") control applied to the swimmer body. Thus, we do not make any small deformation assumptions. For computing shape sensitivities, we use the standard tools of shape calculus [16, 63]. This requires the shape sensitivity of the Stokes equation but also the shape sensitivity of the body's center position through the additional boundary integral equation. We adopt a Lagrangian approach to incorporate both the Stokes constraint and the evolution of the body's center, treating the latter as an additional constraint. This enables us to derive the adjoint system, which solves a backward-in-time ODE that is coupled to Stokes.

There are several contributions in the literature on the stationary or space–time control of a deforming domain that models rigid bodies settling in a Stokes flow [18, 50]. In [50, Chapter 7], a two dimensional flexible structure in rigid motion has been considered, which shares similar features with our problem. The model is a Navier-Stokes equation coupled to an ODE describing the displacement of the structure in the viscous fluid, and kinematic continuity conditions at the fluid-structure interface. In contrast to our work, the moving shape is built as the flow of a vector field that depends on the solution of an ODE coupled with the fluid equation. Another important difference is that in [50, Chapter 7], the control enters as a non-homogeneous Dirichlet condition on a fixed boundary in the Navier-Stokes equation, while in our case the control is the time-dependent geometry of the swimmer body. In [24], the control of droplet deformation in Stokes flow is studied, with a focus on surface tension-driven flows. The interface deformation is governed by the local fluid velocity, and shape calculus is employed to derive optimality conditions. In [75], the authors study an infinite-dimensional, geometrically constrained shape optimization problem for magnetically driven microswimmers in three-dimensional Stokes flow, but the shape is static in time.

The paper is outlined as follows. Section 2 describes the mathematical model, shape optimization problem and shape controls. Section 3 is dedicated to the basic analysis of a modified Stokes system for the forward problem that includes the fluid velocity, pressure and body's center position. In Section 4 the sensitivity analysis of the objective functional with respect to the shape and swimmer thrust controls is performed using a Lagrangian approach. Section 5 describes our unfitted finite element scheme for simulating the forward and adjoint problem, along with a basic consistency and stability analysis. Numerical results are given in Section 6 to illustrate our approach, followed by some remarks in Section 7. Supplemental material on some of the analysis and implementation details are given in the appendices.

2 Model problem

2.1 Fluid mechanics

Consider a tank domain $\mathfrak{D}$, filled with a viscous fluid, and a deforming body $\mathcal{B}$, with $\Gamma := \partial\mathcal{B}$. The boundary of the tank decomposes as $\partial\mathfrak{D} = \Gamma_{\text{in}} \cup \Gamma_{\text{D}}$. The fluid domain is denoted $\Omega = \mathfrak{D} \setminus \overline{\mathcal{B}}$, with boundary decomposing as $\partial\Omega = \partial\mathfrak{D} \cup \Gamma$. The outer unit normal of Ω is $\boldsymbol{\nu}$. See Figure 1.

Let $\boldsymbol{v} = \boldsymbol{v}(t, \boldsymbol{x})$ be the velocity field of the fluid flow, which obeys the Stokes equations:

$$\begin{aligned} -\nabla\cdot\boldsymbol{\sigma} = \boldsymbol{f}^{\mathsf{T}}, \qquad \nabla\cdot\boldsymbol{v} = 0, \text{ in } \Omega, \\ \boldsymbol{v} = \boldsymbol{0}, \text{ on } \Gamma_{\text{D}}, \quad \boldsymbol{v} = \boldsymbol{b}, \text{ on } \Gamma, \quad \boldsymbol{\sigma}\boldsymbol{\nu} = \boldsymbol{0}, \text{ on } \Gamma_{\text{in}}, \end{aligned} \tag{1}$$

$$\boldsymbol{\sigma}(\boldsymbol{v}, p) := -p\boldsymbol{I} + 2\boldsymbol{\varepsilon}(\nabla\boldsymbol{v}), \quad \boldsymbol{\varepsilon}(\nabla\boldsymbol{v}) := \frac{\nabla\boldsymbol{v} + (\nabla\boldsymbol{v})^{\mathsf{T}}}{2}, \tag{2}$$

where $\boldsymbol{0}$ is the zero vector, $\boldsymbol{f}$ is a body force, $\boldsymbol{\sigma}$ is the stress tensor, p is the pressure, and $\boldsymbol{b}(t, \boldsymbol{x})$ is the velocity field of $\mathcal{B}$ (in the lab frame), defined for all $(t, \boldsymbol{x})$ such that $\boldsymbol{x} \in \mathcal{B}(t)$. Note that the PDE itself is steady and that the time-dependence of $\boldsymbol{v}$ is due to the time-dependence of $\boldsymbol{b}$.

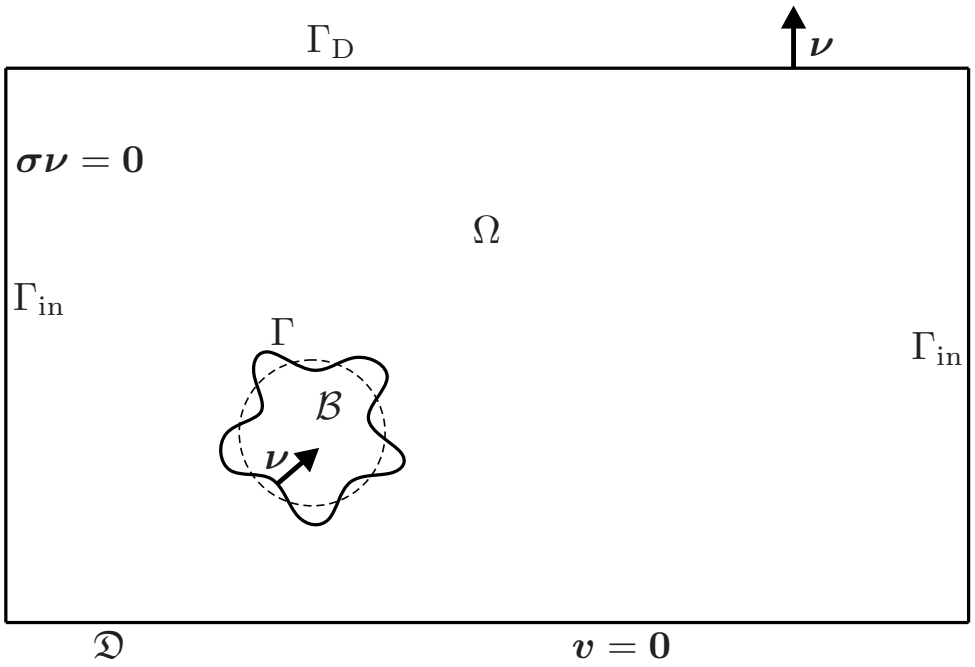

Figure 1: Diagram of 2-D tank with swimming body in Stokes Flow. Here $\mathfrak{D} = \Omega \cup \overline{\mathcal{B}}$ and $\Gamma = \partial\mathcal{B}$. The reference shape of $\mathcal{B}$ is a disk (dashed curve); the deformed shape is shown by the solid curve. Note that Γ_{in} is on the left and right.

2.2 The swimmer

The system of equations is not closed, as the motion of $\mathcal{B}$ must also be taken into account. Let $B(\mathbf{0}, R)$ be the ball in $\mathbb{R}^n$, centered at the origin, with radius R. For simplicity, assume $n = 2$ or 3 and let $\boldsymbol{c}(t) \in \mathbb{R}^n$ be a time-dependent coordinate that represents the center of the body $\mathcal{B}(t)$. Then, assume that the body is given by $\mathcal{B}(t) = \boldsymbol{\Phi}(t, B(\mathbf{0}, 1))$, where the map $\boldsymbol{\Phi}$ is a *homeomorphism* defined by

$$\boldsymbol{\Phi}(t, \hat{\boldsymbol{x}}) := (1 + u(t, \hat{\boldsymbol{x}}))R_0\hat{\boldsymbol{x}} + \boldsymbol{c}(t), \quad \text{for all } \hat{\boldsymbol{x}} \in \mathbb{R}^n, \tag{3}$$

where $u(t, \cdot) : \mathbb{R}^n \to \mathbb{R}$ is our time-dependent *shape control function* that satisfies the following properties

$$u(t, \cdot) \in C^2(\mathbb{R}^n \setminus \{\mathbf{0}\}), \qquad u(t, \hat{\boldsymbol{x}}) = u\left(t, \frac{\hat{\boldsymbol{x}}}{|\hat{\boldsymbol{x}}|}\right), \text{ for all } \hat{\boldsymbol{x}} \in \mathbb{R}^n \setminus \{\mathbf{0}\}, \tag{4}$$

i.e., $u(t, \cdot)$ is essentially a function defined on $\partial B(\mathbf{0}, 1)$ (see [45] which also assumes a radial shape control). Note that $\boldsymbol{\Phi}$ enjoys these properties as a consequence:

$$\begin{gathered}\boldsymbol{\Phi}(t, \cdot) \in C^0(\mathbb{R}^n, \mathbb{R}^n), \quad \boldsymbol{\Phi}(t, \cdot) \in W^{1,\infty}(\mathbb{R}^n, \mathbb{R}^n), \quad \boldsymbol{\Phi}(t, \cdot) \in C^2(\mathbb{R}^n \setminus \{\mathbf{0}\}, \mathbb{R}^n), \\ \boldsymbol{\Phi}^{-1}(t, \boldsymbol{x}) = \frac{\boldsymbol{x} - \boldsymbol{c}(t)}{(1 + u(t, \boldsymbol{x} - \boldsymbol{c}(t))R_0}, \quad \text{for all } \boldsymbol{x} \in \mathbb{R}^n.\end{gathered} \tag{5}$$

Note that if $u = 0$ and $\boldsymbol{c} = \mathbf{0}$, then $\mathcal{B}$ is simply $B(\mathbf{0}, R_0)$.

Remark 1. *We always assume that u is sufficiently small such that $\boldsymbol{\Phi}(t, \cdot) : B(\mathbf{0}, 1) \to \mathcal{B}(t)$ is a homeomorphism. This requires $u(t, \cdot) > -1$ for all t.*

Since $\Gamma(t) = \partial\mathcal{B}(t)$, then for any *material point* $\boldsymbol{x}(t) \in \Gamma(t)$, there is a unique pre-image $\hat{\boldsymbol{x}} \in \partial B(0,1)$, that is *independent* of $\boldsymbol{\Phi}$ and t, given by $\hat{\boldsymbol{x}} = \boldsymbol{\Phi}^{-1}(t, \boldsymbol{x}(t))$. Moreover, because of the form of (3), (4), it is evident that

$$\hat{\boldsymbol{x}} = \frac{\boldsymbol{x}(t) - \boldsymbol{c}(t)}{|\boldsymbol{x}(t) - \boldsymbol{c}(t)|} \quad \Rightarrow \quad \frac{d}{dt}\frac{\boldsymbol{x}(t) - \boldsymbol{c}(t)}{|\boldsymbol{x}(t) - \boldsymbol{c}(t)|} = \boldsymbol{0}. \tag{6}$$

Next, we connect $\boldsymbol{b}$ to $\boldsymbol{\Phi}$. For any material point $\boldsymbol{x}(t) \in \Gamma(t)$, this is simply

$$\begin{aligned} \boldsymbol{b}(t,\boldsymbol{x}) &:= \dot{\boldsymbol{x}} = \partial_t \boldsymbol{\Phi}(t,\hat{\boldsymbol{x}}) = R_0 \partial_t u(t,\hat{\boldsymbol{x}})\hat{\boldsymbol{x}} + \dot{\boldsymbol{c}}(t), \quad \text{where } \hat{\boldsymbol{x}} = \boldsymbol{\Phi}^{-1}(t,\boldsymbol{x}), \\ \text{or} \quad \boldsymbol{b}(t,\boldsymbol{x}) &= R_0 \partial_t u\left(t, \boldsymbol{x}(t) - \boldsymbol{c}(t)\right) \frac{\boldsymbol{x}(t) - \boldsymbol{c}(t)}{|\boldsymbol{x}(t) - \boldsymbol{c}(t)|} + \dot{\boldsymbol{c}}(t), \quad \forall\ \boldsymbol{x} \in \Gamma(t), \end{aligned} \tag{7}$$

because $\hat{\boldsymbol{x}} \in \partial B(\boldsymbol{0}, 1)$. With this, we introduce some notation:

$$\begin{aligned} \hat{\boldsymbol{\beta}}(t,\hat{\boldsymbol{x}};u) &:= R_0 \partial_t u\left(t,\hat{\boldsymbol{x}}\right) \frac{\hat{\boldsymbol{x}}}{|\hat{\boldsymbol{x}}|}, \ \forall\ \hat{\boldsymbol{x}} \neq \boldsymbol{0}, \\ \boldsymbol{\beta}(t,\boldsymbol{x};u,\boldsymbol{c}) &:= \hat{\boldsymbol{\beta}}(t,\boldsymbol{x} - \boldsymbol{c}(t);u)\zeta(\boldsymbol{x}) \equiv R_0 \partial_t u\left(t, \boldsymbol{x} - \boldsymbol{c}(t)\right) \frac{\boldsymbol{x} - \boldsymbol{c}(t)}{|\boldsymbol{x} - \boldsymbol{c}(t)|}\zeta(\boldsymbol{x}), \end{aligned} \tag{8}$$

where ζ is a cutoff function (see (16)) to make $\boldsymbol{\beta}$ satisfy the Dirichlet conditions on the boundary of the box (note that $\boldsymbol{\beta}$ is defined for all $\boldsymbol{x}$ because we can extend u to all of $\mathbb{R}^n$). Also, $\boldsymbol{\beta}$ is C^2 with respect to $\boldsymbol{x}$ for all $\boldsymbol{x} \neq \boldsymbol{c}(t)$. Therefore, the condition $\boldsymbol{v} = \boldsymbol{b}$ on Γ, in (1), is in fact

$$\begin{aligned} \boldsymbol{v}(t,\boldsymbol{x}) &= \boldsymbol{\beta}(t,\boldsymbol{x};u,\boldsymbol{c}) + \dot{\boldsymbol{c}}(t), \quad \text{for all } \boldsymbol{x} \text{ on } \Gamma(t), \\ \int_\Gamma \boldsymbol{\sigma}\boldsymbol{\nu}\, dS(\boldsymbol{x}) &= \boldsymbol{h}(t), \end{aligned} \tag{9}$$

where $\boldsymbol{h}$ is another "force" (thruster) control that acts on the body. Note that the second equation is required to determine the velocity of the center $\dot{\boldsymbol{c}}$, as all forces are balanced in Stokes flow.

2.3 Shape control

In two dimensions, we give a specific example of $u(t,\cdot)$ that satisfies (4). Let $t_\mathrm{f} > 0$ be a given final time and $\tilde{u} \in H^1(0, t_\mathrm{f}; C^2((-\pi,\pi])$ with $\tilde{u}(t,\theta)$ periodic in θ. Then, we take

$$u(t,\hat{\boldsymbol{x}}) = \tilde{u}(t,\theta(\hat{\boldsymbol{x}})), \quad \text{where} \quad \theta(\hat{\boldsymbol{x}}) \equiv \theta(\hat{x},\hat{y}) := \operatorname{atan2}(\hat{y},\hat{x}). \tag{10}$$

Note that $\hat{\boldsymbol{x}} \mapsto \nabla\theta(\hat{\boldsymbol{x}})$ is smooth for all $\hat{\boldsymbol{x}} \neq \boldsymbol{0}$ and is given by

$$\nabla\theta(\hat{x},\hat{y}) = \frac{(-\hat{y},\hat{x})}{\hat{x}^2 + \hat{y}^2}.$$

Moreover, since $\tilde{u}(t,\theta)$ is periodic, $u(t,\hat{\boldsymbol{x}})$ satisfies (4). Section B.1 gives more details on the specific parametrization of $\tilde{u}$. In three dimensions, a similar approach is possible by using spherical coordinate angles.

Note that, for the sake of simplicity, we do not enforce the volume of $\mathcal{B}(t)$ to remain constant in time. In the numerical experiments, we do not observe large deviations from a constant volume; see Section 6. If required, a volume constraint can be imposed explicitly, or deviations from the desired volume can be penalized by adding an appropriate term to the cost functional.

2.4 Optimization problem

We seek to find the optimal u and $\boldsymbol{h}$ that maximize the swimming speed $\dot{\boldsymbol{c}}$. In order to prevent the optimization procedure from achieving trivial or non-convergent results, additional regularizations (penalties) must be included. To this end, we seek to minimize the following objective functional

$$\begin{aligned} J[\boldsymbol{c}, u, \boldsymbol{h}] = \frac{1}{t_{\mathrm{f}}} \int_0^{t_{\mathrm{f}}} -\dot{\boldsymbol{c}}(t) \cdot \boldsymbol{e}_0 dt + \frac{\lambda_{\boldsymbol{h}}}{2t_{\mathrm{f}}} \|\boldsymbol{h}\|^2_{L^2([0,t_{\mathrm{f}}])} + \frac{\lambda_u}{2t_{\mathrm{f}}} (u,u)_{\mathcal{A}_u} \\ + \frac{\lambda_\ell}{t_{\mathrm{f}}} \int_0^{t_{\mathrm{f}}} \int_{-\pi}^{\pi} \mathcal{I}_M \ell(u(t,\theta)) d\theta dt + \frac{1}{4t_{\mathrm{f}}\epsilon_u} \left(\int_0^{t_{\mathrm{f}}} \int_{-\pi}^{\pi} \left(\partial_t u(t,\theta)\right)^2 d\theta dt - E_0 \right)^2. \end{aligned} \tag{11}$$

The first term encourages maximum speed in the constant direction $\boldsymbol{e}_0 \in \mathbb{R}^n$. The second and third terms are standard Tikhonov regularizations for the thrust control $\boldsymbol{h}$ and shape control u with $\lambda_{\boldsymbol{h}}, \lambda_u > 0$. The λ_ℓ term in the last line penalizes the shape control u from becoming too large, or too close to -1, with $\lambda_\ell > 0$ and $\ell(\cdot)$ a penalty function described in Section B.3; the operator $\mathcal{I}_M$ projects to a finite dimensional space (see below).

For the last term, $\int\int \left(\partial_t u(t,\theta)\right)^2 d\theta dt$ is meant to model the energy expended by the swimming body due to the control u. Hence, choosing a small $\epsilon_u > 0$ should encourage the expended energy to be close to the desired value E_0. In other words, this term acts to impose a desired energy "budget" on the swimming motion. One can also consider other notions of efficiency [43]. Note that $\dot{\boldsymbol{c}}$ depends on the controls, u and $\boldsymbol{h}$, through the solution of the forward problem (1), (9).

The admissible set for the controls is defined as follows. For u, let

$$\mathcal{A}_u := H^1(0, t_{\mathrm{f}}; \mathcal{U}_M) \quad \text{or} \quad H^1_{\mathrm{per}}(0, t_{\mathrm{f}}; \mathcal{U}_M), \qquad \mathcal{U}_M \subset C^2(-\pi, \pi) \text{ or } C^2_{\mathrm{per}}(-\pi, \pi), \tag{12}$$

where $H^1_{\mathrm{per}}(0, t_{\mathrm{f}}; \mathcal{U}_M)$ indicates periodic on the time interval $[0, t_{\mathrm{f}}]$ and $\mathcal{U}_M$ is a finite dimensional space (see Section B.1) with projection operator $\mathcal{I}_M : C^2_{\mathrm{per}}(-\pi, \pi) \to \mathcal{U}_M$ (or $\mathcal{I}_M : C^2(-\pi, \pi) \to \mathcal{U}_M$). Periodicity in time is needed to ensure a cyclic motion for the swimmer. The inner product, $(\cdot, \cdot)_{\mathcal{A}_u}$, is given by

$$(u, \eta)_{\mathcal{A}_u} := \int_0^{t_{\mathrm{f}}} \int_{-\pi}^{\pi} \alpha_1 u\eta + \alpha_2 \partial_t u \partial_t \eta + \alpha_3 \partial_\theta u \partial_\theta \eta + \alpha_4 (\partial_t \partial_\theta u)(\partial_t \partial_\theta \eta) d\theta dt, \tag{13}$$

for some non-negative coefficients $\{\alpha_i\}_{i=1}^4$. For the thrust control, we have $\mathcal{A}_{\boldsymbol{h}} := [L^2(0, t_{\mathrm{f}})]^n$. Thus, the concatenated admissible control set is

$$\mathcal{A} := \mathcal{A}_u \times \mathcal{A}_{\boldsymbol{h}}. \tag{14}$$

Thus, we wish to find $(\boldsymbol{c}^*, u^*, \boldsymbol{h}^*)$ that solves

$$J[\boldsymbol{c}^*, u^*, \boldsymbol{h}^*] = \min_{(u,\boldsymbol{h}) \in \mathcal{A}} J[\boldsymbol{c}, u, \boldsymbol{h}], \quad \text{subject to } \boldsymbol{c} \text{ obtained by solving (1), (9),} \tag{15}$$

where we note that $\mathcal{A}$ is obviously closed and convex.

3 Variational formulation of the coupled Stokes swimming body

In writing the weak formulation, we decompose the fluid velocity $\boldsymbol{v}$ in order to account for the (unknown) translation speed $\dot{\boldsymbol{c}}$. This requires the use of a cutoff function $\zeta(t, \boldsymbol{x}) = \zeta(\boldsymbol{x})$ that is

time-independent and at least C^2 such that

$$\zeta(\boldsymbol{x}) = \begin{cases} 1, & \text{if } \boldsymbol{x} \in \mathfrak{D}_\epsilon, \\ \text{positive and} \leq 1, & \text{if } \boldsymbol{x} \in \mathfrak{D} \setminus \mathfrak{D}_\epsilon, \\ 0, & \text{if } \boldsymbol{x} \in \partial\mathfrak{D}, \end{cases} \tag{16}$$

where $\mathfrak{D}_\epsilon \subset \mathfrak{D}$ is the subset satisfying $\operatorname{dist}(\mathfrak{D}_\epsilon, \partial\mathfrak{D}) = \epsilon$. We will assume throughout that $\epsilon > 0$ is small and $\mathcal{B}(t)$ is forever contained in $\mathfrak{D}_\epsilon$. Thus, $\zeta(\boldsymbol{x}) = 1$ for all $\boldsymbol{x} \in \Gamma(t)$ for any t. Moreover, $\nabla\zeta = \boldsymbol{0}$ in an open neighborhood of $\Gamma(t)$. See Section B.2 for a specific example.

3.1 Weak form of the Stokes equations

Let $H^1_{\mathrm{D}}(\mathfrak{D}) = \{v \in H^1(\mathfrak{D}) \mid v|_{\Gamma_{\mathrm{D}}} = 0\}$ and note that $\boldsymbol{v} \in [H^1_{\mathrm{D}}(\mathfrak{D})]^n$ means that each component of $\boldsymbol{v}$ is in $H^1_{\mathrm{D}}(\mathfrak{D})$; $H^1_{\mathrm{D}}(\Omega(t))$ is similarly defined. Next, introduce the function spaces

$$Q^t = L^2(\Omega(t)), \quad W^t(\boldsymbol{z}) = \{\boldsymbol{w} \in [H^1_{\mathrm{D}}(\Omega(t))]^n \mid \boldsymbol{w}|_{\Gamma(t)} = \boldsymbol{z}\}, \tag{17}$$

where $W^t(\boldsymbol{0})$ will be used for *part* of the velocity solution. Note that $\zeta \in H^1_{\mathrm{D}}(\mathfrak{D}) \cap C^2(\mathfrak{D})$ for all t. Now, define the following bilinear forms $a^t(\cdot,\cdot) : [H^1_{\mathrm{D}}(\Omega(t))]^n \times [H^1_{\mathrm{D}}(\Omega(t))]^n \to \mathbb{R}$, $b^t(\cdot,\cdot) : Q^t \times [H^1_{\mathrm{D}}(\Omega(t))]^n \to \mathbb{R}$:

$$a^t(\boldsymbol{v},\boldsymbol{w}) = 2\int_{\Omega(t)} \boldsymbol{\varepsilon}(\nabla\boldsymbol{v}) : \boldsymbol{\varepsilon}(\nabla\boldsymbol{w})\, d\boldsymbol{x}, \quad b^t(q,\boldsymbol{w}) = -\int_{\Omega(t)} q\nabla\cdot\boldsymbol{w}\, d\boldsymbol{x}, \tag{18}$$

where $a^t(\cdot,\cdot)$ is elliptic on $[H^1_{\mathrm{D}}(\Omega(t))]^n$. We also have the indefinite Stokes bilinear form

$$s^t((\boldsymbol{w},q),(\boldsymbol{v},p)) = a^t(\boldsymbol{w},\boldsymbol{v}) + b^t(p,\boldsymbol{w}) + b^t(q,\boldsymbol{v}), \quad \forall\, \boldsymbol{w},\boldsymbol{v} \in [H^1_{\mathrm{D}}(\Omega(t))]^n,\ \forall\, q,p \in Q^t. \tag{19}$$

Next, because of the integral constraint in (9) and the fact that $\dot{\boldsymbol{c}}(t)$ is an unknown to solve for, we are only allowed to test the PDE (1) with functions in $[H^1_{\mathrm{D}}(\Omega(t))]^n$ that are constant on $\Gamma(t)$. We accomplish this by testing with $\tilde{\boldsymbol{w}} + \boldsymbol{r}\zeta$, where $\tilde{\boldsymbol{w}} \in W^t(\boldsymbol{0})$, $\boldsymbol{r} \in \mathbb{R}^n$. Thus, multiplying the Stokes equations (1) by $\tilde{\boldsymbol{w}} + \boldsymbol{r}\zeta$ and $q \in Q^t$, using the second equation in (9), and the fact that $\tilde{\boldsymbol{w}} = \boldsymbol{0}$ on $\Gamma(t)$, we get

$$\begin{aligned} (\tilde{\boldsymbol{w}} + \boldsymbol{r}\zeta, \boldsymbol{f})_{\Omega(t)} &= -(\tilde{\boldsymbol{w}} + \boldsymbol{r}\zeta, \nabla\cdot\boldsymbol{\sigma})_{\Omega(t)} \\ &= (\nabla(\tilde{\boldsymbol{w}} + \boldsymbol{r}\zeta), (-p\boldsymbol{I} + 2\boldsymbol{\varepsilon}(\nabla\boldsymbol{v})))_{\Omega(t)} - (\tilde{\boldsymbol{w}} + \boldsymbol{r}\zeta, \boldsymbol{\sigma}\boldsymbol{\nu})_{\Gamma(t)} \\ &= 2(\nabla\tilde{\boldsymbol{w}}, \boldsymbol{\varepsilon}(\nabla\boldsymbol{v}))_{\Omega(t)} - (\nabla\tilde{\boldsymbol{w}}, p\boldsymbol{I})_{\Omega(t)} + (\boldsymbol{r}\otimes\nabla\zeta, \boldsymbol{\sigma})_{\Omega(t)} - \boldsymbol{r}\cdot(1, \boldsymbol{\sigma}\boldsymbol{\nu})_{\Gamma(t)} \\ &= a^t(\tilde{\boldsymbol{w}},\boldsymbol{v}) + b^t(p,\tilde{\boldsymbol{w}}) + a^t(\boldsymbol{r}\zeta,\boldsymbol{v}) + b^t(p,\boldsymbol{r}\zeta) - (\boldsymbol{r},\boldsymbol{h}(t))_{\mathbb{R}^n}, \\ 0 &= b^t(q,\boldsymbol{v}). \end{aligned} \tag{20}$$

Therefore, using (19), for each $t \in [0,t_{\mathrm{f}}]$ and given $\boldsymbol{c}(t) \in \mathbb{R}^n$, we say $\boldsymbol{v}(t,\cdot) \in [H^1_{\mathrm{D}}(\Omega(t))]^n$, $p(t,\cdot) \in Q^t$, and $\boldsymbol{s}(t) \in \mathbb{R}^n$, is a weak solution of the system (1) and (9), if

$$\begin{aligned} s^t((\tilde{\boldsymbol{w}} + \boldsymbol{r}\zeta, q),(\boldsymbol{v},p)) - (\boldsymbol{r},\boldsymbol{h}(t))_{\mathbb{R}^n} &= (\tilde{\boldsymbol{w}} + \boldsymbol{r}\zeta, \boldsymbol{f})_{\Omega(t)},\ \forall\tilde{\boldsymbol{w}} \in W^t(\boldsymbol{0}),\ \forall\boldsymbol{r} \in \mathbb{R}^n,\ \forall q \in Q^t, \\ \boldsymbol{v}(t,\boldsymbol{x}) &= \boldsymbol{\beta}(t,\boldsymbol{x}) + \boldsymbol{s}(t),\ \forall\boldsymbol{x} \in \Gamma(t), \\ \dot{\boldsymbol{x}} &= \boldsymbol{v}(t,\boldsymbol{x}),\ \forall\boldsymbol{x} \in \Gamma(t), \end{aligned} \tag{21}$$

where $\boldsymbol{x} \in \Gamma(t)$ in the last line refers to material points in $\Gamma(t)$ (i.e., each material point has the same velocity as the fluid). Because of the parameterization of the body motion (recall the derivation of (7)), the last two lines of (21) indicate that the body center satisfies $\dot{\boldsymbol{c}} = \boldsymbol{s}$.

Next, define $\tilde{\boldsymbol{v}}(t,\cdot) \in W^t(\boldsymbol{0})$ such that

$$\boldsymbol{v}(t,\boldsymbol{x}) = \tilde{\boldsymbol{v}}(t,\boldsymbol{x}) + \boldsymbol{\beta}(t,\boldsymbol{x}) + \boldsymbol{s}(t)\zeta(\boldsymbol{x}), \qquad \boldsymbol{x} \in \Omega(t). \tag{22}$$

Then, we rewrite (21) as follows. For each $t \in [0, t_{\mathrm{f}}]$ and given $\boldsymbol{c}(t) \in \mathbb{R}^n$, find $\tilde{\boldsymbol{v}}(t,\cdot) \in W^t(\boldsymbol{0})$, $\boldsymbol{s}(t) \in \mathbb{R}^n$, and $p(t,\cdot) \in Q^t$ such that

$$\begin{aligned} s^t\left((\tilde{\boldsymbol{w}} + \boldsymbol{r}\zeta, q), (\tilde{\boldsymbol{v}} + \boldsymbol{s}(t)\zeta, p)\right) &= -s^t\left((\tilde{\boldsymbol{w}} + \boldsymbol{r}\zeta, q), (\boldsymbol{\beta}, 0)\right) \\ &\quad + (\boldsymbol{r}, \boldsymbol{h}(t))_{\mathbb{R}^n} + (\tilde{\boldsymbol{w}} + \boldsymbol{r}\zeta, \boldsymbol{f})_{\Omega(t)}, \ \forall \tilde{\boldsymbol{w}} \in W^t(\boldsymbol{0}), \ \forall \boldsymbol{r} \in \mathbb{R}^n, \ \forall q \in Q^t. \end{aligned} \tag{23}$$

We point that when we solve the modified Stokes problem (23) at time t, we completely determine the velocity of the body due to $\dot{\boldsymbol{c}} = \boldsymbol{s}$. Furthermore, the evolution of $\Omega(t)$ is completely dictated by $u(t,\cdot)$ and $\boldsymbol{c}(t)$. Thus, $\dot{\boldsymbol{c}}(t) = \boldsymbol{s}(t)$ will play the role of an "ODE" to solve for the evolution of $\boldsymbol{c}(t)$; see Section 3.3.

3.2 Well-posedness of the modified Stokes problem

We wish to determine the solvability of (23). We rewrite (23) as: for each $t \in [0, t_{\mathrm{f}}]$ and given $\boldsymbol{c}(t) \in \mathbb{R}^n$, we seek to find $(\tilde{\boldsymbol{v}}(t,\cdot), \boldsymbol{s}(t)) \in (W^t(\boldsymbol{0}) \times \mathbb{R}^n)$ and $p(t,\cdot) \in Q^t$ such that

$$\begin{aligned} a^t\left(\tilde{\boldsymbol{w}} + \boldsymbol{r}\zeta, \tilde{\boldsymbol{v}} + \boldsymbol{s}(t)\zeta\right) + b^t\left(p, \tilde{\boldsymbol{w}} + \boldsymbol{r}\zeta\right) &= -s^t\left((\tilde{\boldsymbol{w}} + \boldsymbol{r}\zeta, 0), (\boldsymbol{\beta}, 0)\right) \\ + (\tilde{\boldsymbol{w}} + \boldsymbol{r}\zeta, \boldsymbol{f})_{\Omega(t)} + (\boldsymbol{r}, \boldsymbol{h}(t))_{\mathbb{R}^n}, \ \forall \tilde{\boldsymbol{w}} \in W^t(\boldsymbol{0}), \ \forall \boldsymbol{r} \in \mathbb{R}^n, \\ b^t\left(q, \tilde{\boldsymbol{v}} + \boldsymbol{s}(t)\zeta\right) &= -b^t\left(q, \boldsymbol{\beta}\right), \ \forall q \in Q^t, \end{aligned} \tag{24}$$

which is a saddle point problem.

Therefore, we must establish the Ladyzhenskaya-Babuška-Brezzi (LBB) conditions for solvability [4]. First, we establish the coercivity of $a^t\left(\tilde{\boldsymbol{w}} + \boldsymbol{r}\zeta, \tilde{\boldsymbol{w}} + \boldsymbol{r}\zeta\right)$ over the space $W^t(\boldsymbol{0}) \times \mathbb{R}^n$. Obviously, we have

$$a^t\left(\tilde{\boldsymbol{w}} + \boldsymbol{r}\zeta, \tilde{\boldsymbol{w}} + \boldsymbol{r}\zeta\right) \geq 0. \tag{25}$$

Moreover, it is easy to show that $a^t\left(\tilde{\boldsymbol{w}} + \boldsymbol{r}\zeta, \tilde{\boldsymbol{w}} + \boldsymbol{r}\zeta\right) \geq \alpha_0 \|\tilde{\boldsymbol{w}} + \boldsymbol{r}\zeta\|^2_{H^1(\Omega(t))}$, for some $\alpha_0 > 0$, by using the Korn and Poincaré inequalities. Note that $\zeta = 1$ on $\Gamma(t)$, but $\tilde{\boldsymbol{w}} = \boldsymbol{0}$ on $\Gamma(t)$. Then, by a compactness argument [23], one can show that $\|\tilde{\boldsymbol{w}} + \boldsymbol{r}\zeta\|^2_{H^1(\Omega(t))} \geq C_0 \left(\|\tilde{\boldsymbol{w}}\|^2_{H^1(\Omega(t))} + |\boldsymbol{r}|^2\right)$, for some positive constant $C_0 > 0$. Thus, there exists $\tilde{\alpha}_0 > 0$ such that

$$a^t\left(\tilde{\boldsymbol{w}} + \boldsymbol{r}\zeta, \tilde{\boldsymbol{w}} + \boldsymbol{r}\zeta\right) \geq \tilde{\alpha}_0 \left(\|\tilde{\boldsymbol{w}}\|^2_{H^1(\Omega(t))} + |\boldsymbol{r}|^2\right). \tag{26}$$

Next, we establish the inf-sup condition. It is well-known [7] that

$$\sup_{\boldsymbol{z} \in H^1_0(\Omega)} \frac{-\int_\Omega q \nabla \cdot \boldsymbol{z} d\boldsymbol{x}}{\|\boldsymbol{z}\|_{H^1(\Omega)}} \geq c_0 \|q\|_{L^2(\Omega)}, \quad \text{for all } q \in L^2(\Omega), \tag{27}$$

where $c_0 > 0$ depends on Ω. Clearly, there exists a $b_0 > 0$, uniformly in t, such that

$$\sup_{\substack{\tilde{\boldsymbol{w}} \in W^t(\boldsymbol{0}), \\ \boldsymbol{r} \in \mathbb{R}^n}} \frac{b^t\left(q, \tilde{\boldsymbol{w}} + \boldsymbol{r}\zeta\right)}{\left(\|\tilde{\boldsymbol{w}}\|^2_{H^1(\Omega(t))} + |\boldsymbol{r}|^2\right)^{1/2}} \geq b_0 \|q\|_{L^2(\Omega(t))}, \quad \text{for all } q \in Q^t, \tag{28}$$

provided $\mathcal{B}(t)$ is always contained in $\mathfrak{D}_\epsilon$. Together with the obvious continuity bounds

$$\begin{aligned} a^t\left(\tilde{\boldsymbol{w}} + \boldsymbol{r}\zeta, \tilde{\boldsymbol{v}} + \boldsymbol{s}\zeta\right) &\leq C \left(\|\tilde{\boldsymbol{w}}\|^2_{H^1(\Omega(t))} + |\boldsymbol{r}|^2\right)^{1/2} \left(\|\tilde{\boldsymbol{v}}\|^2_{H^1(\Omega(t))} + |\boldsymbol{s}|^2\right)^{1/2}, \\ b^t\left(q, \tilde{\boldsymbol{w}} + \boldsymbol{r}\zeta\right) &\leq C \|q\|_{L^2(\Omega(t))} \left(\|\tilde{\boldsymbol{w}}\|^2_{H^1(\Omega(t))} + |\boldsymbol{r}|^2\right)^{1/2}, \end{aligned} \tag{29}$$

we have that (24) is well-posed.

3.3 ODE for the evolution of the body center

We first introduce notation to compress the modified Stokes system further. Define the space $\mathcal{W}^t := W^t(\mathbf{0}) \times \mathbb{R}^n \times Q^t$, and the following aggregated bilinear and linear forms $S^t(\cdot,\cdot) : \mathcal{W}^t \times \mathcal{W}^t \to \mathbb{R}$, $F^t(\cdot) : \mathcal{W}^t \to \mathbb{R}$:

$$\begin{aligned} S^t\left((\tilde{\boldsymbol{w}}, \boldsymbol{r}, q), (\tilde{\boldsymbol{v}}, \boldsymbol{s}, p)\right) &:= s^t\left((\tilde{\boldsymbol{w}} + \boldsymbol{r}\zeta, q), (\tilde{\boldsymbol{v}} + \boldsymbol{s}\zeta, p)\right), \\ F^t\left((\tilde{\boldsymbol{w}}, \boldsymbol{r}, q); u(t,\cdot), \boldsymbol{h}(t)\right) &:= -s^t\left((\tilde{\boldsymbol{w}} + \boldsymbol{r}\zeta, q), (\boldsymbol{\beta}(u), 0)\right) + (\tilde{\boldsymbol{w}} + \boldsymbol{r}\zeta, \boldsymbol{f})_{\Omega(t)} + (\boldsymbol{r}, \boldsymbol{h}(t))_{\mathbb{R}^n}. \end{aligned} \tag{30}$$

Then, identifying $\boldsymbol{\Theta} \equiv (\tilde{\boldsymbol{w}}, \boldsymbol{r}, q)$ and $\boldsymbol{\Psi}(t) \equiv (\tilde{\boldsymbol{v}}(t), \boldsymbol{s}(t), p(t))$, we write (23) as follows. For each $t \in [0, t_\mathrm{f}]$ and given $\boldsymbol{c}(t) \in \mathbb{R}^n$, we seek to find the state $\boldsymbol{\Psi}(t) \in \mathcal{W}^t$ such that

$$S^t\left(\boldsymbol{\Theta}, \boldsymbol{\Psi}(t)\right) = F^t\left(\boldsymbol{\Theta}; u(t,\cdot), \boldsymbol{h}(t)\right), \quad \forall\ \boldsymbol{\Theta} \in \mathcal{W}^t. \tag{31}$$

Given $t \in [0, t_\mathrm{f}]$ and $(\boldsymbol{c}(t), u(t,\cdot), \boldsymbol{h}(t))$, the solution of (31) exists and is unique. So, for each $t \in [0, t_\mathrm{f}]$, let $\mathcal{S}^t(\cdot)$ be the solution operator for (31), i.e., $\mathcal{S}^t(\cdot)$ maps $(\boldsymbol{c}(t), u(t,\cdot), \boldsymbol{h}(t))$ to the unique solution $\boldsymbol{\Psi}(t) \in \mathcal{W}^t$. Since $\dot{\boldsymbol{c}} = \boldsymbol{s}$, we have the following "ODE" for the evolution of $\boldsymbol{c}$:

$$\dot{\boldsymbol{c}}(t) = (0,1,0) \cdot \boldsymbol{\Psi}(t), \qquad \boldsymbol{\Psi}(t) = \mathcal{S}^t\left(\boldsymbol{c}(t), u(t,\cdot), \boldsymbol{h}(t)\right), \quad \text{for } t \in [0, t_\mathrm{f}], \tag{32}$$

with initial condition $\boldsymbol{c}(0) := \boldsymbol{c}^0$ given by $\Omega(0)$. Again, note that $\mathcal{S}^t(\cdot)$ depends on $\Omega(t)$ which evolves based on $\boldsymbol{c}(t)$ and $u(t)$ through (22).

4 Sensitivity analysis of the optimal control problem

For the numerical approximation of optimal controls $u, \boldsymbol{h}$ minimizing $J[u, \boldsymbol{h}]$, the main task is to perform the sensitivity analysis of $\boldsymbol{c}$ with respect to $u, \boldsymbol{h}$. We explain here the main principles for the sensitivity analysis with respect to u, which is the more complicated case. First, a small perturbation of u results in an explicit perturbation of the shape $\Omega(t)$ via the body shape $\mathcal{B}(t)$ that depends on u. This creates a small variation of the solution $\boldsymbol{v}, p$ of the Stokes equation (1) which depends on the shape $\Omega(t)$. In addition, $\boldsymbol{v}, p$ are also affected by the perturbation of the boundary condition (9). Eventually, this results in the perturbation of $\dot{\boldsymbol{c}}(t)$ via the integral condition in (9). In order to handle these complex interactions, we use a Lagrangian approach that incorporates the cost function, the Stokes PDE constraint and the body center evolution $\dot{\boldsymbol{c}} = \boldsymbol{s}$, also treated as a constraint. Eventually, this results in an adjoint system that includes a modified Stokes PDE, an adjoint body center evolution $\boldsymbol{r}$ and an adjoint body position $\boldsymbol{a}$. The adjoint body position also satisfies an ODE, but backward in time, as usual for the control of evolution problems. The source term of this ODE depends on the forward state $(\boldsymbol{v}, p)$ and the adjoint state $(\boldsymbol{w}, q)$.

For the sensitivity analysis, some quantities such as $\boldsymbol{\beta}(t, \boldsymbol{x}; u, \boldsymbol{c})$ depend explicitly on u and the derivative is straightforward to compute. The challenging task is the sensitivity analysis of the space-time Stokes functional J_{St} (see (35)), which depends on the state variables $\boldsymbol{v}, p$ of the Stokes equation that depend implicitly on the shape $\Omega(t)$. Here we follow a material derivative approach, where the functions defined on the perturbed domain are transported back to a reference domain, and use standard techniques of shape calculus to compute the derivatives.

We first rewrite the objective functional (11) using $\boldsymbol{\Psi}$:

$$\begin{aligned} J[\boldsymbol{\Psi}, u, \boldsymbol{h}] = \frac{1}{t_\mathrm{f}} \int_0^{t_\mathrm{f}} -\boldsymbol{\Psi}_2(t) \cdot \boldsymbol{e}_0 dt + \frac{\lambda_{\boldsymbol{h}}}{2t_\mathrm{f}} \|\boldsymbol{h}\|^2_{L^2([0,t_\mathrm{f}])} + \frac{\lambda_u}{2t_\mathrm{f}} (u,u)_{\mathcal{A}_u} \\ + \frac{\lambda_\ell}{t_\mathrm{f}} \int_0^{t_\mathrm{f}} \int_{-\pi}^{\pi} \mathcal{I}_M \ell(u(t,\theta)) d\theta dt + \frac{1}{4t_\mathrm{f}\epsilon_u} \left(\int_0^{t_\mathrm{f}} \int_{-\pi}^{\pi} \left(\partial_t u(t,\theta)\right)^2 d\theta dt - E_0 \right)^2, \end{aligned} \tag{33}$$

defined for all $\boldsymbol{\Psi} = (\boldsymbol{\Psi}_1, \boldsymbol{\Psi}_2, \boldsymbol{\Psi}_3) = (\tilde{\boldsymbol{v}}, \boldsymbol{s}, p) \in L^2(0, t_\mathrm{f}; \mathcal{W}^t)$, $\boldsymbol{h} \in L^2(0, t_\mathrm{f}; \mathbb{R}^n)$, and $u \in H^1(0, t_\mathrm{f}; \mathcal{U}_M)$. For the optimization, we will have the constraint that $\boldsymbol{\Psi}(t)$ is the solution of (31) for all $t \in [0, t_\mathrm{f}]$, which we note also, implicitly, depends on $\Omega(t)$ through the modified Stokes operator.

We use a Lagrangian approach that incorporates the Stokes PDE constraint, as well as the body center evolution equation $\dot{\boldsymbol{c}} = \boldsymbol{s}$, through Lagrange multipliers [50, Ch. 7] in order to clarify the sensitivity analysis. To this end, $\Omega(t)$ is parameterized by $\boldsymbol{c}(t)$ and $u(t, \cdot)$, but $\boldsymbol{c}(t)$ is decoupled from $\boldsymbol{s}(t)$. Therefore, the Lagrangian is given by

$$\mathcal{L}\left[\boldsymbol{\Psi}, \boldsymbol{c}, u, \boldsymbol{h}, \boldsymbol{\Theta}, \boldsymbol{a}\right] := J\left[\boldsymbol{\Psi}, u, \boldsymbol{h}\right] - \int_0^{t_\mathrm{f}} \boldsymbol{a}(t) \cdot (\dot{\boldsymbol{c}} - \boldsymbol{s})\, dt - J_{\mathrm{St}}\left[\boldsymbol{\Psi}, \boldsymbol{c}, \boldsymbol{\Theta}, u, \boldsymbol{h}\right], \tag{34}$$

defined for all $\boldsymbol{\Theta}, \boldsymbol{\Psi} \in L^2(0, t_\mathrm{f}; \mathcal{W}^t)$, $\boldsymbol{h} \in L^2(0, t_\mathrm{f}; \mathbb{R}^n)$, $\boldsymbol{a} \in L^2(0, t_\mathrm{f}; \mathbb{R}^n)$, $u \in H^1(0, t_\mathrm{f}; \mathcal{U}_M)$, where

$$J_{\mathrm{St}}\left[\boldsymbol{\Psi}, \boldsymbol{c}, \boldsymbol{\Theta}, u, \boldsymbol{h}\right] := \int_0^{t_\mathrm{f}} \left(S^t\left(\boldsymbol{\Theta}, \boldsymbol{\Psi}\right) - F^t\left(\boldsymbol{\Theta}; u, \boldsymbol{h}\right)\right) dt. \tag{35}$$

Here, $\boldsymbol{\Theta}, \boldsymbol{a}$ are the adjoint variables and we emphasize that J_{St} depends on $\boldsymbol{c}(t)$. Computing

$$\delta_{\boldsymbol{a}} \mathcal{L}\left[\boldsymbol{\Psi}, \boldsymbol{c}, u, \boldsymbol{h}, \boldsymbol{\Theta}, \boldsymbol{a}\right](\delta \boldsymbol{a}) = -\int_0^{t_\mathrm{f}} \delta \boldsymbol{a}(t) \cdot (\dot{\boldsymbol{c}} - \boldsymbol{s})\, dt$$

and setting this to zero for all $\delta \boldsymbol{a}$ we recover the constraint $\dot{\boldsymbol{c}} = \boldsymbol{s}$. Moreover, perturbing $\mathcal{L}$ with respect to $\boldsymbol{\Theta}$, and setting to zero, yields the forward problem, (31), for each $t \in [0, t_\mathrm{f}]$ given $\boldsymbol{c}(t) \in \mathbb{R}^n$. Together with $\dot{\boldsymbol{c}} = \boldsymbol{s}$, they deliver the ODE (32).

Next, we need to perturb $\mathcal{L}$ with respect to the forward variables $\boldsymbol{\Psi}$ and $\boldsymbol{c}$ to obtain the adjoint equations. This requires to perform a shape sensitivity analysis in the following subsections, as $J_{\mathrm{St}}\left[\boldsymbol{\Psi}, \boldsymbol{c}, \boldsymbol{\Theta}, u, \boldsymbol{h}\right]$ depends both implicitly on $\boldsymbol{c}$ through the shape $\Omega(t)$ and explicitly through $\boldsymbol{\beta}(u)$.

4.1 Computing the shape derivative via material derivative

We introduce a generic mapping to represent domain perturbations. Let $\mathbf{T}_{\boldsymbol{Z}}^{\rho,t} : \mathfrak{D} \to \mathfrak{D}$ be defined for all $t \in [0, t_\mathrm{f}]$ and $\rho \in (-\epsilon, \epsilon)$, with some $\epsilon > 0$, by

$$\mathbf{T}_{\boldsymbol{Z}}^{\rho,t}(\boldsymbol{x}) := \mathrm{id}_{\mathfrak{D}}(\boldsymbol{x}) + \rho \boldsymbol{Z}(t, \boldsymbol{x}), \quad \text{for all } \boldsymbol{x} \in \mathfrak{D}, \tag{36}$$

where we assume $\boldsymbol{Z}$ is sufficiently smooth and $\boldsymbol{Z}(t, \cdot) = \boldsymbol{0}$ on $\partial\mathfrak{D}$, for all $t \in [0, t_\mathrm{f}]$, so that $\mathbf{T}_{\boldsymbol{Z}}^{\rho,t}(\cdot)$ is a diffeomorphism uniformly in ρ and t. Then, the perturbation of $\Omega(t)$ (at time t) by the field $\boldsymbol{Z}$, is given by

$$\Omega_\rho(t) := \mathbf{T}_{\boldsymbol{Z}}^{\rho,t}(\Omega(t)), \tag{37}$$

where ρ is the scalar perturbation parameter. In other words, fixing $t = t_0$, the mapping (36) is the standard perturbation of the identity approach for deforming the domain $\Omega(t_0)$; the time parameter t simply chooses the particular time-slice to perturb.

Let $g_\rho(t, \cdot)$ be a function defined on $\Omega_\rho(t)$ for all $t \in [0, t_\mathrm{f}]$ and all $\rho \in (-\epsilon, \epsilon)$. Setting $g \equiv g_0$, we define the *material shape derivative* of $g(t, \cdot)$, *at time-slice* t, by

$$D_{\boldsymbol{Z}} g(t, \boldsymbol{x}) := \lim_{\rho \to 0} \frac{g_\rho(t, \mathbf{T}_{\boldsymbol{Z}}^{\rho,t}(\boldsymbol{x})) - g(t, \boldsymbol{x})}{\rho}, \quad \text{for all } \boldsymbol{x} \in \Omega(t), \text{ and each fixed } t. \tag{38}$$

By an appropriate extension of g in $\mathfrak{D}$, one can express (38) more explicitly:

$$D_{\boldsymbol{Z}} g(t, \boldsymbol{x}) = \partial_\rho g_\rho(t, \boldsymbol{x})\Big|_{\rho=0} + \boldsymbol{Z}(t, \boldsymbol{x}) \cdot \nabla_{\boldsymbol{x}} g(t, \boldsymbol{x}), \quad \boldsymbol{x} \in \Omega(t). \tag{39}$$

The mapping (36) is similar to the standard Lagrangian flow map of the domain $\Omega(t)$. Let $\boldsymbol{V} : [0, t_{\mathrm{f}}] \times \mathfrak{D} \to \mathbb{R}^n$ be a smooth velocity field that vanishes on $\partial\mathfrak{D}$ and governs the evolution of $\Omega(t)$, i.e., $\boldsymbol{x} \in \Omega(t)$ moves with velocity $\boldsymbol{V}(t, \boldsymbol{x})$. Next, let $\boldsymbol{X}_t(s, \boldsymbol{x})$ solve the ODE:

$$\begin{aligned} \frac{d}{ds}\boldsymbol{X}_t(s, \boldsymbol{a}) &= \boldsymbol{V}(s, \boldsymbol{X}_t(s, \boldsymbol{a})), \text{ for } s \in (t, t_{\mathrm{f}}) \\ \boldsymbol{X}_t(t, \boldsymbol{a}) &= \boldsymbol{a}, \quad \text{for any } \boldsymbol{a} \in \mathfrak{D}. \end{aligned} \tag{40}$$

Then, $\Omega(s) = \boldsymbol{X}_t(s, \Omega(t))$ for all $s \in [t, t_{\mathrm{f}}]$. Next, for any function $f(t, \cdot)$ defined on $\Omega(t)$ for all $t \in [0, t_{\mathrm{f}}]$, the *material time derivative* of $f(t, \cdot)$, at $t = t_0 \in (0, t_{\mathrm{f}})$, is given by

$$\dot{f}(t_0, \boldsymbol{x}) := \lim_{t \to t_0} \frac{f(t, \boldsymbol{X}_{t_0}(t, \boldsymbol{x})) - f(t_0, \boldsymbol{x})}{t - t_0}, \quad \text{for all } \boldsymbol{x} \in \Omega(t_0), \tag{41}$$

which has the more explicit form

$$\dot{f}(t_0, \boldsymbol{x}) = \partial_t f(t, \boldsymbol{x})\Big|_{t=t_0} + \boldsymbol{V}(t_0, \boldsymbol{x}) \cdot \nabla_{\boldsymbol{x}} f(t_0, \boldsymbol{x}). \tag{42}$$

We emphasize that (38) is not the same as (41), as (38) is a material derivative for a shape perturbation at a *fixed time-slice* t, whereas (41) is a derivative with respect to time.

Next, let $f(t, \boldsymbol{x})$ be defined on $\Omega(t)$ and define the mapped function on $\Omega_\rho(t)$ by

$$f_\rho(t, \boldsymbol{y}) := f\left(t, (\mathbf{T}_{\boldsymbol{Z}}^{\rho,t})^{-1}(\boldsymbol{y})\right), \qquad \boldsymbol{y} \in \Omega_\rho(t). \tag{43}$$

From the definition, $D_{\boldsymbol{Z}} f = 0$. Moreover, we have the identity:

$$(\nabla_{\boldsymbol{y}} f_\rho(t, \boldsymbol{y})) \circ \mathbf{T}_{\boldsymbol{Z}}^{\rho,t}(\boldsymbol{x}) = \nabla_{\boldsymbol{y}}\left(f(t, \cdot) \circ (\mathbf{T}_{\boldsymbol{Z}}^{\rho,t})^{-1}(\boldsymbol{y})\right) \circ \mathbf{T}_{\boldsymbol{Z}}^{\rho,t}(\boldsymbol{x}) = \nabla_{\boldsymbol{x}} f(t, \boldsymbol{x})[\nabla_{\boldsymbol{x}} \mathbf{T}_{\boldsymbol{Z}}^{\rho,t}(\boldsymbol{x})]^{-1}.$$

Then, we get

$$\begin{aligned} D_{\boldsymbol{Z}} \nabla f(t, \boldsymbol{x}) &= \lim_{\rho \to 0} \frac{(\nabla_{\boldsymbol{y}} f_\rho(t, \boldsymbol{y})) \circ \mathbf{T}_{\boldsymbol{Z}}^{\rho,t}(\boldsymbol{x}) - \nabla_{\boldsymbol{x}} f(t, \boldsymbol{x})}{\rho} \\ &= \nabla_{\boldsymbol{x}} f(t, \boldsymbol{x}) \left[\lim_{\rho \to 0} \frac{[\nabla_{\boldsymbol{x}} \mathbf{T}_{\boldsymbol{Z}}^{\rho,t}(\boldsymbol{x})]^{-1} - \boldsymbol{I}}{\rho}\right] = -\nabla_{\boldsymbol{x}} f(t, \boldsymbol{x})[\nabla \boldsymbol{Z}(t, \boldsymbol{x})] = -\sum_{i=1}^{3} (\partial_i f) \partial_j Z_i. \end{aligned} \tag{44}$$

Note that gradients, such as $\nabla_{\boldsymbol{x}} f(t, \boldsymbol{x})$, are treated as row vectors throughout the paper.

4.2 Perturbing the space-time Stokes functional

In order to compute the sensitivity of the Lagrangian, we first perform a simpler, intermediate perturbation analysis of the Stokes functional (35). First, note that

$$J_{\mathrm{St}}\left[\boldsymbol{\Psi}, \boldsymbol{c}, \boldsymbol{\Theta}, u, \boldsymbol{h}\right] = \int_0^{t_{\mathrm{f}}} a^t\left(\boldsymbol{w}, \boldsymbol{v}\right) + b^t\left(p, \boldsymbol{w}\right) + b^t\left(q, \boldsymbol{v}\right) - \left(\boldsymbol{w}, \boldsymbol{f}\right)_{\Omega(t)} - \boldsymbol{r} \cdot \boldsymbol{h}\, dt,$$

with the adjoint variables $\boldsymbol{\Theta}(t) \equiv (\tilde{\boldsymbol{w}}(t), \boldsymbol{r}(t), q(t))$ and the state variables $\boldsymbol{\Psi}(t) \equiv (\tilde{\boldsymbol{v}}(t), \boldsymbol{s}(t), p(t))$, and we set $\boldsymbol{w} = \tilde{\boldsymbol{w}} + \boldsymbol{r}\zeta$, $\boldsymbol{v} = \tilde{\boldsymbol{v}} + \boldsymbol{\beta} + \boldsymbol{s}\zeta$ for simplicity. Note that the Stokes forms depend on $\Omega(t)$. Let us write J_{St} more explicitly

$$J_{\mathrm{St}}\left[\boldsymbol{\Psi}, \boldsymbol{c}, \boldsymbol{\Theta}, u, \boldsymbol{h}\right] = \int_0^{t_{\mathrm{f}}} \mathcal{Q}\left[t, \boldsymbol{\Psi}, \boldsymbol{c}, \boldsymbol{\Theta}, u\right] - \boldsymbol{r}(t) \cdot \boldsymbol{h}(t) dt, \quad \mathcal{Q}\left[t, \boldsymbol{\Psi}, \boldsymbol{c}, \boldsymbol{\Theta}, u\right] := \int_{\Omega(t)} Q(t, \boldsymbol{x})\, d\boldsymbol{x}, \tag{45}$$

where $\mathcal{Q}$ depends on $\Omega(t)$ (which depends on $\boldsymbol{c}$, u), and

$$Q(t,\boldsymbol{x}) := 2\boldsymbol{\varepsilon}(\nabla \boldsymbol{w}) : \boldsymbol{\varepsilon}(\nabla \boldsymbol{v}) - p\nabla\cdot\boldsymbol{w} - q\nabla\cdot\boldsymbol{v} - \boldsymbol{w}\cdot\boldsymbol{f}, \text{ for all } \boldsymbol{x}\in\mathfrak{D},\ t\in[0,t_{\mathrm{f}}]. \tag{46}$$

Note that $\boldsymbol{w}$, $\boldsymbol{v}$, $\boldsymbol{r}$, $\boldsymbol{s}$, q, p are just generic functions and not yet the solutions of the forward and adjoint problems. We use the same notation for the variables and the solutions for the sake of simplicity. However, $\boldsymbol{w}$, $\boldsymbol{v}$ satisfy the following constraints:

$$\begin{aligned} &\boldsymbol{v} = \boldsymbol{s} + \boldsymbol{\beta}, \quad \boldsymbol{w} = \boldsymbol{r}, \quad \text{on } \Gamma(t),\\ &\boldsymbol{v} = \boldsymbol{w} = \boldsymbol{0}, \quad \text{on } \partial\mathfrak{D}. \end{aligned} \tag{47}$$

In the following, we take $\Omega(t)$ to be a prescribed domain evolution and we let $\boldsymbol{Z}$ be a given time-slice perturbation that is *independent* of $\Omega(t)$, $\boldsymbol{s}$, $\boldsymbol{c}$, $\boldsymbol{\beta}$, and u. When we perturb the domain, we must respect (47), namely the first line. This could be done with a Lagrange multiplier (not explored here). Instead, we use a transformation approach to guarantee the constraints are satisfied for any perturbation $\boldsymbol{Z}$.

Due to the way we model the body motion and deformation, we cannot map $\boldsymbol{\beta}$. Thus, we decompose $\boldsymbol{v}$ as

$$\boldsymbol{v} = \bar{\boldsymbol{v}} + \boldsymbol{\beta}, \ \text{ in } \Omega(t), \quad \text{where} \quad \bar{\boldsymbol{v}} \in H^1_{\mathrm{D}}(\Omega(t)), \ \ \bar{\boldsymbol{v}} = \boldsymbol{s}, \ \text{ on } \Gamma(t), \tag{48}$$

where we note that $\boldsymbol{\beta}$ and $\nabla\boldsymbol{\beta}$ are fixed functions (for each t) defined on $\mathfrak{D}$, in the sense that they do not depend on ρ.

Next, recall (36) and (37), note that $\Omega_\rho(t) := \mathbf{T}^{\rho,t}_{\boldsymbol{Z}}(\Omega(t))$, and also note that $\boldsymbol{w}$ lies in $H^1_D(\Omega(t))$ with $\boldsymbol{w} = \boldsymbol{r}$ on $\Gamma(t)$. Now define $\bar{\boldsymbol{v}}_\rho := \bar{\boldsymbol{v}}(t,\cdot)\circ(\mathbf{T}^{\rho,t}_{\boldsymbol{Z}})^{-1}$ and note that $\bar{\boldsymbol{v}}_\rho \in H^1_D(\Omega_\rho(t))$ with $\bar{\boldsymbol{v}}_\rho = \boldsymbol{s}$ on $\Gamma_\rho(t)$. Moreover, since $p(t,\cdot)$ is only defined on $\Omega(t)$, set $p_\rho := p(t,\cdot)\circ(\mathbf{T}^{\rho,t}_{\boldsymbol{Z}})^{-1}$ and note that $p_\rho \in L^2(\Omega_\rho(t))$. We proceed analogously for $\boldsymbol{w}$ and q. Clearly, the (boundary condition) constraints are satisfied on the perturbed domain.

Upon recalling Section 4.1, we have the following material shape derivative formulas

$$\begin{aligned} D_{\boldsymbol{Z}}\bar{\boldsymbol{v}} = D_{\boldsymbol{Z}}\boldsymbol{w} = \boldsymbol{0}, \quad D_{\boldsymbol{Z}}(\nabla\bar{\boldsymbol{v}}) = -(\nabla\bar{\boldsymbol{v}})(\nabla\boldsymbol{Z}),\ D_{\boldsymbol{Z}}(\nabla\boldsymbol{w}) = -(\nabla\boldsymbol{w})(\nabla\boldsymbol{Z}),\\ D_{\boldsymbol{Z}}(\nabla\cdot\bar{\boldsymbol{v}}) = -\nabla\bar{\boldsymbol{v}}^{\mathsf{T}} : \nabla\boldsymbol{Z}, \quad D_{\boldsymbol{Z}}(\nabla\cdot\boldsymbol{w}) = -\nabla\boldsymbol{w}^{\mathsf{T}} : \nabla\boldsymbol{Z},\\ D_{\boldsymbol{Z}}p = D_{\boldsymbol{Z}}q = 0, \quad D_{\boldsymbol{Z}}(\nabla\boldsymbol{\beta}) = \boldsymbol{Z}\cdot\nabla(\nabla\boldsymbol{\beta}), \end{aligned} \tag{49}$$

where we used (44). We now make use of this fundamental result, see for instance [74, Lemma 5.7],

$$R[\Omega,f] := \int_\Omega f\,d\boldsymbol{x}, \quad \delta_\Omega R[\Omega,f](\boldsymbol{Z}) := \lim_{\rho\to 0}\frac{R[\Omega_\rho,f]-R[\Omega,f]}{\rho} = \int_\Omega D_{\boldsymbol{Z}}f\,d\boldsymbol{x} + \int_\Omega f(\nabla\cdot\boldsymbol{Z})d\boldsymbol{x},$$

where Ω_ρ is defined as in (37), and apply it to (45),(46), which gives, using (49),

$$\begin{aligned} \delta_{\Omega(t)}\mathcal{Q}\left[t,\boldsymbol{\Psi},\boldsymbol{c},\boldsymbol{\Theta}\right](\boldsymbol{Z}) = &\int_{\Omega(t)} 2\boldsymbol{\varepsilon}(-\nabla\boldsymbol{w}\nabla\boldsymbol{Z}) : \boldsymbol{\varepsilon}(\nabla\boldsymbol{v})d\boldsymbol{x}\\ &+\int_{\Omega(t)} 2\boldsymbol{\varepsilon}(\nabla\boldsymbol{w}) : \left[\boldsymbol{\varepsilon}(-\nabla\bar{\boldsymbol{v}}\nabla\boldsymbol{Z}) + \boldsymbol{\varepsilon}(D_{\boldsymbol{Z}}(\nabla\boldsymbol{\beta}))\right]d\boldsymbol{x}\\ &+\int_{\Omega(t)} p\nabla\boldsymbol{w}^{\mathsf{T}} : \nabla\boldsymbol{Z} + q\nabla\bar{\boldsymbol{v}}^{\mathsf{T}} : \nabla\boldsymbol{Z} - q\boldsymbol{Z}\cdot\nabla[\nabla\cdot\boldsymbol{\beta}]d\boldsymbol{x}\\ &+\int_{\Omega(t)} -\boldsymbol{w}\cdot[(\nabla\boldsymbol{f})\boldsymbol{Z}] + Q(t,\boldsymbol{x})\nabla\cdot\boldsymbol{Z}\,d\boldsymbol{x}. \end{aligned} \tag{50}$$

Now, we note these simplifications, using (49),

$$\begin{aligned}
&\boldsymbol{\varepsilon}(-\nabla \boldsymbol{w}\nabla \boldsymbol{Z}) : \boldsymbol{\varepsilon}(\nabla \boldsymbol{v}) = -\left(\nabla \boldsymbol{w}\nabla \boldsymbol{Z}\right) : \boldsymbol{\varepsilon}(\nabla \boldsymbol{v}) = -\nabla \boldsymbol{Z} : \nabla \boldsymbol{w}^{\mathsf{T}} \boldsymbol{\varepsilon}(\nabla \boldsymbol{v}),\\
&\boldsymbol{\varepsilon}(\nabla \boldsymbol{w}) : \boldsymbol{\varepsilon}(-\nabla \bar{\boldsymbol{v}}\nabla \boldsymbol{Z}) = -\nabla \boldsymbol{Z} : \nabla \bar{\boldsymbol{v}}^{\mathsf{T}} \boldsymbol{\varepsilon}(\nabla \boldsymbol{w}),\\
&\boldsymbol{\varepsilon}(\nabla \boldsymbol{w}) : \boldsymbol{\varepsilon}(D_{\boldsymbol{Z}}(\nabla \boldsymbol{\beta})) = \boldsymbol{\varepsilon}(\nabla \boldsymbol{w}) : \left[\boldsymbol{Z} \cdot \nabla(\nabla \boldsymbol{\beta})\right] = \sum_{k=1}^{n} \boldsymbol{Z} \cdot \boldsymbol{e}_k \left[\boldsymbol{\varepsilon}(\nabla \boldsymbol{w}) : \partial_k(\nabla \boldsymbol{\beta})\right],
\end{aligned}$$

where we used the symmetry of $\boldsymbol{\varepsilon}$, and $\boldsymbol{e}_k, k = 1, \ldots, n$, are basis vectors in Cartesian coordinates. Plugging into (50), we get the bulk formulation

$$\delta_{\Omega(t)} \mathcal{Q}\left[t, \boldsymbol{\Psi}, \boldsymbol{c}, \boldsymbol{\Theta}\right](\boldsymbol{Z}) = \int_{\Omega(t)} S_1 : \nabla \boldsymbol{Z} + S_0 \cdot \boldsymbol{Z}\, d\boldsymbol{x}, \tag{51}$$

with, using Einstein's summation convention,

$$\begin{aligned}
S_1 &= -2\nabla \boldsymbol{w}^{\mathsf{T}} \boldsymbol{\varepsilon}(\nabla \boldsymbol{v}) - 2\nabla \bar{\boldsymbol{v}}^{\mathsf{T}} \boldsymbol{\varepsilon}(\nabla \boldsymbol{w}) + p\nabla \boldsymbol{w}^{\mathsf{T}} + q\nabla \bar{\boldsymbol{v}}^{\mathsf{T}} + Q(t, \boldsymbol{x})I\\
&= -\nabla \boldsymbol{w}^{\mathsf{T}} \boldsymbol{\sigma}(\boldsymbol{v}, p) - \nabla \bar{\boldsymbol{v}}^{\mathsf{T}} \boldsymbol{\sigma}(\boldsymbol{w}, q) + Q(t, \boldsymbol{x})I,\\
S_0 &= 2\left[\boldsymbol{\varepsilon}(\nabla \boldsymbol{w}) : \partial_k(\nabla \boldsymbol{\beta})\right] \boldsymbol{e}_k - q\nabla[\nabla \cdot \boldsymbol{\beta}] - \boldsymbol{w}^{\mathsf{T}}(\nabla \boldsymbol{f})\\
&= \left[\boldsymbol{\sigma}(\boldsymbol{w}, q) : \partial_k(\nabla \boldsymbol{\beta})\right] \boldsymbol{e}_k - w_i \nabla f_i.
\end{aligned} \tag{52}$$

The tensors S_1, S_0 of the bulk formulation (51) must satisfy the fundamental relation

$$\mathrm{div} S_1 = S_0, \tag{53}$$

valid in general for shape derivatives in distributed form such as (51); see [35, Proposition 1]. The verification of this relation is performed in the appendix; see Section A. In our numerical implementation, there is no problem computing S_0 since $\boldsymbol{\beta}$ is analytically defined.

The bulk formulation (51) is convenient for numerical calculations but it can also be expressed using an interface representation, the so-called Hadamard form [16, 63], provided the data is sufficiently regular in the neighborhood of $\Gamma(t)$. This condition is satisfied here, since $\Gamma(t)$ is smooth. Assuming the higher regularity $S_1 \in W^{1,1}(\Omega(t), \mathbb{R}^{2\times 2})$, using the fact that $\Gamma(t)$ is smooth and that the support of $\boldsymbol{Z}$ is in a neighbourhood of $\Gamma(t)$, we can apply [35, Proposition 1] which yields the Hadamard form of the shape derivative:

$$\delta_{\Omega(t)} \mathcal{Q}\left[t, \boldsymbol{\Psi}, \boldsymbol{c}, \boldsymbol{\Theta}\right](\boldsymbol{Z}) = \int_{\Gamma(t)} (S_1 \boldsymbol{\nu} \cdot \boldsymbol{\nu}) \boldsymbol{Z} \cdot \boldsymbol{\nu}\, dS. \tag{54}$$

with

$$S_1 \boldsymbol{\nu} \cdot \boldsymbol{\nu} = -\boldsymbol{\sigma}(\boldsymbol{v}, p)\boldsymbol{\nu} \cdot \nabla \boldsymbol{w}\boldsymbol{\nu} - \boldsymbol{\sigma}(\boldsymbol{w}, q)\boldsymbol{\nu} \cdot \nabla \bar{\boldsymbol{v}}\boldsymbol{\nu} + Q.$$

When evaluating this expression at the solutions $\boldsymbol{v}$ (state) and $\boldsymbol{w}$ (adjoint) of Stokes equations, we have $\nabla \cdot \boldsymbol{w} = 0$ and $\nabla \cdot \boldsymbol{v} = 0$, thus we have the following simplification:

$$\begin{aligned}
Q(t, \boldsymbol{x}) &= 2\boldsymbol{\varepsilon}(\nabla \boldsymbol{w}) : \boldsymbol{\varepsilon}(\nabla \boldsymbol{v}) - p\nabla \cdot \boldsymbol{w} - q\nabla \cdot \boldsymbol{v} - \boldsymbol{w} \cdot \boldsymbol{f}\\
&= \nabla \boldsymbol{w}\boldsymbol{\nu} \cdot \nabla \boldsymbol{v}\boldsymbol{\nu} + (\nabla \boldsymbol{w}\boldsymbol{\nu} \otimes \boldsymbol{\nu})(\nabla \boldsymbol{v}\boldsymbol{\nu} \otimes \boldsymbol{\nu}) - \boldsymbol{w} \cdot \boldsymbol{f}\\
&= \nabla \boldsymbol{w}\boldsymbol{\nu} \cdot \nabla \boldsymbol{v}\boldsymbol{\nu} - \boldsymbol{w} \cdot \boldsymbol{f}.
\end{aligned}$$

4.3 Perturbing the swimmer shape through $\boldsymbol{\beta}$

4.3.1 Perturbation with respect to $\boldsymbol{c}$

The swimmer shape depends on the control u and the position $\boldsymbol{c}$ which both appear in the function $\boldsymbol{\beta}(t,\boldsymbol{x};u,\boldsymbol{c})$; see (8). In the definition (45) of $\mathcal{Q}[t,\boldsymbol{\Psi},\boldsymbol{c},\boldsymbol{\Theta},u]$, we only consider the terms that depend on $\boldsymbol{\beta}$ and introduce the following subpart of $\mathcal{Q}[t,\boldsymbol{\Psi},\boldsymbol{c},\boldsymbol{\Theta},u]$ for the sake of simplicity:

$$\overline{\mathcal{Q}}[t,\boldsymbol{\beta}] := \int_{\Omega(t)} 2\boldsymbol{\varepsilon}(\nabla\boldsymbol{w}) : \boldsymbol{\varepsilon}(\nabla\boldsymbol{\beta}) - q\nabla\cdot\boldsymbol{\beta}\, d\boldsymbol{x} = \int_{\Omega(t)} \boldsymbol{\sigma}(\boldsymbol{w},q) : \nabla\boldsymbol{\beta}\, d\boldsymbol{x}, \tag{55}$$

where $\boldsymbol{\beta}(t,\boldsymbol{x};u,\boldsymbol{c})$ with u and $\boldsymbol{c}$ treated as *independent* of $\Omega(t)$. Let $\delta\boldsymbol{c}$ be a perturbation of $\boldsymbol{c}$. We first note some preliminary calculations:

$$\begin{aligned}
\nabla|\boldsymbol{x}-\boldsymbol{c}|^{-1} &= -\frac{\boldsymbol{x}-\boldsymbol{c}}{|\boldsymbol{x}-\boldsymbol{c}|^3}, \quad \nabla\left[\frac{\boldsymbol{x}-\boldsymbol{c}}{|\boldsymbol{x}-\boldsymbol{c}|}\right] = \frac{1}{|\boldsymbol{x}-\boldsymbol{c}(t)|}\mathrm{P}^{\perp}_{\boldsymbol{x}-\boldsymbol{c}},\\
\delta_{\boldsymbol{c}}|\boldsymbol{x}-\boldsymbol{c}|^{-1}(\delta\boldsymbol{c}) &= \frac{\boldsymbol{x}-\boldsymbol{c}}{|\boldsymbol{x}-\boldsymbol{c}|^3}\cdot\delta\boldsymbol{c}, \quad \delta_{\boldsymbol{c}}\left[\frac{\boldsymbol{x}-\boldsymbol{c}(t)}{|\boldsymbol{x}-\boldsymbol{c}(t)|}\right](\delta\boldsymbol{c}) = -\frac{1}{|\boldsymbol{x}-\boldsymbol{c}(t)|}\mathrm{P}^{\perp}_{\boldsymbol{x}-\boldsymbol{c}}\delta\boldsymbol{c},
\end{aligned} \tag{56}$$

with

$$\mathrm{P}^{\perp}_{\boldsymbol{x}-\boldsymbol{c}} := \boldsymbol{I} - \frac{\boldsymbol{x}-\boldsymbol{c}(t)}{|\boldsymbol{x}-\boldsymbol{c}(t)|}\otimes\frac{\boldsymbol{x}-\boldsymbol{c}(t)}{|\boldsymbol{x}-\boldsymbol{c}(t)|}. \tag{57}$$

We also compute

$$\begin{aligned}
\nabla\boldsymbol{\beta}(t,\boldsymbol{x}) &= \frac{R_0}{|\boldsymbol{x}-\boldsymbol{c}(t)|}\left[\boldsymbol{\psi}(\boldsymbol{x})\zeta(\boldsymbol{x}) + \partial_t u\left(t,\boldsymbol{x}-\boldsymbol{c}(t)\right)\left\{\mathrm{P}^{\perp}_{\boldsymbol{x}-\boldsymbol{c}}\zeta(\boldsymbol{x}) + (\boldsymbol{x}-\boldsymbol{c}(t))\otimes\nabla\zeta(\boldsymbol{x})\right\}\right],\\
\boldsymbol{\psi}(\boldsymbol{x}) &:= (\boldsymbol{x}-\boldsymbol{c}(t))\otimes\nabla\partial_t u\left(t,\boldsymbol{x}-\boldsymbol{c}(t)\right).
\end{aligned} \tag{58}$$

Again recalling (8), we have

$$\delta_{\boldsymbol{c}}\boldsymbol{\beta}(t,\boldsymbol{x};u,\boldsymbol{c})(\delta\boldsymbol{c}) = -(\delta\boldsymbol{c}\cdot\nabla_{\hat{\boldsymbol{x}}})\hat{\boldsymbol{\beta}}(t,\boldsymbol{x}-\boldsymbol{c}(t);u)\zeta(\boldsymbol{x}) = \mathcal{G}\delta\boldsymbol{c}, \tag{59}$$

with the matrix $\mathcal{G}$ given by

$$\begin{aligned}
\mathcal{G} &:= -\frac{R_0}{|\boldsymbol{x}-\boldsymbol{c}(t)|}\left[\boldsymbol{\psi}(\boldsymbol{x}) + \partial_t u\left(t,\boldsymbol{x}-\boldsymbol{c}(t)\right)\mathrm{P}^{\perp}_{\boldsymbol{x}-\boldsymbol{c}}\right]\zeta(\boldsymbol{x})\\
&= -R_0\left[\frac{\boldsymbol{x}-\boldsymbol{c}(t)}{|\boldsymbol{x}-\boldsymbol{c}(t)|}\otimes\nabla\partial_t u\left(t,\boldsymbol{x}-\boldsymbol{c}(t)\right) + \partial_t u\left(t,\boldsymbol{x}-\boldsymbol{c}(t)\right)\nabla\left(\frac{\boldsymbol{x}-\boldsymbol{c}(t)}{|\boldsymbol{x}-\boldsymbol{c}(t)|}\right)\right]\zeta(\boldsymbol{x}).
\end{aligned} \tag{60}$$

Now we compute

$$\begin{aligned}
\delta_{\boldsymbol{c}}\overline{\mathcal{Q}}[t,\boldsymbol{\beta}](\delta\boldsymbol{c}) &= \int_{\Omega(t)} 2\boldsymbol{\varepsilon}(\nabla\boldsymbol{w}) : \boldsymbol{\varepsilon}(\nabla\delta_{\boldsymbol{c}}\boldsymbol{\beta}(\delta\boldsymbol{c})) - q\nabla\cdot\delta_{\boldsymbol{c}}\boldsymbol{\beta}(\delta\boldsymbol{c})\, d\boldsymbol{x}\\
&= \int_{\Omega(t)} 2\boldsymbol{\varepsilon}(\nabla\boldsymbol{w}) : \boldsymbol{\varepsilon}(\nabla(\mathcal{G}\delta\boldsymbol{c})) - q\nabla\cdot(\mathcal{G}\delta\boldsymbol{c})\, d\boldsymbol{x} = \int_{\Omega(t)} \boldsymbol{\sigma}(\boldsymbol{w},q) : \nabla(\mathcal{G}\delta\boldsymbol{c})\, d\boldsymbol{x}.
\end{aligned} \tag{61}$$

It will turn out that the adjoint state $(\boldsymbol{w},q)$ satisfies $-\nabla\cdot\boldsymbol{\sigma}(\boldsymbol{w},q) = \boldsymbol{0}$ in $\Omega(t)$ and $\boldsymbol{\sigma}(\boldsymbol{w},q)\boldsymbol{\nu} = \boldsymbol{0}$ on Γ_{in}; see Section 4.4 where the strong form of the adjoint is given. Integrating by parts, we get

$$\begin{aligned}
\delta_{\boldsymbol{c}}\overline{\mathcal{Q}}[t,\boldsymbol{\beta}](\delta\boldsymbol{c}) &= \int_{\Omega(t)} \underbrace{(-\nabla\cdot\boldsymbol{\sigma}(\boldsymbol{w},q))}_{=0}\cdot(\mathcal{G}\delta\boldsymbol{c}) + \int_{\partial\Omega(t)} (\mathcal{G}\delta\boldsymbol{c})\cdot\boldsymbol{\sigma}(\boldsymbol{w},q)\boldsymbol{\nu}\, dS(\boldsymbol{x})\\
&= \int_{\Gamma(t)} (\mathcal{G}\delta\boldsymbol{c})\cdot\boldsymbol{\sigma}(\boldsymbol{w},q)\boldsymbol{\nu}\, dS(\boldsymbol{x}),
\end{aligned} \tag{62}$$

where we have used the fact that $\zeta = 0$ on $\partial\mathfrak{D}$.

4.3.2 Perturbation with respect to the shape control u

Let δu be a perturbation of u. Then, from (8), we have

$$\delta_u \boldsymbol{\beta}(t, \boldsymbol{x}; u, \boldsymbol{c})(\delta u) = \boldsymbol{\beta}(t, \boldsymbol{x}; \delta u, \boldsymbol{c}), \tag{63}$$

as $\boldsymbol{\beta}$ is linear in u. Now, treating $u(t, \cdot)$ as independent of $\Omega(t)$, similar to (61), we get

$$\begin{aligned} \delta_u \overline{\mathcal{Q}}\left[t, \boldsymbol{\beta}\right](\delta u) &= \int_{\Omega(t)} 2\boldsymbol{\varepsilon}(\nabla \boldsymbol{w}) : \boldsymbol{\varepsilon}(\nabla \delta_u \boldsymbol{\beta}(\delta u)) - q \nabla \cdot \delta_u \boldsymbol{\beta}(\delta u)\, d\boldsymbol{x} \\ &= \int_{\Omega(t)} \boldsymbol{\sigma}(\boldsymbol{w}, q) : (\nabla \delta_u \boldsymbol{\beta}(\delta u))\, d\boldsymbol{x}. \end{aligned} \tag{64}$$

Also, similar to (62) and assuming $\boldsymbol{w}$, q are the adjoint solutions, an integration by parts gives

$$\delta_u \overline{\mathcal{Q}}\left[t, \boldsymbol{\beta}\right](\delta u) = \int_{\Gamma(t)} \delta_u \boldsymbol{\beta}(\delta u) \cdot \boldsymbol{\sigma}(\boldsymbol{w}, q) \boldsymbol{\nu}\, dS(\boldsymbol{x}). \tag{65}$$

4.4 Sensitivity of the Lagrangian and adjoint equations

We now have the tools to perturb $\mathcal{L}$, see (34), with respect to $\boldsymbol{\Psi}$ and $\boldsymbol{c}$ to obtain the adjoint equations. First, we perturb $\mathcal{L}$ with respect to $\boldsymbol{\Psi}_1$ and $\boldsymbol{\Psi}_3$:

$$\begin{aligned} \delta_{\boldsymbol{\Psi}_1} \mathcal{L}\left[\boldsymbol{\Psi}, \boldsymbol{c}, u, \boldsymbol{h}, \boldsymbol{\Theta}, \boldsymbol{a}\right](\delta \tilde{\boldsymbol{v}}) &= -\int_0^{t_\mathrm{f}} S^t\left(\boldsymbol{\Theta}, (\delta \tilde{\boldsymbol{v}}, \boldsymbol{0}, 0)\right) dt, \\ \delta_{\boldsymbol{\Psi}_3} \mathcal{L}\left[\boldsymbol{\Psi}, \boldsymbol{c}, u, \boldsymbol{h}, \boldsymbol{\Theta}, \boldsymbol{a}\right](\delta p) &= -\int_0^{t_\mathrm{f}} S^t\left(\boldsymbol{\Theta}, (\boldsymbol{0}, \boldsymbol{0}, \delta p)\right) dt. \end{aligned} \tag{66}$$

In view of (33), perturbing $\mathcal{L}$ with respect to $\boldsymbol{\Psi}_2 \equiv \boldsymbol{s}$ gives

$$\delta_{\boldsymbol{\Psi}_2} \mathcal{L}\left[\boldsymbol{\Psi}, \boldsymbol{c}, u, \boldsymbol{h}, \boldsymbol{\Theta}, \boldsymbol{a}\right](\delta \boldsymbol{s}) = -\int_0^{t_\mathrm{f}} S^t\left(\boldsymbol{\Theta}, (\boldsymbol{0}, \delta \boldsymbol{s}, 0)\right) dt - \frac{1}{t_\mathrm{f}} \int_0^{t_\mathrm{f}} \boldsymbol{e}_0 \cdot \delta \boldsymbol{s} dt + \int_0^{t_\mathrm{f}} \boldsymbol{a}(t) \cdot \delta \boldsymbol{s} dt. \tag{67}$$

Equations (66), (67) appear in the adjoint system, but we need another equation that comes from perturbing $\mathcal{L}$ with respect to $\boldsymbol{c}$.

Note that $J\left[\boldsymbol{\Psi}, u, \boldsymbol{h}\right]$ does not depend on $\boldsymbol{c}$, but $J_{\mathrm{St}}\left[\boldsymbol{\Psi}, \boldsymbol{c}, \boldsymbol{\Theta}, u, \boldsymbol{h}\right]$ depends both implicitly on $\boldsymbol{c}$ through the shape $\Omega(t)$ and explicitly through $\boldsymbol{\beta}$. Thus, $\delta_{\boldsymbol{c}} J_{\mathrm{St}}\left[\boldsymbol{\Psi}, \boldsymbol{c}, \boldsymbol{\Theta}, u, \boldsymbol{h}\right]$ contributes with two terms in the derivative. For the first term, the perturbation of $\boldsymbol{c}$ corresponds to a translation of the body $\mathcal{B}(t)$, which deforms $\Omega(t)$, so we can use formula (51) with $\boldsymbol{Z} = \delta \boldsymbol{c} \zeta$. The second term comes from the derivative of $\boldsymbol{\beta}$ with respect to $\boldsymbol{c}$ in $J_{\mathrm{St}}\left[\boldsymbol{\Psi}, \boldsymbol{c}, \boldsymbol{\Theta}, u, \boldsymbol{h}\right]$, but this time with $\Omega(t)$ held fixed for each t; for this we can use formula (61). Hence, we get the following bulk formula

$$\begin{aligned} \delta_{\boldsymbol{c}} J_{\mathrm{St}}\left[\boldsymbol{\Psi}, \boldsymbol{c}, \boldsymbol{\Theta}, u, \boldsymbol{h}\right](\delta \boldsymbol{c}) &= \int_0^{t_\mathrm{f}} \delta_{\Omega(t)} \mathcal{Q}\left[t, \boldsymbol{\Psi}, \boldsymbol{c}, \boldsymbol{\Theta}\right](\delta \boldsymbol{c}) dt + \int_0^{t_\mathrm{f}} \delta_{\boldsymbol{c}} \overline{\mathcal{Q}}\left[t, \boldsymbol{\beta}\right](\delta \boldsymbol{c}) dt \\ &= \int_0^{t_\mathrm{f}} \int_{\Omega(t)} S_1 : \nabla(\delta \boldsymbol{c} \zeta) + S_0 \cdot (\delta \boldsymbol{c} \zeta)\, d\boldsymbol{x} dt + \int_0^{t_\mathrm{f}} \int_{\Omega(t)} \boldsymbol{\sigma}(\boldsymbol{w}, q) : \left[\nabla(\mathcal{G} \delta \boldsymbol{c})\right] d\boldsymbol{x} dt, \end{aligned} \tag{68}$$

with S_0, S_1 defined in (52), and where the terms coming from the derivative of $\boldsymbol{\beta}$ w.r.t. $\boldsymbol{c}$ have been computed in Section 4.3. Alternatively, using (54) and (62), we can also obtain a boundary representation of this derivative:

$$\delta_{\boldsymbol{c}} J_{\mathrm{St}}\left[\boldsymbol{\Psi}, \boldsymbol{c}, \boldsymbol{\Theta}, u, \boldsymbol{h}\right](\delta \boldsymbol{c}) = \int_0^{t_\mathrm{f}} \int_{\Gamma(t)} \left(S_1 \boldsymbol{\nu} \cdot \boldsymbol{\nu}\right) \delta \boldsymbol{c} \cdot \boldsymbol{\nu}\, dS dt + \int_0^{t_\mathrm{f}} \int_{\Gamma(t)} (\mathcal{G} \delta \boldsymbol{c}) \cdot \boldsymbol{\sigma}(\boldsymbol{w}, q) \boldsymbol{\nu}\, dS(\boldsymbol{x}) dt. \tag{69}$$

Gathering these results, we obtain

$$\begin{aligned}\delta_{\boldsymbol{c}}\mathcal{L}\left[\boldsymbol{\Psi},\boldsymbol{c},u,\boldsymbol{h},\boldsymbol{\Theta},\boldsymbol{a}\right](\delta\boldsymbol{c}) &= -\int_0^{t_\mathrm{f}} \boldsymbol{a}(t)\cdot\delta\dot{\boldsymbol{c}}dt - \delta_{\boldsymbol{c}}J_{\mathrm{St}}\left[\boldsymbol{\Psi},\boldsymbol{c},\boldsymbol{\Theta},\boldsymbol{h}\right](\delta\boldsymbol{c})\\ &= -\int_0^{t_\mathrm{f}} \boldsymbol{a}(t)\cdot\delta\dot{\boldsymbol{c}}dt - \int_0^{t_\mathrm{f}}\int_{\Omega(t)} \boldsymbol{\sigma}(\boldsymbol{w},q):\left[\nabla(\mathcal{G}\delta\boldsymbol{c})\right]d\boldsymbol{x}dt\\ &\quad -\int_0^{t_\mathrm{f}}\int_{\Omega(t)} S_1:\nabla(\delta\boldsymbol{c}\zeta)+S_0\cdot(\delta\boldsymbol{c}\zeta)\,d\boldsymbol{x}dt.\end{aligned}$$

Since the initial position $\boldsymbol{c}(0)=\boldsymbol{c}_0$ is fixed, it must hold that $\delta\boldsymbol{c}(0)=\boldsymbol{0}$ for any perturbation. We also impose the terminal condition $\boldsymbol{a}(t_\mathrm{f})=\boldsymbol{0}$ for the adjoint. Hence, an integration by parts in time reveals

$$-\int_0^{t_\mathrm{f}}\boldsymbol{a}(t)\cdot\delta\dot{\boldsymbol{c}}dt=\int_0^{t_\mathrm{f}}\dot{\boldsymbol{a}}(t)\cdot\delta\boldsymbol{c}dt+\left[\boldsymbol{a}\cdot\delta\boldsymbol{c}\right]_0^{t_\mathrm{f}}=\int_0^{t_\mathrm{f}}\dot{\boldsymbol{a}}(t)\cdot\delta\boldsymbol{c}dt.$$

Thus, we obtain

$$\begin{aligned}\delta_{\boldsymbol{c}}\mathcal{L}\left[\boldsymbol{\Psi},\boldsymbol{c},u,\boldsymbol{h},\boldsymbol{\Theta},\boldsymbol{a}\right](\delta\boldsymbol{c}) &= \int_0^{t_\mathrm{f}}\dot{\boldsymbol{a}}(t)\cdot\delta\boldsymbol{c}dt-\int_0^{t_\mathrm{f}}\sum_{i=1}^{d}(\delta\boldsymbol{c}(t)\cdot\boldsymbol{e}_i)\cdot\left[\int_{\Omega(t)}\boldsymbol{\sigma}(\boldsymbol{w},q):\left[\nabla(\mathcal{G}\boldsymbol{e}_i)\right]d\boldsymbol{x}\right]dt\\ &\quad -\int_0^{t_\mathrm{f}}\delta\boldsymbol{c}\cdot\int_{\Omega(t)}S_1\nabla\zeta+S_0\zeta\,d\boldsymbol{x}dt.\end{aligned}$$

Setting this to zero, for all $\delta\boldsymbol{c}$, we get the backward in time ODE in (75), with the terminal condition $\boldsymbol{a}(t_\mathrm{f})=\boldsymbol{0}$.

Now, we perturb $\mathcal{L}$ with respect to u, which involves similar calculations as above. First, note that perturbing u with δu induces a perturbation of $\Omega(t)$ through (3). The induced perturbation is

$$\boldsymbol{V}(t,\boldsymbol{x};\delta u)=R_0\delta u(t,\boldsymbol{x}-\boldsymbol{c})\frac{\boldsymbol{x}-\boldsymbol{c}}{|\boldsymbol{x}-\boldsymbol{c}|}\zeta, \tag{70}$$

where δu satisfies the same properties as in (4). Whence, as in (68), we have, also using (65),

$$\begin{aligned}\delta_u J_{\mathrm{St}}\left[\boldsymbol{\Psi},\boldsymbol{c},\boldsymbol{\Theta},u,\boldsymbol{h}\right](\delta u) &= \int_0^{t_\mathrm{f}}\delta_{\Omega(t)}\mathcal{Q}\left[t,\boldsymbol{\Psi},\boldsymbol{c},\boldsymbol{\Theta}\right](\boldsymbol{V}(t,\cdot;\delta u))dt+\int_0^{t_\mathrm{f}}\delta_u\overline{\mathcal{Q}}\left[t,\boldsymbol{\beta}\right](\delta u)dt\\ &= \int_0^{t_\mathrm{f}}\int_{\Omega(t)} S_1:\nabla\boldsymbol{V}(t,\boldsymbol{x};\delta u)+S_0\cdot\boldsymbol{V}(t,\boldsymbol{x};\delta u)\,d\boldsymbol{x}dt\\ &\quad +\int_0^{t_\mathrm{f}}\int_{\Omega(t)}\boldsymbol{\sigma}(\boldsymbol{w},q):\nabla\boldsymbol{\beta}(t,\boldsymbol{x};\delta u,\boldsymbol{c})\,d\boldsymbol{x}dt.\end{aligned} \tag{71}$$

Then, the perturbation of the Lagrangian is

$$\begin{aligned}\delta_u\mathcal{L}\left[\boldsymbol{\Psi},\boldsymbol{c},u,\boldsymbol{h},\boldsymbol{\Theta},\boldsymbol{a}\right](\delta u) &= \delta_u J\left[\boldsymbol{\Psi},u,\boldsymbol{h}\right](\delta u)-\delta_u J_{\mathrm{St}}\left[\boldsymbol{\Psi},\boldsymbol{c},\boldsymbol{\Theta},u,\boldsymbol{h}\right](\delta u)\\ &= \frac{\lambda_u}{t_\mathrm{f}}\left(u,\delta u\right)_{\mathcal{A}_u}+\frac{\lambda_\ell}{t_\mathrm{f}}\int_0^{t_\mathrm{f}}\int_{-\pi}^{\pi}\mathcal{I}_M\left(\ell'(u(t,\theta))\delta u(t,\theta)\right)d\theta dt\\ &\quad +\frac{1}{t_\mathrm{f}\epsilon_u}\left(\int_0^{t_\mathrm{f}}\int_{-\pi}^{\pi}\left(\partial_t u(t,\theta)\right)^2 d\theta dt-E_0\,d\theta dt\right)\int_0^{t_\mathrm{f}}\int_{-\pi}^{\pi}\partial_t u(t,\theta)\partial_t\delta u(t,\theta)d\theta dt\\ &\quad -\int_0^{t_\mathrm{f}}\int_{\Omega(t)}\boldsymbol{\sigma}(\boldsymbol{w},q):\nabla\boldsymbol{\beta}(t,\boldsymbol{x};\delta u,\boldsymbol{c})\,d\boldsymbol{x}dt\\ &\quad -\int_0^{t_\mathrm{f}}\int_{\Omega(t)}S_1:\nabla\boldsymbol{V}(t,\boldsymbol{x};\delta u)+S_0\cdot\boldsymbol{V}(t,\boldsymbol{x};\delta u)\,d\boldsymbol{x}dt.\end{aligned} \tag{72}$$

Finally, perturbing $\mathcal{L}$ with respect to the force control $\boldsymbol{h}$ gives

$$\begin{aligned}\delta_{\boldsymbol{h}}\mathcal{L}\left[\boldsymbol{\Psi},\boldsymbol{c},u,\boldsymbol{h},\boldsymbol{\Theta},\boldsymbol{a}\right](\delta\boldsymbol{h}) &= \delta_{\boldsymbol{h}}J\left[\boldsymbol{\Psi},u,\boldsymbol{h}\right](\delta\boldsymbol{h}) + \int_0^{t_\mathrm{f}} \left(\boldsymbol{\Theta}_2(t),\delta\boldsymbol{h}(t)\right)_{\mathbb{R}^n} dt \\ &= \int_0^{t_\mathrm{f}} \left(\frac{\lambda_{\boldsymbol{h}}}{t_\mathrm{f}}\boldsymbol{h}(t) + \boldsymbol{\Theta}_2(t)\right)\cdot\delta\boldsymbol{h}(t)\,dt,\end{aligned} \tag{73}$$

where $\boldsymbol{\Theta}_2(t) \equiv \boldsymbol{r}(t)$.

Let us write the adjoint system more explicitly. Let $\boldsymbol{\Theta}(t) \equiv (\tilde{\boldsymbol{w}}(t),\boldsymbol{r}(t),q(t))$ be the adjoint. In view of (66), (67), marching backward in time, for each $t \in (0,t_\mathrm{f})$, we seek to find $(\tilde{\boldsymbol{w}}(t),\boldsymbol{r}(t),q(t)) \in \mathcal{W}^t$ such that

$$S^t\left((\tilde{\boldsymbol{w}}(t),\boldsymbol{r}(t),q(t)),(\tilde{\boldsymbol{y}},\boldsymbol{j},z)\right) = \frac{1}{t_\mathrm{f}}\left(-\boldsymbol{e}_0,\boldsymbol{j}\right)_{\mathbb{R}^n} + \left(\boldsymbol{a}(t),\boldsymbol{j}\right)_{\mathbb{R}^n},\ \forall\,(\tilde{\boldsymbol{y}},\boldsymbol{j},z) \in \mathcal{W}^t, \tag{74}$$

while solving the following backward in time ODE for $t \in [0,t_\mathrm{f})$:

$$\begin{aligned}&\boldsymbol{\Upsilon}(t) := \int_{\Omega(t)} \left[\boldsymbol{\sigma}(\boldsymbol{w},q) : [\nabla(\mathcal{G}\boldsymbol{e}_1)], \boldsymbol{\sigma}(\boldsymbol{w},q) : [\nabla(\mathcal{G}\boldsymbol{e}_2)]\right]^{\mathsf{T}} d\boldsymbol{x} + \int_{\Omega(t)} S_1\nabla\zeta + S_0\zeta\,d\boldsymbol{x}, \\ &\dot{\boldsymbol{a}}(t) = \boldsymbol{\Upsilon}(t), \qquad \boldsymbol{a}(t_\mathrm{f}) = \boldsymbol{0},\end{aligned} \tag{75}$$

with $\boldsymbol{v} = \tilde{\boldsymbol{v}} + \boldsymbol{\beta} + \boldsymbol{s}(t)\zeta$ and $\boldsymbol{w} = \tilde{\boldsymbol{w}} + \boldsymbol{r}(t)\zeta$. Note that on the right-hand side of (74), $\frac{1}{t_\mathrm{f}}\left(-\boldsymbol{e}_0,\boldsymbol{j}\right)_{\mathbb{R}^n}$ is the usual source term in the adjoint equation that comes from the derivative of the integrand in the cost function J, while the term $\left(\boldsymbol{a}(t),\boldsymbol{j}\right)_{\mathbb{R}^n}$ is due to the implicit dependence of $\Omega(t)$ on the controls u, $\boldsymbol{h}$. Observe also that (75) is a bulk formulation, but alternatively one could also write a boundary formulation for (75), using (69) instead of (68).

Finally, we also provide the strong form corresponding to the variational formulation (74). Taking the test function $\boldsymbol{j} = \boldsymbol{0}$ and integrating by parts, we obtain the following system of equations for $\boldsymbol{w}$ and q:

$$\begin{aligned}&-\nabla\cdot\boldsymbol{\sigma}(\boldsymbol{w},q) = \boldsymbol{0}, \qquad \nabla\cdot\boldsymbol{w} = 0,\ \text{in}\ \Omega(t), \\ &\qquad \boldsymbol{w} = \boldsymbol{0},\ \text{on}\ \Gamma_\mathrm{D}, \quad \boldsymbol{w} = \boldsymbol{r}(t),\ \text{on}\ \Gamma(t), \quad \boldsymbol{\sigma}(\boldsymbol{w},q)\boldsymbol{\nu} = \boldsymbol{0},\ \text{on}\ \Gamma_\mathrm{in},\end{aligned} \tag{76}$$

$$\boldsymbol{\sigma}(\boldsymbol{w},q) := -q\boldsymbol{I} + 2\boldsymbol{\varepsilon}(\nabla\boldsymbol{w}), \quad \boldsymbol{\varepsilon}(\nabla\boldsymbol{w}) := \frac{\nabla\boldsymbol{w} + (\nabla\boldsymbol{w})^{\mathsf{T}}}{2}. \tag{77}$$

Next, taking the test functions $\tilde{\boldsymbol{y}} \equiv \boldsymbol{0}$ and $z \equiv 0$ in (74), using also the definitions (19),(30), we obtain

$$\int_{\Omega(t)} 2\boldsymbol{\varepsilon}(\nabla(\boldsymbol{j}\zeta)) : \boldsymbol{\varepsilon}(\nabla\boldsymbol{w}) - q\nabla\cdot(\boldsymbol{j}\zeta) = \frac{1}{t_\mathrm{f}}\left(-\boldsymbol{e}_0,\boldsymbol{j}\right)_{\mathbb{R}^n} + \left(\boldsymbol{a}(t),\boldsymbol{j}\right)_{\mathbb{R}^n} \quad \forall\boldsymbol{j} \in \mathbb{R}^n.$$

We can rewrite it as

$$\boldsymbol{j}\cdot\int_{\Omega(t)} 2\boldsymbol{\varepsilon}(\nabla\boldsymbol{w})\nabla\zeta - q\nabla\zeta = \frac{1}{t_\mathrm{f}}\left(-\boldsymbol{e}_0,\boldsymbol{j}\right)_{\mathbb{R}^n} + \left(\boldsymbol{a}(t),\boldsymbol{j}\right)_{\mathbb{R}^n} \quad \forall\boldsymbol{j} \in \mathbb{R}^n,$$

or equivalently

$$\int_{\Omega(t)} \boldsymbol{\sigma}(\boldsymbol{w},q)\nabla\zeta = -\frac{\boldsymbol{e}_0}{t_\mathrm{f}} + \boldsymbol{a}(t). \tag{78}$$

Alternatively, using an integration by parts and $\zeta = 0$ on Γ_{D}, $\zeta = 1$ on $\Gamma(t)$, one can also write this integral equation as follows:

$$\begin{aligned}\int_{\Omega(t)} 2\boldsymbol{\varepsilon}(\nabla(\boldsymbol{j}\zeta)) : \boldsymbol{\varepsilon}(\nabla \boldsymbol{w}) - q\nabla\cdot(\boldsymbol{j}\zeta) &= \int_{\Omega(t)} \boldsymbol{\sigma}(\boldsymbol{w},q) : \nabla(\boldsymbol{j}\zeta) \\ &= \int_{\Omega(t)} \underbrace{-\nabla\cdot\boldsymbol{\sigma}(\boldsymbol{w},q)}_{=0}\cdot(\boldsymbol{j}\zeta) + \int_{\partial\Omega(t)} \boldsymbol{\sigma}(\boldsymbol{w},q)\boldsymbol{\nu}\cdot(\boldsymbol{j}\zeta) \\ &= \int_{\Gamma_{\mathrm{in}}} \underbrace{\boldsymbol{\sigma}(\boldsymbol{w},q)\boldsymbol{\nu}}_{=0}\cdot(\boldsymbol{j}\zeta) + \int_{\Gamma_{\mathrm{D}}} \boldsymbol{\sigma}(\boldsymbol{w},q)\boldsymbol{\nu}\cdot(\boldsymbol{j}\zeta) + \boldsymbol{j}\cdot\int_{\Gamma(t)} \boldsymbol{\sigma}(\boldsymbol{w},q)\boldsymbol{\nu}\end{aligned}$$

which yields

$$\int_{\Gamma(t)} \boldsymbol{\sigma}(\boldsymbol{w},q)\boldsymbol{\nu} = -\frac{\boldsymbol{e}_0}{t_{\mathrm{f}}} + \boldsymbol{a}(t). \tag{79}$$

Note that (79) is analogous to the integral equation (9) for the forward state. Since $\boldsymbol{w} = \tilde{\boldsymbol{w}} + \boldsymbol{r}(t)\zeta$, (76),(79) is the strong form of the PDE system for the adjoint variables $(\tilde{\boldsymbol{w}}, \boldsymbol{r}, q)$.

5 Unfitted finite element method for the forward problem

Several numerical schemes have been developed for fluid-structure interaction problems. For instance, a conforming mesh approach can be quite accurate for direct simulation [41, 17], but is less convenient for shape optimization because of inconsistent gradients. In addition, for large deformations that are unknown a priori, remeshing is needed which can present additional difficulties.

Another approach to fluid-structure interaction is the immersed boundary method (IBM) [53, 5, 6, 27], which has been shown to be quite effective, even with large deformations of the structure. Nonetheless, there can be numerical artifacts at the boundary that can lead to a loss of accuracy in computing boundary stresses. These artifacts can be alleviated by filtering/smoothing strategies, as well as adaptive mesh refinement [42, 26].

We also want to mention level-set methods (outside of the unfitted FEM context), which are quite popular [52, 58, 22, 60, 47, 68, 67, 69, 70, 72, 29, 30, 64]. In particular, there are level-set methods for fluid-structure interaction [13, 14] and structural optimization [71, 3]. Another potential option is phase field methods [76, 66, 25], but these models include an additional equation for the phase variable which results in a more complicated PDE system.

For the discretization of the modified Stokes problem, we employ an unfitted finite element method which has the advantage of easy handling of complex geometric motions [9, 40]. However, this approach requires introducing stabilization terms into both the state and adjoint Stokes systems to deal with "cut" elements [8]. We then show the consistency and stability of our discrete scheme, and describe the time discretization for the forward and adjoint problems.

5.1 Discretization

Let $\widehat{\mathcal{T}}_h$ be a conforming shape regular mesh of $\mathfrak{D}$ (the tank) and let $B_h \subset W^{1,\infty}(\mathfrak{D})$, $W_h \subset [H^1(\mathfrak{D})]^n$ be continuous, degree 2, Lagrange, finite element spaces. Similarly, let $Q_h \subset L^2(\mathfrak{D})$ be a continuous, degree 1, Lagrange, finite element space (i.e. the Taylor-Hood space for the velocity). We approximate the fluid domain by $\Omega_h(t) = \Omega_h(\phi_h(t,\cdot))$ with a level set function $\phi_h(t,\cdot) \in B_h$ that approximates the signed distance function of $\Gamma(t)$ that is easily computed from $u(t,\cdot)$, $\boldsymbol{c}(t)$ (i.e. $\Gamma_h(t) = \{\phi_h(t,\cdot) = 0\}$).

We follow [10, 28, 38, 73] in posing an unfitted FEM for the modified Stokes problem; see also [48, 32]. We take a finite element subspace $\mathring{W}_h \subset W_h$, where $\boldsymbol{v} \in \mathring{W}_h$ satisfies $\boldsymbol{v}|_{\Gamma_\mathrm{D}} = \boldsymbol{0}$ (where $\Gamma_\mathrm{D} \subset \partial\mathfrak{D}$). Next, let $\mathfrak{D}_{h,\delta}(t) \subset \mathfrak{D}$ be a domain consisting of all elements $T \in \widehat{\mathcal{T}}_h$ that are within δ of $\Omega_h(t)$, for some small $\delta > 0$. This gives the restricted finite element space: $V_h^t = \mathring{W}_h|_{\mathfrak{D}_{h,\delta}(t)}$. Furthermore, let $\mathcal{F}_\delta^t$ be the set of mesh *facets* that are within δ of $\partial\Omega_h(t)$.

We recall the standard forms for the Stokes problem in (18) and the standard Nitsche bilinear form for zero velocity boundary conditions on $\Gamma_h(t)$ is given by

$$N_h(\boldsymbol{w},\boldsymbol{v}) := -\left(2\boldsymbol{\varepsilon}(\nabla\boldsymbol{w})\boldsymbol{\nu},\boldsymbol{v}\right)_{\Gamma_h(t)} - \left(2\boldsymbol{\varepsilon}(\nabla\boldsymbol{v})\boldsymbol{\nu},\boldsymbol{w}\right)_{\Gamma_h(t)} + \frac{\gamma_\mathrm{D}}{h}\left(\boldsymbol{w},\boldsymbol{v}\right)_{\Gamma_h(t)}, \ \gamma_\mathrm{D} > 0, \tag{80}$$

In order to account for the coupled body motion, we define the following discrete bilinear and linear forms

$$\begin{aligned} a_h^t((\tilde{\boldsymbol{w}},\boldsymbol{r}),(\tilde{\boldsymbol{v}},\boldsymbol{s})) &:= a^t(\tilde{\boldsymbol{w}}+\boldsymbol{r}\zeta,\tilde{\boldsymbol{v}}+\boldsymbol{s}\zeta) + \frac{\gamma_\mathrm{vel}}{h^2}s_h\left(\mathcal{F}_\delta^t;\tilde{\boldsymbol{w}},\tilde{\boldsymbol{v}}\right) + N_h(\tilde{\boldsymbol{w}},\tilde{\boldsymbol{v}}) \\ b_h^t(q,(\tilde{\boldsymbol{w}},\boldsymbol{r})) &:= b^t(q,\tilde{\boldsymbol{w}}+\boldsymbol{r}\zeta) + (\tilde{\boldsymbol{w}}\cdot\boldsymbol{\nu},q)_{\Gamma_h(t)}, \end{aligned} \tag{81}$$

where we have introduced the facet stabilization term $s_h\left(\mathcal{F}_\delta^t;\tilde{\boldsymbol{w}},\tilde{\boldsymbol{v}}\right)$ [40, Sec. 4.3] with constant $\gamma_\mathrm{vel} > 0$.

Next, we define the big bilinear form for the modified Stokes problem, i.e.,

$$S_h^t((\tilde{\boldsymbol{w}},\boldsymbol{r},q),(\tilde{\boldsymbol{v}},\boldsymbol{s},p)) := a_h^t((\tilde{\boldsymbol{w}},\boldsymbol{r}),(\tilde{\boldsymbol{v}},\boldsymbol{s})) + b_h^t(q,(\tilde{\boldsymbol{v}},\boldsymbol{s})) + b_h^t(p,(\tilde{\boldsymbol{w}},\boldsymbol{r})) - \gamma_\mathrm{p}s_h\left(\mathcal{F}_\delta^t;q,p\right), \tag{82}$$

where we have introduced the facet stabilization term $s_h\left(\mathcal{F}_\delta^t;q,p\right)$ with constant $\gamma_\mathrm{p} > 0$; this is needed to ensure an inf-sup condition for the pressure. The augmented linear form is given by

$$F_h^t(\tilde{\boldsymbol{w}},\boldsymbol{r},q) := (\tilde{\boldsymbol{w}}+\boldsymbol{r}\zeta,\boldsymbol{f})_{\Omega_h(t)} + \boldsymbol{r}\cdot\boldsymbol{h} - a^t(\tilde{\boldsymbol{w}}+\boldsymbol{r}\zeta,\boldsymbol{\beta}) - b^t(q,\boldsymbol{\beta}) + (\tilde{\boldsymbol{w}},2\boldsymbol{\varepsilon}(\nabla\boldsymbol{\beta})\boldsymbol{\nu})_{\Gamma_h(t)}. \tag{83}$$

Thus, the unfitted method is as follows. Given the initial center position $\boldsymbol{c}_h(0) = \boldsymbol{c}_0$, for all $t \in [0,t_\mathrm{f}]$, we seek to find $\tilde{\boldsymbol{v}}_h(t,\cdot) \in V_h^t$, $\boldsymbol{s}_h(t) \in \mathbb{R}^n$, and $p_h(t,\cdot) \in Q_h^t$ such that

$$S_h^t((\tilde{\boldsymbol{w}}_h,\boldsymbol{r}_h,q_h),(\tilde{\boldsymbol{v}}_h,\boldsymbol{s}_h,p_h)) = F_h^t(\tilde{\boldsymbol{w}}_h,\boldsymbol{r}_h,q_h), \quad \dot{\boldsymbol{c}}_h = \boldsymbol{s}_h, \tag{84}$$

for all $\tilde{\boldsymbol{w}}_h \in V_h^t$, $\boldsymbol{r}_h \in \mathbb{R}^n$, $q_h \in Q_h^t$. Note that we will take an interpolant of $\boldsymbol{\beta}$.

5.2 Consistency

We ignore the geometric approximation of the domain, i.e., we replace Ω_h, Γ_h by Ω, Γ. Note that the geometric error can be estimated through the usual arguments.

To check consistency, we replace $(\tilde{\boldsymbol{v}}_h,\boldsymbol{s}_h,p_h)$ in (84) by the exact solution $(\tilde{\boldsymbol{v}},\boldsymbol{s},p)$ of (1) and (9) (note that $\boldsymbol{s} \equiv \dot{\boldsymbol{c}}$). Note that $\boldsymbol{v} = \tilde{\boldsymbol{v}} + \boldsymbol{s}\zeta + \boldsymbol{\beta}$. Thus, (84) becomes

$$S_h^t((\tilde{\boldsymbol{w}}_h,\boldsymbol{r}_h,q_h),(\tilde{\boldsymbol{v}},\boldsymbol{s},p)) = F_h^t(\tilde{\boldsymbol{w}}_h,\boldsymbol{r}_h,q_h), \text{ for all } \tilde{\boldsymbol{w}}_h \in V_h^t,\ \boldsymbol{r}_h \in \mathbb{R}^n,\ q_h \in Q_h^t. \tag{85}$$

Rewriting this more explicitly, we have

$$\begin{aligned} a_h^t((\tilde{\boldsymbol{w}}_h,\boldsymbol{r}_h),(\tilde{\boldsymbol{v}},\boldsymbol{s})) + b_h^t(q_h,(\tilde{\boldsymbol{v}},\boldsymbol{s})) + b_h^t(p,(\tilde{\boldsymbol{w}}_h,\boldsymbol{r}_h)) - \gamma_\mathrm{p}s_h\left(\mathcal{F}_\delta^t;q_h,p\right) \\ = (\tilde{\boldsymbol{w}}_h+\boldsymbol{r}_h\zeta,\boldsymbol{f})_{\Omega(t)} + \boldsymbol{r}_h\cdot\boldsymbol{h} - a^t(\tilde{\boldsymbol{w}}_h+\boldsymbol{r}_h\zeta,\boldsymbol{\beta}) - b^t(q_h,\boldsymbol{\beta}) \\ + (\tilde{\boldsymbol{w}}_h,2\boldsymbol{\varepsilon}(\nabla\boldsymbol{\beta})\boldsymbol{\nu})_{\Gamma(t)}, \end{aligned} \tag{86}$$

where we note that both stabilization terms vanish because we assume that the exact solution satisfies $\tilde{\boldsymbol{v}} \in H^2(\Omega)$ and $p \in H^1(\Omega)$, i.e. the jump terms vanish. Then, using (18), we get

$$\begin{aligned}
&(\boldsymbol{\varepsilon}(\nabla(\tilde{\boldsymbol{w}}_h + \boldsymbol{r}_h\zeta)), 2\boldsymbol{\varepsilon}(\nabla(\tilde{\boldsymbol{v}} + \boldsymbol{s}\zeta)))_\Omega - (2\boldsymbol{\varepsilon}(\nabla\tilde{\boldsymbol{w}}_h)\boldsymbol{\nu}, \tilde{\boldsymbol{v}})_{\Gamma(t)} - (2\boldsymbol{\varepsilon}(\nabla\tilde{\boldsymbol{v}})\boldsymbol{\nu}, \tilde{\boldsymbol{w}}_h)_{\Gamma(t)} \\
&+\frac{\gamma_{\mathrm{D}}}{h}(\tilde{\boldsymbol{w}}_h, \tilde{\boldsymbol{v}})_{\Gamma(t)} - (\nabla\cdot(\tilde{\boldsymbol{v}} + \boldsymbol{s}\zeta), q_h)_\Omega + (\tilde{\boldsymbol{v}}\cdot\boldsymbol{\nu}, q_h)_{\Gamma(t)} - (\nabla\cdot(\tilde{\boldsymbol{w}}_h + \boldsymbol{r}_h\zeta), p)_\Omega + (\tilde{\boldsymbol{w}}_h\cdot\boldsymbol{\nu}, p)_{\Gamma(t)} \\
&\qquad = (\tilde{\boldsymbol{w}}_h + \boldsymbol{r}_h\zeta, \boldsymbol{f})_{\Omega(t)} + \boldsymbol{r}_h\cdot\boldsymbol{h}(t) - (\boldsymbol{\varepsilon}(\nabla(\tilde{\boldsymbol{w}}_h + \boldsymbol{r}_h\zeta)), 2\boldsymbol{\varepsilon}(\nabla\boldsymbol{\beta}))_\Omega \\
&\qquad\qquad + (\nabla\cdot\boldsymbol{\beta}, q_h)_\Omega + (\tilde{\boldsymbol{w}}_h, 2\boldsymbol{\varepsilon}(\nabla\boldsymbol{\beta})\boldsymbol{\nu})_{\Gamma(t)},
\end{aligned} \tag{87}$$

where we plugged in (80). Note that $\tilde{\boldsymbol{v}} = \boldsymbol{0}$ on Γ_h. Thus, after moving some terms around, we obtain

$$\begin{aligned}
&(\nabla(\tilde{\boldsymbol{w}}_h + \boldsymbol{r}_h\zeta), \boldsymbol{\sigma}(\boldsymbol{v}, p))_\Omega - (2\boldsymbol{\varepsilon}(\nabla(\tilde{\boldsymbol{v}} + \boldsymbol{s}\zeta))\boldsymbol{\nu}, \tilde{\boldsymbol{w}}_h)_{\Gamma(t)} - (\nabla\cdot\boldsymbol{v}, q_h)_\Omega + (\tilde{\boldsymbol{w}}_h\cdot\boldsymbol{\nu}, p)_{\Gamma(t)} \\
&\qquad = (\tilde{\boldsymbol{w}}_h + \boldsymbol{r}_h\zeta, \boldsymbol{f})_{\Omega(t)} + \boldsymbol{r}_h\cdot\boldsymbol{h}(t) + (\tilde{\boldsymbol{w}}_h, 2\boldsymbol{\varepsilon}(\nabla\boldsymbol{\beta})\boldsymbol{\nu})_{\Gamma(t)},
\end{aligned} \tag{88}$$

where we also used (2). Again, using (2), and $\nabla\cdot\boldsymbol{v} = 0$, we get

$$(\nabla(\tilde{\boldsymbol{w}}_h + \boldsymbol{r}_h\zeta), \boldsymbol{\sigma}(\boldsymbol{v}, p))_\Omega - (\boldsymbol{\sigma}(\boldsymbol{v}, p)\boldsymbol{\nu}, \tilde{\boldsymbol{w}}_h)_{\Gamma(t)} = (\tilde{\boldsymbol{w}}_h + \boldsymbol{r}_h\zeta, \boldsymbol{f})_{\Omega(t)} + \boldsymbol{r}_h\cdot\boldsymbol{h}(t). \tag{89}$$

Now, integrate by parts on the first term, and use that $\tilde{\boldsymbol{w}}_h = \boldsymbol{0}$, $\zeta = 0$ on Γ_{D} and $\boldsymbol{\sigma}(\boldsymbol{v}, p)\boldsymbol{\nu} = \boldsymbol{0}$, on Γ_{in}, to get

$$\left(\tilde{\boldsymbol{w}}_h + \boldsymbol{r}_h\zeta, -\nabla\cdot\boldsymbol{\sigma}(\boldsymbol{v}, p) - \boldsymbol{f}^{\mathsf{T}}\right)_{\Omega(t)} + (\tilde{\boldsymbol{w}}_h + \boldsymbol{r}_h, \boldsymbol{\sigma}(\boldsymbol{v}, p)\boldsymbol{\nu})_{\Gamma(t)} - (\boldsymbol{\sigma}(\boldsymbol{v}, p)\boldsymbol{\nu}, \tilde{\boldsymbol{w}}_h)_{\Gamma(t)} = \boldsymbol{r}_h\cdot\boldsymbol{h}(t). \tag{90}$$

From (1), $-\nabla\cdot\boldsymbol{\sigma} = \boldsymbol{f}^{\mathsf{T}}$, so

$$\boldsymbol{r}_h\cdot(\boldsymbol{\sigma}(\boldsymbol{v}, p)\boldsymbol{\nu}, 1)_{\Gamma(t)} = \boldsymbol{r}_h\cdot\boldsymbol{h}(t), \tag{91}$$

which is obviously satisfied because (9) states that $(\boldsymbol{\sigma}(\boldsymbol{v}, p)\boldsymbol{\nu}, 1)_{\Gamma(t)} = \boldsymbol{h}(t)$. So, everything vanishes and the scheme is consistent.

5.3 Stability

The main thing is to check coercivity of the first line in (81). Recall

$$\begin{aligned}
a_h^t\left((\tilde{\boldsymbol{w}}, \boldsymbol{r}), (\tilde{\boldsymbol{v}}, \boldsymbol{s})\right) &:= a^t\left(\tilde{\boldsymbol{w}} + \boldsymbol{r}\zeta, \tilde{\boldsymbol{v}} + \boldsymbol{s}\zeta\right) + \frac{\gamma_{\mathrm{vel}}}{h^2}s_h\left(\mathcal{F}_\delta^t; \tilde{\boldsymbol{w}}, \tilde{\boldsymbol{v}}\right) \\
&\quad - (2\boldsymbol{\varepsilon}(\nabla\tilde{\boldsymbol{w}})\boldsymbol{\nu}, \tilde{\boldsymbol{v}})_{\Gamma_h(t)} - (2\boldsymbol{\varepsilon}(\nabla\tilde{\boldsymbol{v}})\boldsymbol{\nu}, \tilde{\boldsymbol{w}})_{\Gamma_h(t)} + \frac{\gamma_{\mathrm{D}}}{h}(\tilde{\boldsymbol{w}}, \tilde{\boldsymbol{v}})_{\Gamma_h(t)}.
\end{aligned} \tag{92}$$

Let us concentrate on one term. Using Korn's inequality, we have

$$\begin{aligned}
a^t(\tilde{\boldsymbol{w}} + \boldsymbol{r}\zeta, \tilde{\boldsymbol{w}} + \boldsymbol{r}\zeta) &= 2\|\boldsymbol{\varepsilon}(\nabla(\tilde{\boldsymbol{w}} + \boldsymbol{r}\zeta))\|_{L^2(\Omega_h)}^2 \geq C_0\|\nabla(\tilde{\boldsymbol{w}} + \boldsymbol{r}\zeta)\|_{L^2(\Omega_h)}^2 \\
&\geq C_1\|\tilde{\boldsymbol{w}} + \boldsymbol{r}\zeta\|_{H^1(\Omega_h)}^2,
\end{aligned} \tag{93}$$

because $\tilde{\boldsymbol{w}} = \boldsymbol{0}$ and $\zeta = 0$ on Γ_{D}. We now claim that

$$\|\tilde{\boldsymbol{w}} + \boldsymbol{r}\zeta\|_{H^1(\Omega_h)}^2 + \|\tilde{\boldsymbol{w}}\|_{L^2(\Gamma_h)}^2 \approx \|\tilde{\boldsymbol{w}}\|_{H^1(\Omega_h)}^2 + |\boldsymbol{r}|^2, \text{ for all } \tilde{\boldsymbol{w}} \in H_D^1(\Omega_h),\ \boldsymbol{r} \in \mathbb{R}^n. \tag{94}$$

This follows from a compactness argument, which is proved by noting that $\|\tilde{\boldsymbol{w}} + \boldsymbol{r}\zeta\|_{H^1(\Omega_h)}^2 + \|\tilde{\boldsymbol{w}}\|_{L^2(\Gamma_h)}^2 = 0$ implies that $\tilde{\boldsymbol{w}} = -\boldsymbol{r}\zeta$ in Ω_h. However, $\tilde{\boldsymbol{w}} = \boldsymbol{0}$ on Γ_h which means that $\boldsymbol{r} = \boldsymbol{0}$. Ergo, $\tilde{\boldsymbol{w}} = \boldsymbol{0}$ on Ω_h.

Returning to (92) and using (94), we have

$$\begin{aligned} a_h^t\left((\tilde{\boldsymbol{w}},\boldsymbol{r}),(\tilde{\boldsymbol{w}},\boldsymbol{r})\right) &\geq C_1\|\tilde{\boldsymbol{w}}+\boldsymbol{r}\zeta\|^2_{H^1(\Omega_h)}+\|\tilde{\boldsymbol{w}}\|^2_{L^2(\Gamma_h)}-4\left(\boldsymbol{\varepsilon}(\nabla\tilde{\boldsymbol{w}})\boldsymbol{\nu},\tilde{\boldsymbol{w}}\right)_{\Gamma_h}+\left(\frac{\gamma_{\mathrm{D}}}{h}-1\right)\|\tilde{\boldsymbol{w}}\|^2_{L^2(\Gamma_h)}\\ &\quad+\frac{\gamma_{\mathrm{vel}}}{h^2}s_h\left(\mathcal{F}_\delta^t;\tilde{\boldsymbol{w}},\tilde{\boldsymbol{w}}\right)\\ &\geq C_2\|\tilde{\boldsymbol{w}}\|^2_{H^1(\Omega_h)}-4\left(\boldsymbol{\varepsilon}(\nabla\tilde{\boldsymbol{w}})\boldsymbol{\nu},\tilde{\boldsymbol{w}}\right)_{\Gamma_h}+\left(\frac{\gamma_{\mathrm{D}}}{h}-1\right)\|\tilde{\boldsymbol{w}}\|^2_{L^2(\Gamma_h)}\\ &\quad+C_2|\boldsymbol{r}|^2+\frac{\gamma_{\mathrm{vel}}}{h^2}s_h\left(\mathcal{F}_\delta^t;\tilde{\boldsymbol{w}},\tilde{\boldsymbol{w}}\right). \end{aligned} \tag{95}$$

Recall that $\tilde{\boldsymbol{w}}$ is a discrete function here. Now, apply a weighted Cauchy inequality to the non-symmetric term, i.e.,

$$\left(\boldsymbol{\varepsilon}(\nabla\tilde{\boldsymbol{w}})\boldsymbol{\nu},\tilde{\boldsymbol{w}}\right)_{\Gamma_h}\leq\|\nabla\tilde{\boldsymbol{w}}\|_{L^2(\Gamma_h)}\|\tilde{\boldsymbol{w}}\|_{L^2(\Gamma_h)}\leq\frac{h}{2a_0}\|\nabla\tilde{\boldsymbol{w}}\|^2_{L^2(\Gamma_h)}+\frac{a_0}{2h}\|\tilde{\boldsymbol{w}}\|^2_{L^2(\Gamma_h)},$$

for some constant $a_0>0$ to be chosen. Then,

$$\begin{aligned} a_h^t\left((\tilde{\boldsymbol{w}},\boldsymbol{r}),(\tilde{\boldsymbol{w}},\boldsymbol{r})\right) &\geq C_2\|\nabla\tilde{\boldsymbol{w}}\|^2_{L^2(\Omega_h)}-\frac{2}{a_0}h\|\nabla\tilde{\boldsymbol{w}}\|^2_{L^2(\Gamma_h)}+\left(\frac{\gamma_{\mathrm{D}}-2a_0}{h}-1\right)\|\tilde{\boldsymbol{w}}\|^2_{L^2(\Gamma_h)}\\ &\quad+C_2\|\tilde{\boldsymbol{w}}\|^2_{L^2(\Omega_h)}+C_2|\boldsymbol{r}|^2+\frac{\gamma_{\mathrm{vel}}}{h^2}s_h\left(\mathcal{F}_\delta^t;\tilde{\boldsymbol{w}},\tilde{\boldsymbol{w}}\right). \end{aligned} \tag{96}$$

We recall an inverse trace estimate for finite element functions:

$$h\|\nabla\tilde{\boldsymbol{w}}\|^2_{L^2(\Gamma_h)}\leq C_3\|\nabla\tilde{\boldsymbol{w}}\|^2_{L^2(\Omega_h)}.$$

This gives

$$\begin{aligned} a_h^t\left((\tilde{\boldsymbol{w}},\boldsymbol{r}),(\tilde{\boldsymbol{w}},\boldsymbol{r})\right) &\geq\left(C_2-\frac{2C_3}{a_0}\right)\|\nabla\tilde{\boldsymbol{w}}\|^2_{L^2(\Omega_h)}+\left(\frac{\gamma_{\mathrm{D}}-2a_0}{h}-1\right)\|\tilde{\boldsymbol{w}}\|^2_{L^2(\Gamma_h)}\\ &\quad+C_2\|\tilde{\boldsymbol{w}}\|^2_{L^2(\Omega_h)}+C_2|\boldsymbol{r}|^2+\frac{\gamma_{\mathrm{vel}}}{h^2}s_h\left(\mathcal{F}_\delta^t;\tilde{\boldsymbol{w}},\tilde{\boldsymbol{w}}\right). \end{aligned} \tag{97}$$

Now, choose $a_0=3C_3/C_2$ and choose $\gamma_{\mathrm{D}}=3a_0=9C_3/C_2$. Thus,

$$\begin{aligned} a_h^t\left((\tilde{\boldsymbol{w}},\boldsymbol{r}),(\tilde{\boldsymbol{w}},\boldsymbol{r})\right) &\geq\frac{C_2}{3}\|\nabla\tilde{\boldsymbol{w}}\|^2_{L^2(\Omega_h)}+\left(\frac{a_0}{h}-1\right)\|\tilde{\boldsymbol{w}}\|^2_{L^2(\Gamma_h)}\\ &\quad+C_2\|\tilde{\boldsymbol{w}}\|^2_{L^2(\Omega_h)}+C_2|\boldsymbol{r}|^2+\frac{\gamma_{\mathrm{vel}}}{h^2}s_h\left(\mathcal{F}_\delta^t;\tilde{\boldsymbol{w}},\tilde{\boldsymbol{w}}\right)\\ &\geq\frac{C_2}{3}\|\tilde{\boldsymbol{w}}\|^2_{H^1(\Omega_h)}+\frac{\gamma_{\mathrm{vel}}}{h^2}s_h\left(\mathcal{F}_\delta^t;\tilde{\boldsymbol{w}},\tilde{\boldsymbol{w}}\right)+C_2|\boldsymbol{r}|^2, \end{aligned} \tag{98}$$

provided $h\leq a_0$ (a very mild restriction). This proves the coercivity of $a_h^t(\cdot,\cdot)$. Note that the stabilization part is to give coercivity in a discrete norm to control the effect of cut elements.

5.4 Unfitted method for the adjoint

In view of (74), we introduce the augmented linear form

$$G_h^t\left(\boldsymbol{y},\boldsymbol{j},z;\boldsymbol{s},\boldsymbol{a}\right):=\boldsymbol{j}\cdot\left(\frac{-\boldsymbol{e}_0}{t_{\mathrm{f}}}+\boldsymbol{a}(t)\right). \tag{99}$$

Thus, the unfitted method is as follows. Given the final adjoint position $\boldsymbol{a}_h(t_\mathrm{f}) = \mathbf{0}$, marching backward in time for $t \in [0, t_\mathrm{f}]$, we seek to find $\tilde{\boldsymbol{w}}_h(t,\cdot) \in V_h^t$, $\boldsymbol{r}_h(t) \in \mathbb{R}^n$, and $q_h(t,\cdot) \in Q_h^t$ such that

$$S_h^t\left((\tilde{\boldsymbol{w}}_h, \boldsymbol{r}_h, q_h), (\tilde{\boldsymbol{y}}_h, \boldsymbol{j}_h, z_h)\right) = G_h^t\left(\tilde{\boldsymbol{y}}_h, \boldsymbol{j}_h, z_h; \boldsymbol{s}_h, \boldsymbol{a}_h\right), \quad \dot{\boldsymbol{a}}_h = \boldsymbol{\Upsilon}_h(t), \tag{100}$$

for all $\tilde{\boldsymbol{y}}_h \in V_h^t$, $\boldsymbol{j}_h \in \mathbb{R}^n$, $z_h \in Q_h^t$ (compare with (74)). Note that the exact solution of the adjoint equation satisfies $\boldsymbol{w} = \tilde{\boldsymbol{w}} + \boldsymbol{r}\zeta$ in $\Omega(t)$.

5.5 Time discretization

Discretizing in time, we have a sequence of times $\{t_k\}_{k=0}^K$, that are uniformly spaced with time-step δt with $t_0 = 0$ and $t_K = t_\mathrm{f}$. We put time indices as a superscript, so $\Omega^k \equiv \Omega(t_k)$, $\Gamma^k \equiv \Gamma(t_k)$, and $\boldsymbol{v}_h^k(x) \equiv \boldsymbol{v}_h(t_k, x)$, $\boldsymbol{c}^k \equiv \boldsymbol{c}(t_k)$, etc., and function spaces $V_h^k \equiv V_h^{t_k}$, etc. The algorithm is as follows. Let Ω^0 be given, which implies that Γ^0 and $\boldsymbol{c}^0$ are also given. Then, for $k = 0, 1, ..., K$, do the following.

(1) On Ω^k, solve for $\tilde{\boldsymbol{v}}_h^k \in V_h^k$, $\boldsymbol{s}_h^k \in \mathbb{R}^n$, and $p_h^k \in Q_h^k$ such that

$$S_h^k\left((\tilde{\boldsymbol{w}}_h, \boldsymbol{r}_h, q_h), (\tilde{\boldsymbol{v}}_h^k, \boldsymbol{s}_h^k, p_h^k)\right) = F_h^k\left(\tilde{\boldsymbol{w}}_h, \boldsymbol{r}_h, q_h\right), \tag{101}$$

for all $\tilde{\boldsymbol{w}}_h \in V_h^k$, $\boldsymbol{r}_h \in \mathbb{R}^n$, $q_h \in Q_h^k$.

(2) If $k < K$, update $\Omega^k \to \Omega^{k+1}$ using the given function $u(t_k, \cdot)$ and

$$\boldsymbol{c}_h^{k+1} = \boldsymbol{c}_h^k + \delta t \boldsymbol{s}_h^k. \tag{102}$$

Note that we do not have to solve an ODE for all points evolving in time to determine Ω^{k+1}. Due to the specific parameterization of $\Omega(t)$, we can just update the body position and use u.

For completeness, we state the fully discrete method for the adjoint system. Note that the sequence of domains $\{\Omega^k\}_{k=0}^K$ has already been determined by solving the forward problem. The algorithm is as follows. Given $\boldsymbol{a}_h^K = \mathbf{0}$, for $k = K-1, ..., 0$ (in reverse), do the following.

(1) On Ω^k, given $\boldsymbol{c}_h^k$ and $(\tilde{\boldsymbol{v}}_h^k, \boldsymbol{s}_h^k, p_h^k)$, solve for $\tilde{\boldsymbol{w}}_h^k \in V_h^k$, $\boldsymbol{r}_h^k \in \mathbb{R}^n$, and $q_h^k \in Q_h^k$ such that

$$S_h^k\left((\tilde{\boldsymbol{w}}_h^k, \boldsymbol{r}_h^k, q_h^k), (\tilde{\boldsymbol{y}}_h, \boldsymbol{j}_h, z_h)\right) = G_h^k\left(\tilde{\boldsymbol{y}}_h, \boldsymbol{j}_h, z_h; \boldsymbol{s}_h^k, \boldsymbol{a}_h^k\right), \tag{103}$$

for all $\tilde{\boldsymbol{y}}_h \in V_h^k$, $\boldsymbol{j}_h \in \mathbb{R}^n$, $z_h \in Q_h^k$.

(2) If $k > 0$, update $\boldsymbol{a}_h^k \to \boldsymbol{a}_h^{k-1}$ with

$$\boldsymbol{a}_h^{k-1} = \begin{cases} \boldsymbol{a}_h^K - (\delta t/2)\boldsymbol{\Upsilon}_h^K, & \text{if } k = K, \\ \boldsymbol{a}_h^k - \delta t \boldsymbol{\Upsilon}_h^k, & \text{for } k = K-1, K-2, ..., 2, \\ 2\boldsymbol{a}_h^1 - 2\delta t \boldsymbol{\Upsilon}_h^1, & \text{if } k = 1, \end{cases} \tag{104}$$

where $\boldsymbol{\Upsilon}_h^k$ depends on the forward and adjoint solutions at time index k; see (75). The form of (104) is due to the use of the trapezoidal rule in evaluating the time integral (See Section B.4.3 and (146)).

6 Numerical results

All simulations were implemented in `NGSolve` [57] with the add-on package `ngsxfem` for unfitted methods [39]. The optimization was done using `scipy` with the `l-BFGS` option. The hardware used for the simulations was the following desktop: PC, Intel(R) Xeon(R) Silver 4216, 2.10GHz, 16 Cores, 32 Logical Processors, 64 GB of RAM.

In all three experiments, we set the thrust control to zero, i.e. $\boldsymbol{h} = \mathbf{0}$. For a low number of body modes (Section 6.1), the locomotion is relatively elementary. With more modes (Sections 6.2, 6.3), the locomotion profile looks more like a traveling wave around the swimmer body. All of the locomotion profiles are time-irreversible.

6.1 Sliding bar ($M = 4$)

The tank domain is taken to be $\mathfrak{D} = [0, 2]^2$ in two dimensions and is triangulated with a uniform mesh of size $h = 0.1$. We assume that $\epsilon = 0.2$ in (16) and the other numerical parameters are given by

$$\delta = 0.2, \quad \gamma_{\text{vel}} = 0.05, \quad \gamma_{\text{p}} = 0.05, \quad \gamma_{\text{D}} = 150, \tag{105}$$

where these parameters are used in the unfitted finite element method (see Section 5.1). The final time is $t_{\text{f}} = 1.0$ with $K = 40$ time steps. We use $M = 4$ for the body parameterization (i.e., 8 basis functions) with a base radius of $R_0 = 0.4$. The initial body position is $\boldsymbol{c}(0) = (1.0, 1.0)$.

The optimal control parameters are as follows. The thrust is not used and is set to zero: $\boldsymbol{h}(t) \equiv \mathbf{0}$. The shape control is given by $u(t, \theta) := \boldsymbol{\rho}(t) \cdot \boldsymbol{\varphi}(\theta)$ (see Appendix B.4.1), where $\boldsymbol{\rho}$ is periodic on the interval $[0, t_{\text{f}}]$, is piecewise linear with respect to the time discretization, and $\boldsymbol{\rho}(t) \in \mathbb{R}^{2M}$ for each t. The initial guess for the shape optimization is given by

$$\begin{aligned} \rho_{-3}(t) := 0.0, \quad \rho_{-2}(t) := -0.3\sin(2\pi t), \quad \rho_{-1}(t) := 0.0, \quad \rho_0(t) := 0.3\cos(2\pi t), \\ \rho_1(t) := 0.0, \quad \rho_2(t) := -0.3\sin(2\pi t), \quad \rho_3(t) := 0.0, \quad \rho_4(t) := -0.3\cos(2\pi t), \end{aligned} \tag{106}$$

which are interpolated on the piecewise linear time mesh. Using (106) gives a time-periodic, irreversible motion, which is necessary to achieve a net displacement after one cycle of motion because of the scallop theorem [55, 34]; see the discussion in the introduction. The rest of the optimization parameters are given by

$$\begin{aligned} \boldsymbol{e}_0 = (1.0, 0.0), \quad \lambda_u = 0.02, \quad \lambda_\ell = 0.01, \quad \epsilon_u = 0.05, \quad E_0 = 4.36, \\ (u, \eta)_{\mathcal{A}_u} := (\partial_t u, \partial_t \eta)_{(0, t_{\text{f}}) \times (-\pi, \pi)}, \end{aligned} \tag{107}$$

and the shape control barrier function parameters (see Appendix B.3) are given by

$$\gamma_- = -0.5, \quad \gamma_+ = 0.8, \quad \gamma_0 = 1.0. \tag{108}$$

We let $\boldsymbol{d}$ be the net displacement of the body after one full cycle of motion, i.e. $0 \le t \le t_{\text{f}}$. The initial shape control results in $\boldsymbol{d} = (1.66983, 0.0053075) \cdot 10^{-2}$. We use the built-in `Python/scipy` optimization routine `minimize` with the following parameters:

$$\texttt{method} = \texttt{'L-BFGS-B'}, \quad \texttt{maxcor} = 5, \quad \texttt{ftol} = 10^{-8}, \quad \texttt{gtol} = 10^{-8}, \tag{109}$$

and we provide the objective function evaluation and its jacobian using the formulas we have derived in this paper. After running 104 iterations, the net displacement is $\boldsymbol{d} = (3.81017, 0.0046781) \cdot 10^{-2}$,

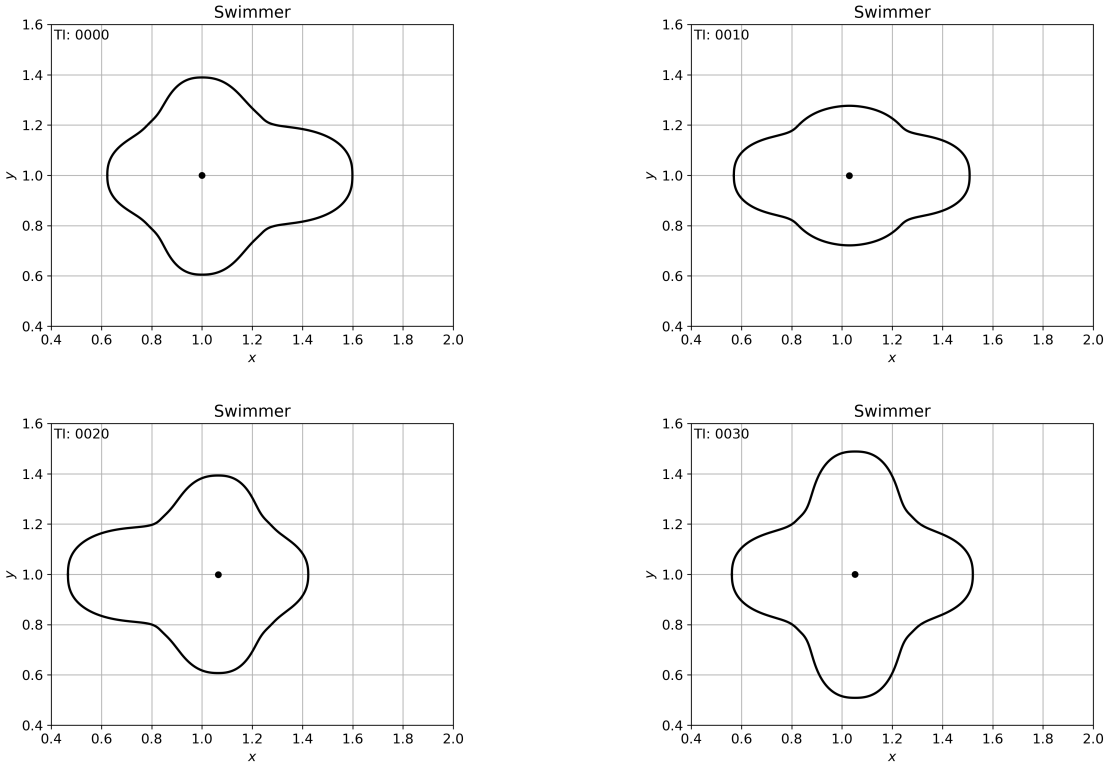

Figure 2: Optimized swimmer motion (Section 6.1). Four time indices are shown $k = 0, 10, 20, 30$ with "center" $\boldsymbol{c}$ shown as the black dot. When $k = 40$, the shape matches the $k = 0$ case, except $\boldsymbol{c}$ has displaced by $\boldsymbol{d} = (3.81017, 0.0046781) \cdot 10^{-2}$.

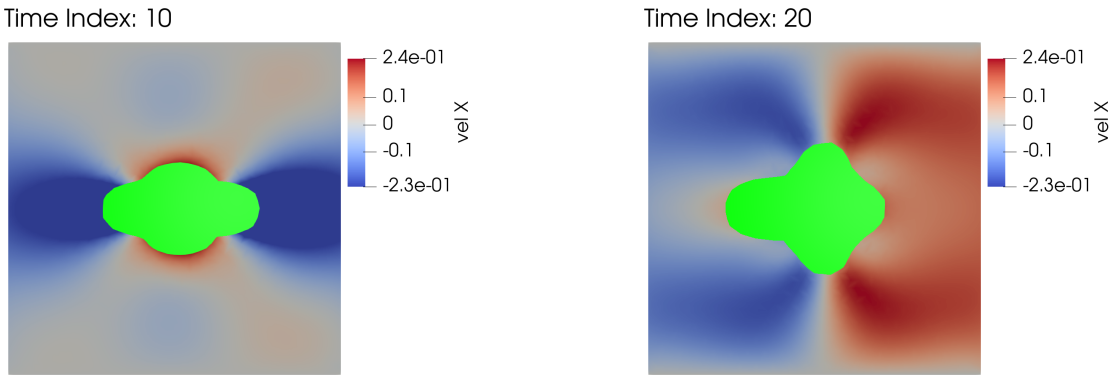

Figure 3: Optimized swimmer motion (Section 6.1) with velocity field. Two time indices are shown $k = 10, 20$ with the x-component of the velocity field shown in color.

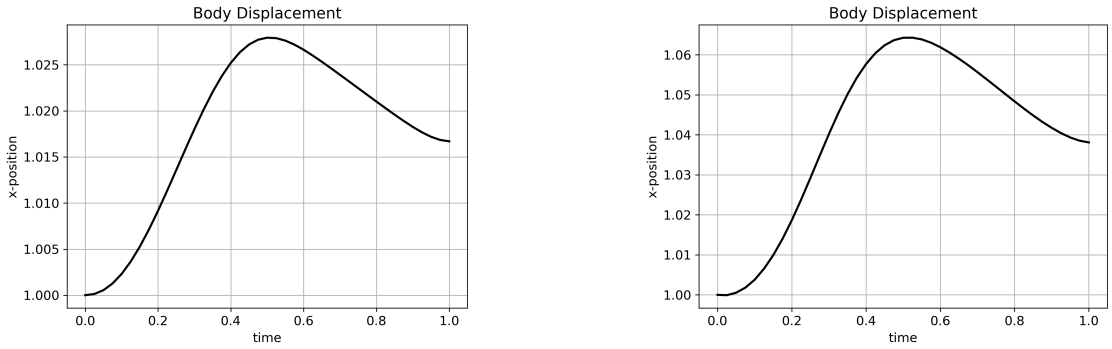

Figure 4: Body position motion for initial control (left) and final optimized control (right) (Section 6.1). Only the x-component of $\boldsymbol{c}(t)$ is shown; the y-component stays close to constant.

which is an improvement of 2.282 times in the x-direction. Figure 2 shows snapshots of the body motion which exhibits a "sliding bar" like motion. We observe that the area of the body slightly varies in time, which is expected because no area or volume constraint has been imposed.

Figure 3 shows the velocity field surrounding the swimmer, while Figure 4 plots the body position $\boldsymbol{c}(t)$ for the initial control and final optimized control. Note how $\boldsymbol{c}(t) \cdot \boldsymbol{e}_1$ is not monotonically increasing with time. This is because swimming bodies in Stokes flow require a "recovery" stroke as part of their locomotion.

6.2 Traveling wave $M = 8$

The tank domain is taken to be $\mathfrak{D} = [0, 2]^2$ in two dimensions and is triangulated with a uniform mesh of size $h = 0.04$. We assume that $\epsilon = 0.2$ in (16) and the other unfitted numerical parameters are given in (105). The final time is $t_\mathrm{f} = 1.0$ with $K = 80$ time steps. We use $M = 8$ for the body parameterization (i.e., 16 basis functions) with a base radius of $R_0 = 0.4$. The initial body position is $\boldsymbol{c}(0) = (1.0, 1.0)$.

The optimal control parameters are as follows. The thrust is not used and is set to zero: $\boldsymbol{h}(t) \equiv \boldsymbol{0}$. The shape control is given by $u(t, \theta) := \boldsymbol{\rho}(t) \cdot \boldsymbol{\varphi}(\theta)$ (see Appendix B.4.1), where $\boldsymbol{\rho}$ is periodic on the interval $[0, t_\mathrm{f}]$, is piecewise linear with respect to the time discretization, and $\boldsymbol{\rho}(t) \in \mathbb{R}^{2M}$ for each t. The initial guess for the shape optimization is randomly chosen in the following way. First, we choose

each component of $\boldsymbol{\rho}(t)$ by

$$\rho_j(t) := A_0 \sin(2\pi f_0 t - \phi_0) \quad \text{or} \quad A_0 \cos(2\pi f_0 t - \phi_0), \quad j = -7, -6, ..., 7, 8, \tag{110}$$

where $A_0 \in [-0.5, 0.5]$ is a uniform random variable, $f_0 \in \{1, 2\}$ is randomly chosen (with equal probability), and $\phi_0 \in [-\pi/2, \pi/2]$ is a uniform random variable; the choice between sin or cos is randomly chosen with equal probability. Next, we compute a new $\widetilde{\boldsymbol{\rho}}(t)$ through symmetrization, i.e.

$$\widetilde{\rho}_j(t) = \widetilde{\rho}_{-j}(t) := \frac{1}{2}\left(\rho_j(t) + \rho_{-j}(t)\right), \quad \text{for } j = 1, ..., M-1, \tag{111}$$

and $\widetilde{\rho}_0(t) := \rho_0(t)$ and $\widetilde{\rho}_M(t) := \rho_M(t)$. This ensures that the resulting body shape will be symmetric across the x-axis. These functions are then interpolated on the piecewise linear time mesh. The rest of the optimization parameters are given in (107), (108), except

$$(u, \eta)_{\mathcal{A}_u} := (\partial_t u, \partial_t \eta)_{(0,t_\mathrm{f})\times(-\pi,\pi)} + (\partial_\theta u, \partial_\theta \eta)_{(0,t_\mathrm{f})\times(-\pi,\pi)}\,. \tag{112}$$

We let $\boldsymbol{d}$ be the net displacement of the body after one full cycle of motion, i.e. $0 \le t \le t_\mathrm{f}$. The initial shape control results in $\boldsymbol{d} = (-0.153566, 0.00031711)\cdot 10^{-2}$. We use the built-in `Python/scipy` optimization routine `minimize` with the parameters given in (109), where we provide the objective function evaluation and its jacobian using the formulas we have derived in this paper. After running 1049 iterations, the net displacement is $\boldsymbol{d} = (8.9161, 0.0005741)\cdot 10^{-2}$. Figure 5 shows snapshots of the body motion which exhibits a "traveling wave" like motion. This corroborates well-established results in the literature, which show that generating traveling wavelike deformations constitute an effective swimming mechanism and are frequently observed in microorganisms; see [19, 59, 65].

Figure 6 shows the velocity field surrounding the swimmer, while Figure 7 plots the body position $\boldsymbol{c}(t)$ for the initial control and final optimized control. Again, we see that $\boldsymbol{c}(t)\cdot\boldsymbol{e}_1$ is not monotonically increasing with time because of the need for a "recovery" stroke as part of the locomotion profile.

6.3 Traveling wave $M = 10$

The tank domain is taken to be $\mathfrak{D} = [0, 2]^2$ in two dimensions and is triangulated with a uniform mesh of size $h = 0.05$. We assume that $\epsilon = 0.2$ in (16) and the other unfitted numerical parameters are given in (105). The final time is $t_\mathrm{f} = 1.0$ with $K = 80$ time steps. We use $M = 10$ for the body parameterization (i.e., 20 basis functions) with a base radius of $R_0 = 0.4$. The initial body position is $\boldsymbol{c}(0) = (1.0, 1.0)$.

The optimal control parameters are as follows. The thrust is not used and is set to zero: $\boldsymbol{h}(t) \equiv \boldsymbol{0}$. The shape control is given by $u(t, \theta) := \boldsymbol{\rho}(t) \cdot \boldsymbol{\varphi}(\theta)$ (see Appendix B.4.1), where $\boldsymbol{\rho}$ is periodic on the interval $[0, t_\mathrm{f}]$, is piecewise linear with respect to the time discretization, and $\boldsymbol{\rho}(t) \in \mathbb{R}^{2M}$ for each t. The initial guess for the shape optimization is randomly chosen in the following way. First, we choose each component of $\boldsymbol{\rho}(t)$ by

$$\rho_j(t) := A_0 \sin(2\pi f_0 t - \phi_0) \quad \text{or} \quad A_0 \cos(2\pi f_0 t - \phi_0), \quad j = -7, -6, ..., 7, 8, \tag{113}$$

where $A_0 \in [-0.25, 0.25]$ is a uniform random variable, $f_0 = 1$, and $\phi_0 \in [-\pi/8, \pi/8]$ is a uniform random variable; the choice between sin or cos is randomly chosen with equal probability. Next, we compute a new $\widetilde{\boldsymbol{\rho}}(t)$ through symmetrization as in (111), which ensures that the resulting body shape will be symmetric across the x-axis. These functions are then interpolated on the piecewise linear time mesh. The rest of the optimization parameters are given in (107), (108), with (112) replacing the inner product.

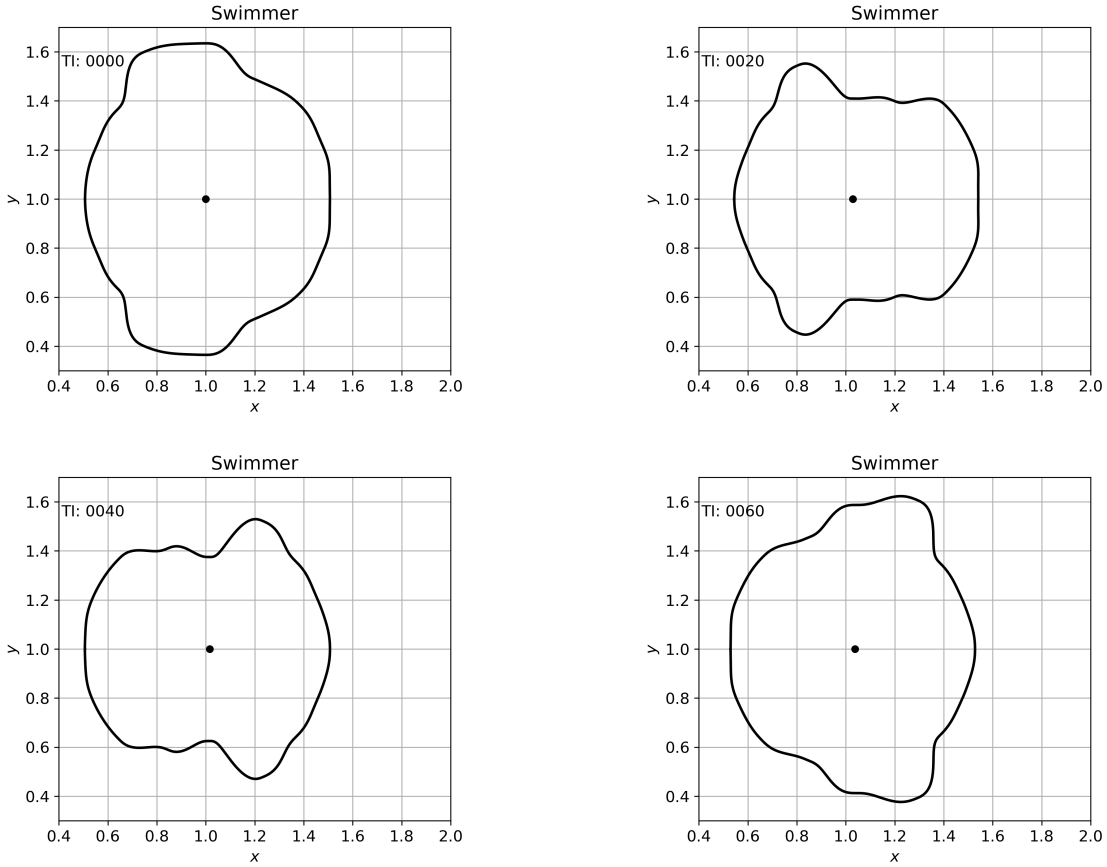

Figure 5: Optimized swimmer motion (Section 6.2). Four time indices are shown $k = 0, 20, 40, 60$ with "center" $\boldsymbol{c}$ shown as the black dot. When $k = 80$, the shape matches the $k = 0$ case, except $\boldsymbol{c}$ has displaced by $\boldsymbol{d} = (8.9161, 0.0005741) \cdot 10^{-2}$.

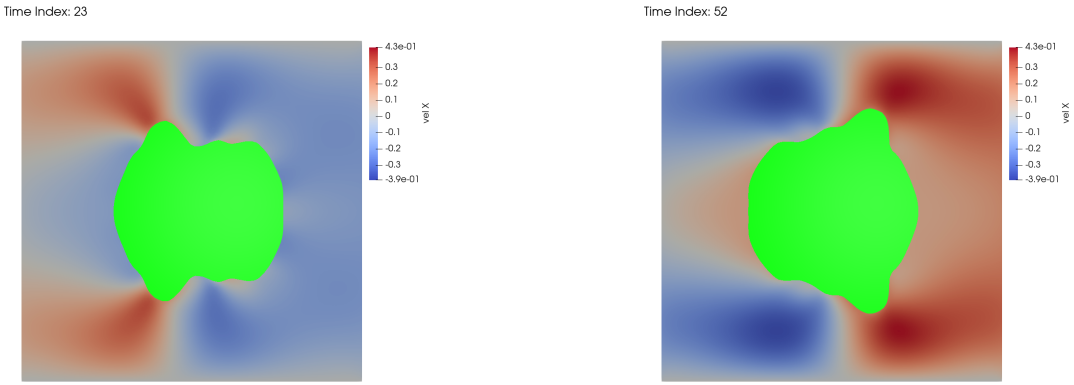

Figure 6: Optimized swimmer motion (Section 6.2) with velocity field. Two time indices are shown $k = 23, 52$ with the x-component of the velocity field shown in color.

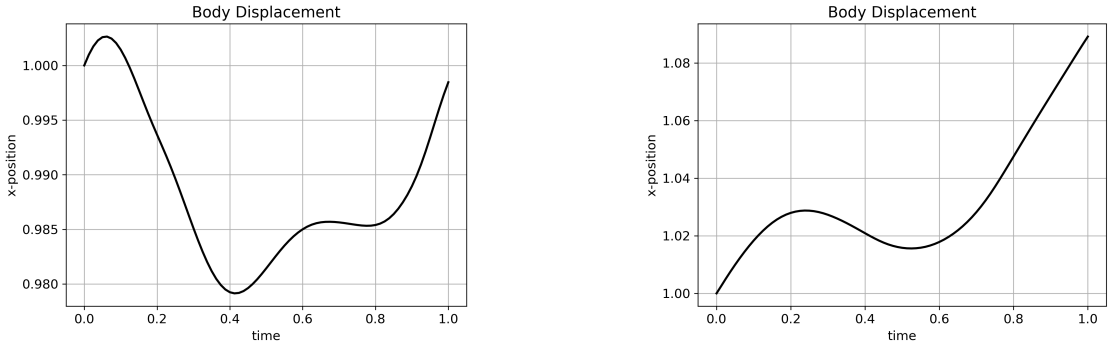

Figure 7: Body position motion for initial control (left) and final optimized control (right) (Section 6.2). Only the x-component of $\boldsymbol{c}(t)$ is shown; the y-component stays close to constant.

We let $\boldsymbol{d}$ be the net displacement of the body after one full cycle of motion, i.e. $0 \leq t \leq t_{\mathrm{f}}$. The initial shape control results in $\boldsymbol{d} = (0.4867148, 0.00452654) \cdot 10^{-2}$. We use the built-in `Python/scipy` optimization routine `minimize` with the parameters given in (109), where we provide the objective function evaluation and its jacobian using the formulas we have derived in this paper. After running 848 iterations, the net displacement is $\boldsymbol{d} = (9.68153, 0.00460076) \cdot 10^{-2}$. Figure 8 shows snapshots of the body motion which exhibits a "traveling wave" like motion (similar to Figure 5).

Figure 9 shows the velocity field surrounding the swimmer, while Figure 10 plots the body position $\boldsymbol{c}(t)$ for the initial control and final optimized control. Again, we see that $\boldsymbol{c}(t) \cdot \boldsymbol{e}_1$ is not monotonically increasing with time because of the need for a "recovery" stroke as part of the locomotion profile.

7 Remarks

We have developed a methodology for performing the optimal control of a self-deforming swimming body within a Stokesian fluid. The methodology is general and can be applied to similar frameworks with other PDE constraints, for instance a swimmer in a Navier-Stokes flow. This work provides new tools for the study of the control of free boundary problems, expanding the authors' previous work on this topic [31, 33, 36, 37]. A notable and novel feature of this work is the hybrid nature of the free boundary problem, where the body's shape is the control, while its center position is defined implicitly. This leads to several technical challenges in the shape sensitivity analysis.

In addition, we present an effective numerical scheme based on an unfitted finite element method in order to accurately handle the complex geometric motion of the swimmer, and a discrete optimization method for finding an optimal control that minimizes our objective functional. The numerical results show the efficacy of the method, as the optimal control leads to a notable improvement in the net displacement of the swimmer. Our results are consistent with the known fact that generating traveling wavelike deformations constitute an effective swimming mechanism in microorganisms [19, 59, 65].

The present work opens several possible lines for further research. Natural extensions are the refinement of the model, for instance adding volume or geometric constraints, the development of fully three-dimensional models or the incorporation of more complex fluid dynamics, such as the Navier–Stokes equations when moderate Reynolds numbers become relevant. Another promising but challenging direction is the investigation of actuation mechanisms for microswimmers, particularly magnetic actuation for nanoscale swimmers [20]. Incorporating such effects would require an

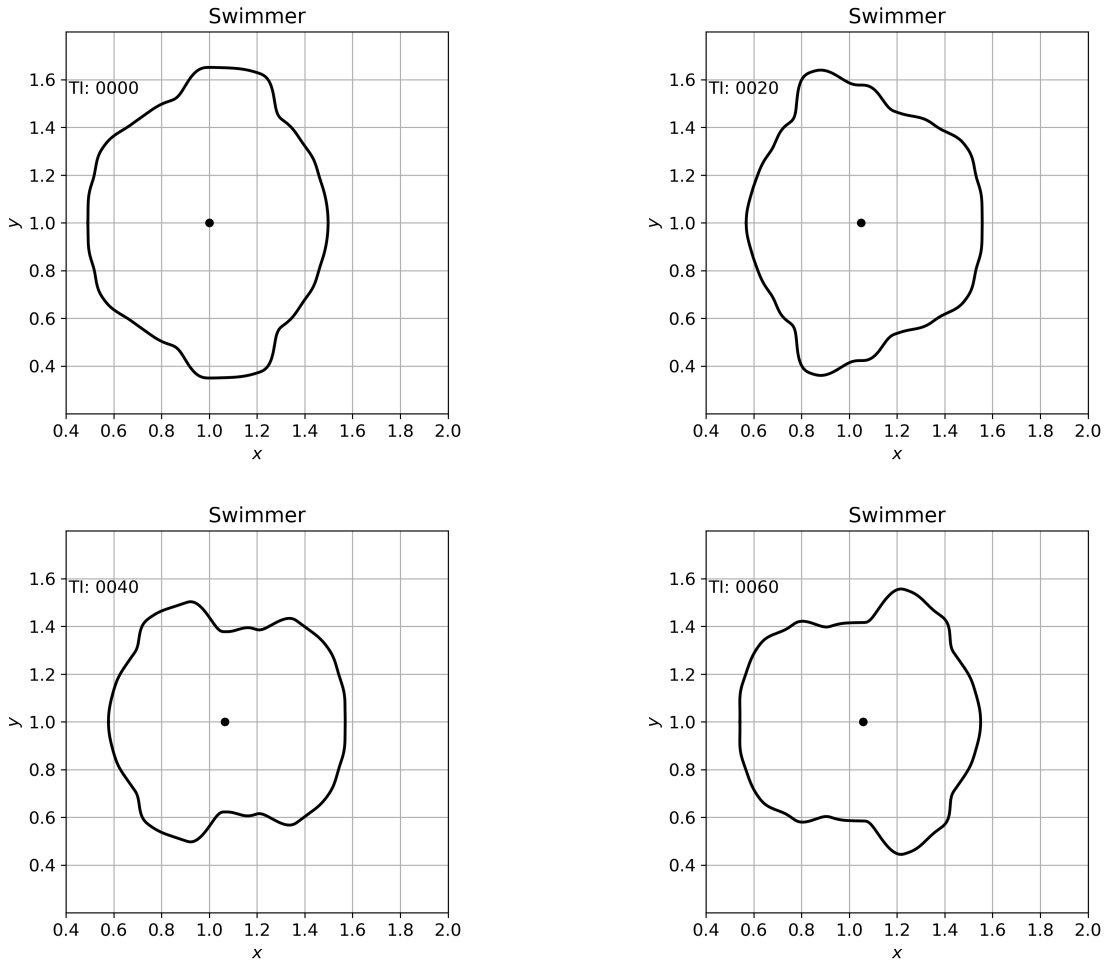

Figure 8: Optimized swimmer motion (Section 6.3). Four time indices are shown $k = 0, 20, 40, 60$ with "center" $\boldsymbol{c}$ shown as the black dot. When $k = 80$, the shape matches the $k = 0$ case, except $\boldsymbol{c}$ has displaced by $\boldsymbol{d} = (9.68153, 0.00460076) \cdot 10^{-2}$.

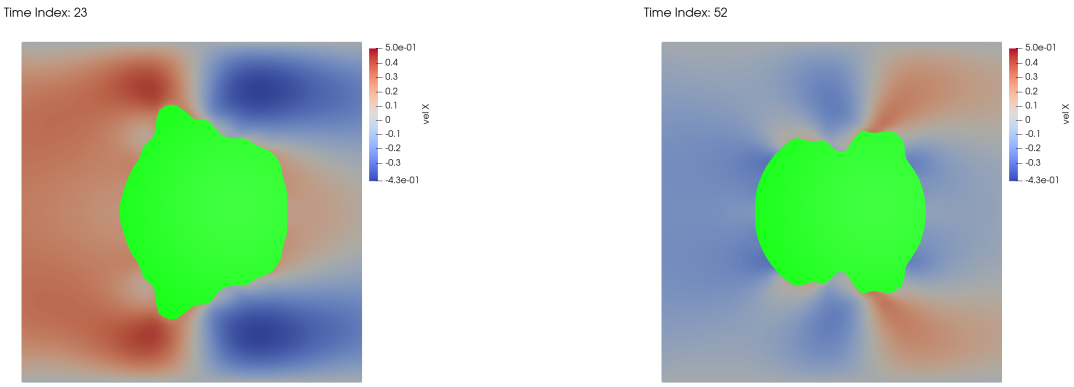

Figure 9: Optimized swimmer motion (Section 6.3) with velocity field. Two time indices are shown $k = 23, 52$ with the x-component of the velocity field shown in color.

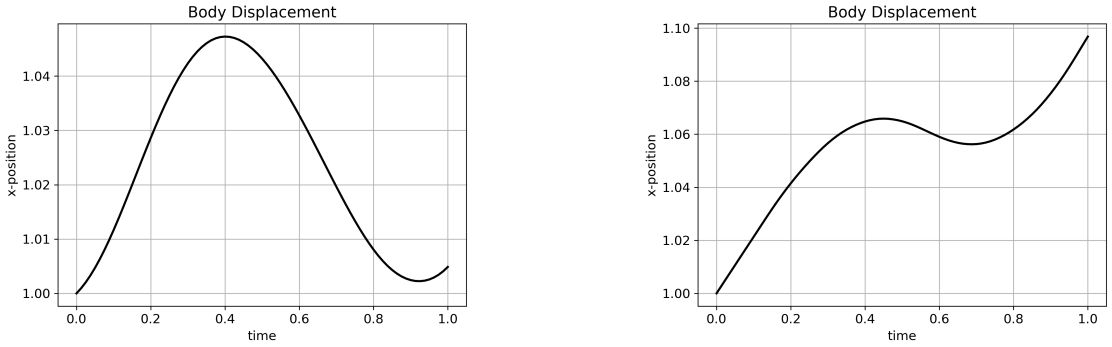

Figure 10: Body position motion for initial control (left) and final optimized control (right) (Section 6.3). Only the x-component of $\boldsymbol{c}(t)$ is shown; the y-component stays close to constant.

additional layer in the optimization framework to account for the external magnetic field and its coupling with the swimmer's deformation.

Acknowledgments

Antoine Laurain acknowledges the support, since May 2023, of the Collaborating Researcher Program of the Institute of Mathematics and Statistics at the University of São Paulo. Shawn Walker acknowledges financial support by the National Science Foundation (NSF) through DMS-2111474, DMS-2513843.

A Shape derivative results

Here we prove the relation $\mathrm{div} S_1 = S_0$, see (53). On one hand, the bulk formulation (51), also called *weak formulation* of the shape derivative, arises naturally from the use of weak formulations of the PDEs in the Lagrangian framework. On the other hand, the Hadamard form (54) of the shape derivative is associated to the strong formulation of the PDEs, and is obtained from (51) by applying the divergence theorem, i.e., integrating by parts. In connection with this, the key element to prove $\mathrm{div} S_1 = S_0$ is to use the strong forms of the state and adjoint.

Using index notation with the Einstein summation convention, we can write

$$\begin{aligned} (S_1)_{ij} &= -\partial_i \boldsymbol{w}_k \boldsymbol{\sigma}(\boldsymbol{v}, p)_{kj} - \partial_i \bar{\boldsymbol{v}}_k \boldsymbol{\sigma}(\boldsymbol{w}, q)_{kj} + Q(t, \boldsymbol{x})\delta_{ij}, \\ (S_0)_j &= \boldsymbol{\sigma}(\boldsymbol{w}, q)_{ij} \partial_k \partial_j \boldsymbol{\beta}_i - w_i \partial_j f_i. \end{aligned} \tag{114}$$

Next, we compute $(\mathrm{div} Q(t, \boldsymbol{x}) I)_{ij} = \partial_j (Q(t, \boldsymbol{x})\delta_{ij}) = \partial_i Q(t, \boldsymbol{x})$ and

$$\begin{aligned} \partial_i Q(t, \boldsymbol{x}) &= \partial_i \left[2[\boldsymbol{\varepsilon}(\nabla \boldsymbol{w})]_{kj} [\boldsymbol{\varepsilon}(\nabla \boldsymbol{v})]_{kj} - p \partial_k \boldsymbol{w}_k - q \partial_k \boldsymbol{v}_k - \boldsymbol{w}_k \boldsymbol{f}_k \right] \\ &= 2(\partial_i \partial_j \boldsymbol{w}_k)[\boldsymbol{\varepsilon}(\nabla \boldsymbol{v})]_{kj} + 2[\boldsymbol{\varepsilon}(\nabla \boldsymbol{w})]_{kj} (\partial_i \partial_j \boldsymbol{v}_k) - (\partial_i p) \partial_k \boldsymbol{w}_k - p(\partial_i \partial_k \boldsymbol{w}_k) \\ &\quad - (\partial_i q) \partial_k \boldsymbol{v}_k - q(\partial_i \partial_k \boldsymbol{v}_k) - (\partial_i \boldsymbol{w}_k) f_k - \boldsymbol{w}_k (\partial_i f_k). \end{aligned} \tag{115}$$

Thus, we obtain

$$\begin{aligned} (\mathrm{div} S_1)_i &= \partial_j (S_1)_{ij} \\ &= -\partial_j \partial_i \boldsymbol{w}_k \boldsymbol{\sigma}(\boldsymbol{v}, p)_{kj} - \partial_i \boldsymbol{w}_k \partial_j \boldsymbol{\sigma}(\boldsymbol{v}, p)_{kj} - \partial_j \partial_i \bar{\boldsymbol{v}}_k \boldsymbol{\sigma}(\boldsymbol{w}, q)_{kj} - \partial_i \bar{\boldsymbol{v}}_k \partial_j \boldsymbol{\sigma}(\boldsymbol{w}, q)_{kj} \\ &\quad + 2(\partial_i \partial_j \boldsymbol{w}_k)[\boldsymbol{\varepsilon}(\nabla \boldsymbol{v})]_{kj} + 2[\boldsymbol{\varepsilon}(\nabla \boldsymbol{w})]_{kj} (\partial_i \partial_j \boldsymbol{v}_k) - (\partial_i p) \partial_k \boldsymbol{w}_k - p(\partial_i \partial_k \boldsymbol{w}_k) \\ &\quad - (\partial_i q) \partial_k \boldsymbol{v}_k - q(\partial_i \partial_k \boldsymbol{v}_k) - (\partial_i \boldsymbol{w}_k) f_k - \boldsymbol{w}_k (\partial_i f_k). \end{aligned}$$

First, using the strong form of the forward state (1) we get $-\partial_j \boldsymbol{\sigma}(\boldsymbol{v},p)_{kj} = f_k$ and using the strong form of the adjoint state we also have $\partial_j \boldsymbol{\sigma}(\boldsymbol{w},q)_{kj} = 0$. In addition, the strong form of the forward and adjoint states also yield $\partial_k \boldsymbol{v}_k = \nabla \cdot \boldsymbol{w} = 0$ and $\partial_k \boldsymbol{w}_k = \nabla \cdot \boldsymbol{w} = 0$

Next, employing $\boldsymbol{\sigma}(\boldsymbol{v},p) = -p\boldsymbol{I} + 2\boldsymbol{\varepsilon}(\nabla \boldsymbol{v})$, see (2), we get

$$-\partial_j \partial_i \boldsymbol{w}_k \boldsymbol{\sigma}(\boldsymbol{v},p)_{kj} = -2(\partial_j \partial_i \boldsymbol{w}_k)[\boldsymbol{\varepsilon}(\nabla \boldsymbol{v})]_{kj} + p(\partial_k \partial_i \boldsymbol{w}_k).$$

In a similar way, using $\boldsymbol{v} = \bar{\boldsymbol{v}} + \boldsymbol{\beta}$, we have

$$\begin{aligned} -(\partial_j \partial_i \bar{\boldsymbol{v}}_k)\boldsymbol{\sigma}(\boldsymbol{w},q)_{kj} &= -(\partial_j \partial_i \boldsymbol{v}_k)\boldsymbol{\sigma}(\boldsymbol{w},q)_{kj} + (\partial_j \partial_i \boldsymbol{\beta}_k)\boldsymbol{\sigma}(\boldsymbol{w},q)_{kj} \\ &= -2(\partial_j \partial_i \boldsymbol{v}_k)[\boldsymbol{\varepsilon}(\nabla \boldsymbol{w})]_{kj} + q(\partial_k \partial_i \boldsymbol{v}_k) + (\partial_j \partial_i \boldsymbol{\beta}_k)\boldsymbol{\sigma}(\boldsymbol{w},q)_{kj}. \end{aligned}$$

Gathering these results, most terms cancel out and we obtain

$$(\mathrm{div} S_1)_i = \partial_j (S_1)_{ij} = (\partial_j \partial_i \boldsymbol{\beta}_k)\boldsymbol{\sigma}(\boldsymbol{w},q)_{kj} - \boldsymbol{w}_k(\partial_i f_k) = (S_0)_i,$$

which proves $\mathrm{div} S_1 = S_0$.

B Implementation details

B.1 Parameterizing the body shape control

Recall $\tilde{u} \in \mathcal{A}_u$ from Section 2.3. For a fixed t, set $\rho(\theta) = \tilde{u}(t,\theta)$ and take a Galerkin expansion for $\rho(\theta)$:

$$\rho(\theta) := \sum_k \rho_k \varphi_k(\theta), \tag{116}$$

where $\{\varphi_k\}$ are convenient basis functions and $\{\rho_k\}$ are coefficients in $\mathbb{R}$. The body basis functions, φ_k, are defined in the following way. We start with a reference basis function $\hat{\varphi} \in C^2(\mathbb{R})$ centered at $\theta = 0$:

$$\hat{\varphi}(\theta) = \begin{cases} 1 + \theta^3(10 + 15\theta + 6\theta^2), & -1 \le \theta \le 0, \\ 1 - \theta^3(10 - 15\theta + 6\theta^2), & 0 \le \theta \le 1, \\ 0, & \text{else.} \end{cases} \tag{117}$$

Next, for a positive integer M, subdivide $(-\pi, \pi]$ into $2M$ sub-intervals, which induces $2M$ points in $(-\pi, \pi]$ that will be the nodal points of our basis functions:

$$\theta_k = k d_0, \text{ for } k = (-M+1), ..., -1, 0, 1, ..., M, \qquad d_0 = \frac{\pi}{M}. \tag{118}$$

Then, we define the basis function, centered at 0 by:

$$\varphi_0(\theta) = \hat{\varphi}\left(\frac{\theta}{d_0}\right). \tag{119}$$

In general, the basis functions are given by

$$\begin{aligned} \varphi_k(\theta) &= \hat{\varphi}\left(\frac{\theta - \theta_k}{d_0}\right), \text{ for } k = (-M+1), ..., -1, 0, 1, ..., (M-1), \\ \varphi_M(\theta) &= \begin{cases} \hat{\varphi}\left((\theta + \pi)/d_0\right), & -\pi \le \theta \le -\pi + d_0, \\ \hat{\varphi}\left((\theta - \pi)/d_0\right), & \pi - d_0 \le \theta \le \pi, \\ 0, & \text{else.} \end{cases} \end{aligned} \tag{120}$$

Note that this collection of basis functions is a *partition of unity*.

Next, set $\boldsymbol{\rho} = (\rho_{-M+1}, \rho_{-M+2}, ..., \rho_{M-1}, \rho_M)^{\mathsf{T}} \in \mathbb{R}^{2M}$. Letting $\boldsymbol{\varphi}(\theta) = (\varphi_{-M+1}(\theta), ..., \varphi_M(\theta))^{\mathsf{T}} \in \mathbb{R}^{2M}$, then (116) becomes

$$\rho(\theta) = \boldsymbol{\rho} \cdot \boldsymbol{\varphi}(\theta). \tag{121}$$

Therefore, we get the definition of the finite dimensional control space for $u(t, \cdot)$ for each fixed t:

$$\mathcal{U}_M \equiv \mathcal{U}_M(-\pi, \pi) := \{\boldsymbol{\rho} \cdot \boldsymbol{\varphi}(\theta) \mid \boldsymbol{\rho} \in \mathbb{R}^{2M}\} \subset C^2_{\text{per}}(-\pi, \pi) \text{ or } C^2((-\pi, \pi]), \tag{122}$$

with interpolation operator $\mathcal{I}_M : C^2_{\text{per}}(-\pi, \pi) \to \mathcal{U}_M$ (or $\mathcal{I}_M : C^2(-\pi, \pi) \to \mathcal{U}_M$) given by

$$\mathcal{I}_M \rho := \sum_{k=-M+1}^{M} \rho(\theta_k)\varphi_k. \tag{123}$$

One can also use an L^2-projection for $\mathcal{I}_M$.

B.2 Cutoff function

The specific formula for $\zeta \in C^2$ is as follows. Define a reference cutoff function:

$$\begin{aligned}
\bar{\zeta}(\xi; \xi_0, \xi_1) &= \begin{cases} 1 + \left(\frac{\xi - (\xi_0 + \delta)}{\delta}\right)^3, & \xi_0 \le \xi \le \xi_0 + \delta, \\ 1, & \xi_0 + \delta \le \xi \le \xi_1 - \delta, \\ 1 - \left(\frac{\xi - (\xi_1 - \delta)}{\delta}\right)^3, & \xi_1 - \delta \le \xi \le \xi_1, \end{cases} \\
\bar{\zeta}'(\xi; \xi_0, \xi_1) &= \begin{cases} \frac{3}{\delta}\left(\frac{\xi - (\xi_0 + \delta)}{\delta}\right)^2, & \xi_0 \le \xi \le \xi_0 + \delta, \\ 0, & \xi_0 + \delta \le \xi \le \xi_1 - \delta, \\ -\frac{3}{\delta}\left(\frac{\xi - (\xi_1 - \delta)}{\delta}\right)^2, & \xi_1 - \delta \le \xi \le \xi_1, \end{cases}
\end{aligned} \tag{124}$$

where $\delta > 0$ is small. Then, ζ is given by

$$\begin{aligned}
\zeta(x, y) &= \bar{\zeta}(x; x_0, x_1)\bar{\zeta}(y; y_0, y_1), \\
\nabla\zeta(x, y) &= \left(\bar{\zeta}'(x; x_0, x_1)\bar{\zeta}(y; y_0, y_1), \bar{\zeta}(x; x_0, x_1)\bar{\zeta}'(y; y_0, y_1)\right),
\end{aligned} \tag{125}$$

with the box domain defined by $\mathfrak{D} = [x_0, x_1] \times [y_0, y_1]$.

B.3 Control penalty

The penalty function $\ell \in C^2(\gamma_-, \gamma_+)$ for u, appearing in (33), is defined as follows:

$$\ell(u) = \begin{cases} +\infty, & u \le \gamma_-, \\ -\gamma_0\left(\frac{1}{\gamma_- - u} - \frac{1}{\gamma_-}\right)u^2, & \gamma_- < u \le 0, \\ \gamma_0\left(\frac{1}{\gamma_+ - u} - \frac{1}{\gamma_+}\right)u^2, & 0 \le u < \gamma_+, \\ +\infty, & \gamma_+ \le u, \end{cases} \tag{126}$$

where $-1 < \gamma_- < 0$, $\gamma_0 > 0$, and $\gamma_+ > 0$ are bounded, chosen constants. Formulas for ℓ' and ℓ'' are

$$\ell'(u) = \begin{cases} -\gamma_0\left(\frac{1}{\gamma_- - u}\right)^2 u^2 - 2\gamma_0\left(\frac{1}{\gamma_- - u} - \frac{1}{\gamma_-}\right)u, & \gamma_- < u \le 0, \\ \gamma_0\left(\frac{1}{\gamma_+ - u}\right)^2 u^2 + 2\gamma_0\left(\frac{1}{\gamma_+ - u} - \frac{1}{\gamma_+}\right)u, & 0 \le u < \gamma_+, \end{cases} \tag{127}$$

$$\ell''(u) = \begin{cases} -2\gamma_0 \left(\frac{1}{\gamma_- - u}\right)^3 u^2 - 4\gamma_0 \left(\frac{1}{\gamma_- - u}\right)^2 u - 2\gamma_0 \left(\frac{1}{\gamma_- - u} - \frac{1}{\gamma_-}\right), & \gamma_- < u \leq 0, \\ 2\gamma_0 \left(\frac{1}{\gamma_+ - u}\right)^3 u^2 + 4\gamma_0 \left(\frac{1}{\gamma_+ - u}\right)^2 u + 2\gamma_0 \left(\frac{1}{\gamma_+ - u} - \frac{1}{\gamma_+}\right), & 0 \leq u < \gamma_+. \end{cases} \tag{128}$$

B.4 Time semi-discrete optimal control problem

We start by discretizing the interval $[0, t_\mathrm{f}]$ with $K+1$ uniformly spaced time points $\{t_k\}_{k=0}^K$, with spacing $\delta t > 0$, $t_0 = 0$, and $t_K = t_\mathrm{f}$. The time discretization introduces some additional technical issues, which we now explain.

B.4.1 Discretizing the shape control u

The first issue is the time discretization of $u \in H^1(0, t_\mathrm{f}; \mathcal{U}_M)$ or $u \in H^1_{\mathrm{per}}(0, t_\mathrm{f}; \mathcal{U}_M)$. Since both $u(t, \cdot)$ and $\partial_t u(t, \cdot)$ appear when solving the forward problem, care must be taken to ensure consistency, especially with the forward Euler scheme in (101), (102).

First consider the case $u \in H^1(0, t_\mathrm{f}; \mathcal{U}_M)$. We must approximate both $u(t, \cdot)$ and $\partial_t u(t, \cdot)$ and be able to evaluate at the time points $\{t_k\}_{k=0}^K$. For instance, one could take

$$u(t, \theta) := \boldsymbol{\rho}(t) \cdot \boldsymbol{\varphi}(\theta),$$

where $\boldsymbol{\rho}(t) \in \mathbb{R}^{2M}$ is a piecewise linear function over the time mesh $\{t_k\} \subset [0, t_\mathrm{f}]$. Evaluating $u(t_k, \cdot)$ is easily done. An obvious choice for $\partial_t u(t, \cdot)$, consistent with the body center update (102) is

$$\partial_t u(t_k, \cdot) \approx \frac{u(t_{k+1}, \cdot) - u(t_k, \cdot)}{\delta t}, \quad \text{for } k = 0, 1, ..., K. \tag{129}$$

Unfortunately, this requires evaluating $u(t_{K+1}, \cdot)$ at the undefined point t_{K+1}. Moreover, the simple "remedy" given by

$$\partial_t u(t_K, \cdot) \approx \frac{u(t_K, \cdot) - u(t_{K-1}, \cdot)}{\delta t}, \tag{130}$$

performs extremely poorly when running our optimization algorithm, as demonstrated by our own experience.

For the forward problem, (130) is an acceptable approximation since it is done at the end of the interval $[0, t_\mathrm{f}]$. On the other hand, solving parabolic optimal control problems requires solving both forward *and* backward (adjoint) problems. Whence, $u(t, \cdot)$ must satisfy "boundary conditions" at t_0 and t_K. Since $u(t_K, \cdot)$ is free in the optimization, it implies a Neumann condition for $\partial_t u(t_K, \cdot)$. It is well-known (see [62, 49]) that finite difference approximations of Neumann conditions require fictitious, or ghost, points to avoid degradation of accuracy. We take this approach in what follows.

Let $\{t_k\}_{k=0}^{K+1}$ be a uniform discretization of the interval $[0, t_\mathrm{f} + \delta t]$, i.e. $t_{K+1} = t_\mathrm{f} + \delta t$ will play the role of a *ghost point*. Next, we let $\Xi_{\delta t} \subset H^1(0, t_\mathrm{f} + \delta t)$ be a Lagrange finite element space of degree 1 over $\{t_k\}_{k=0}^{K+1}$, with basis functions $\{\chi_i\}_{k=0}^{K+1}$. Then, we approximate u by $u(t, \theta) = \boldsymbol{\rho}(t) \cdot \boldsymbol{\varphi}(\theta)$, where $\boldsymbol{\rho} \in [\Xi_{\delta t}]^{2M}$. In other words, define

$$\mathcal{A}_{u, \delta t} := \left\{ \boldsymbol{\rho}(t) \cdot \boldsymbol{\varphi}(\theta) \mid \boldsymbol{\rho} \in [\Xi_{\delta t}]^{2M} \right\} \subset H^1(0, t_\mathrm{f} + \delta t; \mathcal{U}_M), \tag{131}$$

and take $u \in \mathcal{A}_{u, \delta t}$. Since the forward problem (101) is only solved at t_k for $k = 0, ..., K$, it is straightforward to evaluate $u(t_k, \cdot)$ and $\partial_t u(t_k, \cdot)$ using (129).

Periodic in time. If $u(t,\cdot)$ is periodic in time, then the ghost point disappears. In this case, we let $\Xi_{\delta t} \subset H^1_{\text{per}}(0,t_{\text{f}})$ be a Lagrange finite element space of degree 1 over $\{t_k\}_{k=0}^K$ where we identify the Degree-of-Freedom (DoF) at t_K with the DoF at t_0. Thus, only K basis functions $\{\chi_i\}_{k=0}^{K-1}$ are needed when periodicity is enforced. Then, we approximate u by $u(t,\theta) = \boldsymbol{\rho}(t)\cdot\boldsymbol{\varphi}(\theta)$, where $\boldsymbol{\rho} \in [\Xi_{\delta t}]^{2M}$ and $\mathcal{A}_{u,\delta t} \subset H^1_{\text{per}}(0,t_{\text{f}};\mathcal{U}_M)$.

We define the number of augmented time points $\widetilde{K} := K+1$ when no periodicity in time is assumed; if time periodicity is assumed, then $\widetilde{K} := K-1$. Furthermore, we set $\widetilde{t_{\text{f}}} := t_{\text{f}} + \delta t$ when no periodicity in time is assumed; if time periodicity is assumed, then $\widetilde{t_{\text{f}}} := t_{\text{f}}$.

Next, we write the expansion of $u \in \mathcal{A}_{\delta t}$ more explicitly:

$$u(t,\theta) = \sum_{p=-M+1}^{M}\sum_{k=0}^{\widetilde{K}} U_{pk}\chi_k(t)\varphi_p(\theta), \tag{132}$$

where $[U_{pk}] \equiv \underline{\underline{\mathsf{U}}} \in \mathbb{R}^{2M\times(\widetilde{K}+1)}$ and let $\underline{\mathsf{U}} \in \mathbb{R}^{2M(\widetilde{K}+1)}$ be the flattened version of $\underline{\underline{\mathsf{U}}}$ along rows, i.e.

$$(\underline{\mathsf{U}})_{\widetilde{K}(p+M-1)+k} = (\underline{\underline{\mathsf{U}}})_{pk}, \text{ for } -M+1 \le p \le M, \quad 0 \le k \le \widetilde{K}.$$

Moreover, for a "test" function, or perturbation of u, denoted η we have the expansion

$$\eta(t,\theta) = \sum_{p=-M+1}^{M}\sum_{k=0}^{\widetilde{K}} D_{pk}\chi_k(t)\varphi_p(\theta), \tag{133}$$

where $[D_{pk}] \equiv \underline{\underline{\mathsf{D}}} \in \mathbb{R}^{2M\times(\widetilde{K}+1)}$ and $\underline{\mathsf{D}} \in \mathbb{R}^{2M(\widetilde{K}+1)}$ the flattened version of $\underline{\underline{\mathsf{D}}}$.

B.4.2 Bilinear forms with u

It is useful in the optimization to compute bilinear forms mapping $\mathcal{A}_{\delta t}\times\mathcal{A}_{\delta t} \to \mathbb{R}$. For instance, define the bilinear form:

$$\begin{aligned} e\left(\underline{\underline{\mathsf{U}}},\underline{\underline{\mathsf{D}}}\right) &= \int_0^{\widetilde{t_{\text{f}}}}\int_{-\pi}^{\pi} u(t,\theta)\eta(t,\theta)\,d\theta dt \\ &= \sum_{p=-M+1}^{M}\sum_{k=0}^{\widetilde{K}}\sum_{q=-M+1}^{M}\sum_{j=0}^{\widetilde{K}} U_{pk}D_{qj}\left[\int_{-\pi}^{\pi}\varphi_p(\theta)\varphi_q(\theta)d\theta\right]\left[\int_0^{\widetilde{t_{\text{f}}}}\chi_k(t)\chi_j(t)dt\right]. \end{aligned} \tag{134}$$

Next, let $\underline{\underline{\mathcal{H}}} = [\mathcal{H}_{pq}] \in \mathbb{R}^{2M\times 2M}$ and $\underline{\underline{\mathcal{M}}} = [\mathcal{M}_{kj}] \in \mathbb{R}^{(\widetilde{K}+1)\times(\widetilde{K}+1)}$ be given by

$$\mathcal{H}_{pq} := \int_{-\pi}^{\pi}\varphi_p(\theta)\varphi_q(\theta)d\theta, \qquad \mathcal{M}_{kj} := \int_0^{\widetilde{t_{\text{f}}}}\chi_k(t)\chi_j(t)dt. \tag{135}$$

Let $\underline{\underline{\mathcal{H}}}\otimes\underline{\underline{\mathcal{M}}} \in \mathbb{R}^{2M(\widetilde{K}+1)\times 2M(\widetilde{K}+1)}$ be a re-indexed Kronecker product:

$$(\underline{\underline{\mathcal{H}}}\otimes\underline{\underline{\mathcal{M}}})_{(\widetilde{K}+1)(p+M-1)+k,(\widetilde{K}+1)(q+M-1)+j} = \mathcal{H}_{pq}\mathcal{M}_{kj}, \text{ for } -M+1 \le p,q \le M,\ 0 \le k,j \le \widetilde{K}. \tag{136}$$

Then, (134) can be written as

$$
\begin{aligned}
e\left(\underline{\mathsf{U}}, \underline{\underline{\mathsf{D}}}\right) &= \sum_{p=-M+1}^{M} \sum_{k=0}^{\widetilde{K}} \sum_{q=-M+1}^{M} \sum_{j=0}^{\widetilde{K}} (\underline{\mathsf{U}})_{(\widetilde{K}+1)(p+M-1)+k} (\underline{\mathsf{D}})_{(\widetilde{K}+1)(q+M-1)+j} \cdot \\
&\qquad \cdot (\underline{\underline{\mathcal{H}}} \otimes \underline{\underline{\mathcal{M}}})_{(\widetilde{K}+1)(p+M-1)+k,(\widetilde{K}+1)(q+M-1)+j} \\
&= \underline{\mathsf{U}}^{\mathsf{T}} (\underline{\underline{\mathcal{H}}} \otimes \underline{\underline{\mathcal{M}}}) \underline{\mathsf{D}}.
\end{aligned}
\tag{137}
$$

Note that $\underline{\underline{\mathcal{H}}}$ can be computed using a simple for loop, while $\underline{\underline{\mathcal{M}}}$ can be computed using standard finite element software.

B.4.3 Time discretization of the Lagrangian

In this section, we describe the time discretization of $\mathcal{L}$ and derive the various resulting perturbation equations. First, we let the time integral be discretized by the trapezoidal rule:

$$
\int_0^{t_\mathrm{f}} f(t)dt \approx Q(f) := \sum_{k=0}^{K} f(t_k)\mu_k, \quad \mu_k = \begin{cases} \delta t, & \text{if } 0 < k < K, \\ \delta t/2, & \text{else.} \end{cases}
\tag{138}
$$

With this, we have the time semi-discrete version of J:

$$
\begin{aligned}
J[\boldsymbol{\Psi}, u, \boldsymbol{h}] &= \frac{1}{t_\mathrm{f}} Q(-\boldsymbol{\Psi}_2(t) \cdot \boldsymbol{e}_0) + \frac{\lambda_{\boldsymbol{h}}}{2t_\mathrm{f}} \|\boldsymbol{h}\|^2_{L^2(0,t_\mathrm{f})} + \frac{\lambda_u}{2t_\mathrm{f}} (u,u)_{\mathcal{A}_u} \\
&\quad + \frac{\lambda_\ell}{t_\mathrm{f}} \int_0^{\widetilde{t_\mathrm{f}}} \int_{-\pi}^{\pi} \mathcal{I}_M \ell(u(t,\theta)) d\theta dt + \frac{1}{4t_\mathrm{f}\epsilon_u} \left(\int_0^{\widetilde{t_\mathrm{f}}} \int_{-\pi}^{\pi} \left(\partial_t u(t,\theta)\right)^2 d\theta dt - E_0 \right)^2,
\end{aligned}
\tag{139}
$$

where $u \in \mathcal{A}_{u,\delta t}$ and $\boldsymbol{h} \in [\Xi_{\delta t}]^n$ (without periodicity enforced). Note that the time integrals for the last two terms are computed exactly with respect to the finite element space $\mathcal{A}_{u,\delta t}$ (i.e. $\Xi_{\delta t}$).

The time semi-discrete version of J_{St} is:

$$
\begin{aligned}
J_{\mathrm{St}}[\boldsymbol{\Psi}, \boldsymbol{c}, \boldsymbol{\Theta}, u, \boldsymbol{h}] &= Q\left(S^t(\boldsymbol{\Theta}, \boldsymbol{\Psi}) - F^t(\boldsymbol{\Theta}; u, \boldsymbol{h})\right) \\
&= Q(\mathcal{Q}[\cdot, \boldsymbol{\Psi}, \boldsymbol{c}, \boldsymbol{\Theta}, u]) - Q(\boldsymbol{r} \cdot \boldsymbol{h}), \quad \mathcal{Q}[t, \boldsymbol{\Psi}, \boldsymbol{c}, \boldsymbol{\Theta}, u] := \int_{\Omega(t)} Q(t, \boldsymbol{x})\, d\boldsymbol{x},
\end{aligned}
\tag{140}
$$

where Q is given in (46). Note that $\partial_t u(t,\cdot)$ is replaced by

$$
\partial_t u(t_k, \theta^k) \approx \frac{u(t_{k+1}, \theta^k) - u(t_k, \theta^k)}{\delta t}, \text{ where } \theta^k = \theta(\boldsymbol{x} - \boldsymbol{c}(t_k)), \quad \text{for } k = 0, ..., K, \quad \text{(non-periodic)},
$$

$$
\partial_t u(t_k, \theta^k) \approx \begin{cases} \frac{u(t_{k+1}, \theta^k) - u(t_k, \theta^k)}{\delta t}, & \text{if } k = 0, ..., K-2, \\ \frac{u(t_0, \theta^k) - u(t_{K-1}, \theta^k)}{\delta t}, & \text{if } k = K-1, \\ \frac{u(t_1, \theta^k) - u(t_0, \theta^k)}{\delta t}, & \text{if } k = K, \end{cases} \qquad \text{(periodic)},
$$

and that the time discrete u controls consist of $\widetilde{K}$ values for each basis function φ_p.

The time semi-discrete Lagrangian is then:

$$
\mathcal{L}[\boldsymbol{\Psi}, \boldsymbol{c}, u, \boldsymbol{h}, \boldsymbol{\Theta}, \boldsymbol{a}] := J[\boldsymbol{\Psi}, u, \boldsymbol{h}] - \sum_{k=0}^{K} \boldsymbol{a}^k \cdot \left(\frac{\boldsymbol{c}^{k+1} - \boldsymbol{c}^k}{\delta t} - \boldsymbol{s}^k \right) \mu_k - J_{\mathrm{St}}[\boldsymbol{\Psi}, \boldsymbol{c}, \boldsymbol{\Theta}, u, \boldsymbol{h}].
\tag{141}
$$

First, we perturb $\mathcal{L}$ with respect to $\boldsymbol{\Theta}$:

$$\delta_{\boldsymbol{\Theta}}\mathcal{L}\left[\boldsymbol{\Psi},\boldsymbol{c},u,\boldsymbol{h},\boldsymbol{\Theta},\boldsymbol{a}\right](\delta\boldsymbol{\Theta}) = -Q\left(S^t\left(\delta\boldsymbol{\Theta},\boldsymbol{\Psi}\right) - F^t\left(\delta\boldsymbol{\Theta};u,\boldsymbol{h}\right)\right), \tag{142}$$

and taking $\delta\boldsymbol{\Theta}$ to be non-vanishing at t_k only, we get the modified Stokes problem at time t_k, i.e. (31) is evaluated at $t = t_k$.

Next, we perturb $\mathcal{L}$ with respect to $\boldsymbol{\Psi}_1$ and $\boldsymbol{\Psi}_3$:

$$\begin{aligned}\delta_{\boldsymbol{\Psi}_1}\mathcal{L}\left[\boldsymbol{\Psi},\boldsymbol{c},u,\boldsymbol{h},\boldsymbol{\Theta},\boldsymbol{a}\right](\delta\tilde{\boldsymbol{v}}) &= -Q(S^t\left(\boldsymbol{\Theta},(\delta\tilde{\boldsymbol{v}},\boldsymbol{0},0)\right)),\\ \delta_{\boldsymbol{\Psi}_3}\mathcal{L}\left[\boldsymbol{\Psi},\boldsymbol{c},u,\boldsymbol{h},\boldsymbol{\Theta},\boldsymbol{a}\right](\delta p) &= -Q(S^t\left(\boldsymbol{\Theta},(\boldsymbol{0},\boldsymbol{0},\delta p)\right)),\end{aligned} \tag{143}$$

and perturbing $\mathcal{L}$ with respect to $\boldsymbol{\Psi}_2 \equiv \boldsymbol{s}$ gives

$$\begin{aligned}\delta_{\boldsymbol{\Psi}_2}\mathcal{L}\left[\boldsymbol{\Psi},\boldsymbol{c},u,\boldsymbol{h},\boldsymbol{\Theta},\boldsymbol{a}\right](\delta\boldsymbol{s}) = &-Q(S^t\left(\boldsymbol{\Theta},(\boldsymbol{0},\delta\boldsymbol{s},0)\right))\\ &+\frac{1}{t_{\mathrm{f}}}Q\left((\boldsymbol{\Psi}_2-\boldsymbol{e}_0)\cdot\delta\boldsymbol{s}\right)+Q(\boldsymbol{a}\cdot\delta\boldsymbol{s}),\end{aligned} \tag{144}$$

and taking the perturbations to be non-vanishing at t_k only, we get part of the adjoint system at time t_k, i.e. (74) is evaluated at $t = t_k$.

Next,

$$\begin{aligned}\delta_{\boldsymbol{c}}\mathcal{L}\left[\boldsymbol{\Psi},\boldsymbol{c},u,\boldsymbol{h},\boldsymbol{\Theta},\boldsymbol{a}\right](\delta\boldsymbol{c}) &= -\sum_{k=0}^{K}\boldsymbol{a}^k\cdot\left(\frac{\delta\boldsymbol{c}^{k+1}-\delta\boldsymbol{c}^k}{\delta t}\right)\mu_k - \delta_{\boldsymbol{c}}J_{\mathrm{St}}\left[\boldsymbol{\Psi},\boldsymbol{c},\boldsymbol{\Theta},\boldsymbol{h}\right](\delta\boldsymbol{c})\\ &= -\sum_{k=0}^{K}\boldsymbol{a}^k\cdot\left(\frac{\delta\boldsymbol{c}^{k+1}-\delta\boldsymbol{c}^k}{\delta t}\right)\mu_k - Q\left(\int_{\Omega(t)}\boldsymbol{\sigma}(\boldsymbol{w},q):\left[\nabla(\mathcal{G}\delta\boldsymbol{c})\right]d\boldsymbol{x}\right)\\ &\quad - Q\left(\int_{\Omega(t)}S_1:\nabla(\delta\boldsymbol{c}\zeta)+S_0\cdot(\delta\boldsymbol{c}\zeta)\,d\boldsymbol{x}\right).\end{aligned} \tag{145}$$

As we want to keep the same initial position $\boldsymbol{c}^0$ we take $\delta\boldsymbol{c}^0 = \boldsymbol{0}$ for the perturbation. We also impose the terminal condition $\boldsymbol{a}^K = \boldsymbol{0}$ for the adjoint. Under these conditions, summation by parts reveals

$$\begin{aligned}-\frac{1}{\delta t}\sum_{k=0}^{K}\mu_k\boldsymbol{a}^k\cdot\left(\delta\boldsymbol{c}^{k+1}-\delta\boldsymbol{c}^k\right) &= -\frac{1}{\delta t}\sum_{k=0}^{K-1}\mu_k\boldsymbol{a}^k\cdot\left(\delta\boldsymbol{c}^{k+1}-\delta\boldsymbol{c}^k\right)\\ &= -\frac{1}{\delta t}\left[\mu_K\boldsymbol{a}^K\delta\boldsymbol{c}^K-\mu_0\boldsymbol{a}^0\delta\boldsymbol{c}^0\right]+\frac{1}{\delta t}\sum_{k=0}^{K-1}\delta\boldsymbol{c}^{k+1}\cdot\left(\mu_{k+1}\boldsymbol{a}^{k+1}-\mu_k\boldsymbol{a}^k\right)\\ &= \frac{1}{\delta t}\sum_{k=1}^{K-2}\mu_k\delta\boldsymbol{c}^{k+1}\cdot\left(\boldsymbol{a}^{k+1}-\boldsymbol{a}^k\right)\\ &\quad+\frac{1}{\delta t}\delta\boldsymbol{c}^1\cdot\left(\mu_1\boldsymbol{a}^1-\mu_0\boldsymbol{a}^0\right)+\frac{1}{\delta t}\delta\boldsymbol{c}^K\cdot\left(\boldsymbol{0}-\mu_{K-1}\boldsymbol{a}^{K-1}\right)\\ &= \frac{1}{\delta t}\sum_{k=1}^{K-1}\mu_k\delta\boldsymbol{c}^{k+1}\cdot\left(\boldsymbol{a}^{k+1}-\boldsymbol{a}^k\right)+\frac{1}{\delta t}\delta\boldsymbol{c}^1\cdot\left(\mu_1\boldsymbol{a}^1-\mu_0\boldsymbol{a}^0\right)\\ &= \frac{1}{\delta t}\sum_{k=2}^{K}\mu_{k-1}\delta\boldsymbol{c}^k\cdot\left(\boldsymbol{a}^k-\boldsymbol{a}^{k-1}\right)+\frac{1}{\delta t}\mu_0\delta\boldsymbol{c}^1\cdot\left(\boldsymbol{a}^1-\boldsymbol{a}^0\right)+\frac{1}{\delta t}\delta\boldsymbol{c}^1\cdot\boldsymbol{a}^1(\mu_1-\mu_0)\\ &= \frac{1}{\delta t}\sum_{k=0}^{K-1}\mu_k\delta\boldsymbol{c}^{k+1}\cdot\left(\boldsymbol{a}^{k+1}-\boldsymbol{a}^k\right)+\frac{1}{2}\delta\boldsymbol{c}^1\cdot\boldsymbol{a}^1.\end{aligned}$$

So, we get

$$\begin{aligned}\delta_{\boldsymbol{c}}\mathcal{L}\left[\boldsymbol{\Psi},\boldsymbol{c},u,\boldsymbol{h},\boldsymbol{\Theta},\boldsymbol{a}\right](\delta\boldsymbol{c}) = \frac{1}{\delta t}\sum_{k=0}^{K-1}\mu_k\delta\boldsymbol{c}^{k+1}\cdot\left(\boldsymbol{a}^{k+1}-\boldsymbol{a}^k\right)+\frac{1}{2}\delta\boldsymbol{c}^1\cdot\boldsymbol{a}^1\\ -\sum_{k=0}^{K}\left[\sum_{r=1}^{d}(\delta\boldsymbol{c}^k\cdot\boldsymbol{e}_r)\cdot\left[\int_{\Omega^k}\boldsymbol{\sigma}(\boldsymbol{w}^k,q^k):\left[\nabla(\mathcal{G}^k\boldsymbol{e}_r)\right]d\boldsymbol{x}\right]\right]\mu_k\\ -\sum_{k=0}^{K}\delta\boldsymbol{c}^k\cdot\left[\int_{\Omega^k}S_1^k(\nabla\zeta)+S_0^k\zeta\,d\boldsymbol{x}\right]\mu_k.\end{aligned}$$

Setting this to zero, for all $\{\delta\boldsymbol{c}^k\}$, we get a backward in time difference equation. For instance, setting (see (75)):

$$\boldsymbol{\Upsilon}^k := \int_{\Omega^k}\boldsymbol{\sigma}(\boldsymbol{w}^k,q^k):\left[\nabla(\mathcal{G}^k\{\boldsymbol{e}_1,\boldsymbol{e}_2\})\right]d\boldsymbol{x}+\int_{\Omega^k}S_1^k(\nabla\zeta)+S_0^k\zeta\,d\boldsymbol{x},\ \forall\,k,$$

for $\delta\boldsymbol{c}^k$, for $k=2,...,K$, we get

$$\mu_{k-1}\frac{\boldsymbol{a}^k-\boldsymbol{a}^{k-1}}{\delta t}=\mu_k\boldsymbol{\Upsilon}^k,$$

and for $\delta\boldsymbol{c}^1$:

$$\mu_0\frac{\boldsymbol{a}^1-\boldsymbol{a}^0}{\delta t}+\frac{1}{2}\boldsymbol{a}^1=\mu_1\boldsymbol{\Upsilon}^1.$$

Thus, given $\boldsymbol{a}^K=\boldsymbol{0}$, we solve the following backward in time:

$$\begin{aligned}\text{for } k=K: &\quad \frac{\boldsymbol{a}^K-\boldsymbol{a}^{K-1}}{\delta t}=\frac{1}{2}\boldsymbol{\Upsilon}^K,\quad\Rightarrow\quad \text{get } \boldsymbol{a}^{K-1},\\ \text{iter. for } k=K-1,...,2: &\quad \frac{\boldsymbol{a}^k-\boldsymbol{a}^{k-1}}{\delta t}=\boldsymbol{\Upsilon}^k,\quad\Rightarrow\quad \text{get } \{\boldsymbol{a}^{K-2},...,\boldsymbol{a}^1\},\\ \text{for } k=1: &\quad \frac{\boldsymbol{a}^1-\boldsymbol{a}^0}{\delta t}=2\boldsymbol{\Upsilon}^1-\frac{1}{\delta t}\boldsymbol{a}^1,\quad\Rightarrow\quad \text{get } \boldsymbol{a}^0.\end{aligned}\tag{146}$$

Note that we solve $\boldsymbol{\Upsilon}^K$ first, then the first equation in (146). Essentially, just "forward" Euler while taking into account the quadrature weights.

Next, recalling (72), we have

$$\begin{aligned}\delta_u\mathcal{L}\left[\boldsymbol{\Psi},\boldsymbol{c},u,\boldsymbol{h},\boldsymbol{\Theta},\boldsymbol{a}\right](\delta u) = \frac{\lambda_u}{t_{\mathrm{f}}}\left(u,\delta u\right)_{\mathcal{A}_u}+\frac{\lambda_\ell}{t_{\mathrm{f}}}\int_0^{\widetilde{t_{\mathrm{f}}}}\int_{-\pi}^{\pi}\mathcal{I}_M\left(\ell'(u(t,\theta))\delta u(t,\theta)\right)d\theta dt\\ +\frac{1}{t_{\mathrm{f}}\epsilon_u}\left(\int_0^{\widetilde{t_{\mathrm{f}}}}\int_{-\pi}^{\pi}\left(\partial_t u(t,\theta)\right)^2 d\theta dt-E_0\right)\int_0^{\widetilde{t_{\mathrm{f}}}}\int_{-\pi}^{\pi}\partial_t u(t,\theta)\partial_t\delta u(t,\theta)d\theta dt\\ -Q\left(\int_{\Omega(\cdot)}\boldsymbol{\sigma}(\boldsymbol{w},q):\nabla\boldsymbol{\beta}(\cdot,\boldsymbol{x};\delta u,\boldsymbol{c})\,d\boldsymbol{x}\right)\\ -Q\left(\int_{\Omega(\cdot)}S_1:\nabla\boldsymbol{V}(\cdot,\boldsymbol{x};\delta u)+S_0\cdot\boldsymbol{V}(\cdot,\boldsymbol{x};\delta u)\,d\boldsymbol{x}\right).\end{aligned}\tag{147}$$

Finally, perturbing $\mathcal{L}$ with respect to the force control $\boldsymbol{h}$ gives

$$\delta_{\boldsymbol{h}}\mathcal{L}\left[\boldsymbol{\Psi},\boldsymbol{c},u,\boldsymbol{h},\boldsymbol{\Theta},\boldsymbol{a}\right](\delta\boldsymbol{h})=\delta_{\boldsymbol{h}}J\left[\boldsymbol{\Psi},u,\boldsymbol{h}\right](\delta\boldsymbol{h})+Q\left(\boldsymbol{r}\cdot\delta\boldsymbol{h}\right)=\frac{\lambda_{\boldsymbol{h}}}{t_{\mathrm{f}}}\left(\boldsymbol{h},\delta\boldsymbol{h}\right)_{L^2(0,t_{\mathrm{f}})}+Q\left(\boldsymbol{r}\cdot\delta\boldsymbol{h}\right).\tag{148}$$

B.5 FE approximation of $\boldsymbol{\beta}$

Let $I_h : C^0 \to B_h$ be the interpolation operator onto the background finite element space. After recalling (8), in the numerical implementation, we have

$$\begin{aligned}\boldsymbol{\beta}_h(t, \boldsymbol{x}; u, \boldsymbol{c}) &:= (I_h\boldsymbol{\beta})(t, \boldsymbol{x}; u, \boldsymbol{c}) \\ &= R_0 \sum_i \left[\partial_t u\left(t, \boldsymbol{x}_i - \boldsymbol{c}(t)\right) \frac{\boldsymbol{x}_i - \boldsymbol{c}(t)}{|\boldsymbol{x}_i - \boldsymbol{c}(t)|}\zeta(\boldsymbol{x}_i)\right] \phi_i,\end{aligned} \tag{149}$$

where $\{\boldsymbol{x}_i\}$ are the nodal points of B_h and $\{\phi_i\}$ are the finite element basis functions. Thus, the gradient is simply

$$\nabla_{\boldsymbol{x}}\boldsymbol{\beta}_h(t, \boldsymbol{x}) = R_0 \sum_i \left[\partial_t u\left(t, \boldsymbol{x}_i - \boldsymbol{c}(t)\right) \frac{\boldsymbol{x}_i - \boldsymbol{c}(t)}{|\boldsymbol{x}_i - \boldsymbol{c}(t)|}\zeta(\boldsymbol{x}_i)\right] \otimes \nabla\phi_i(\boldsymbol{x}), \tag{150}$$

which is automatically computed within the finite element framework. Now, using the linearity of I_h, we have a discrete version of (59),

$$\delta_{\boldsymbol{c}}\boldsymbol{\beta}_h(t, \boldsymbol{x})(\delta\boldsymbol{c}) = \sum_i (\mathcal{G}_i\delta\boldsymbol{c})\phi_i, \tag{151}$$

with the matrix $\mathcal{G}_i = \mathcal{G}|_{\boldsymbol{x}=\boldsymbol{x}_i}$ given by (60):

$$\mathcal{G}_i := -\frac{R_0}{|\boldsymbol{x}_i - \boldsymbol{c}(t)|}\left[(\boldsymbol{x}_i - \boldsymbol{c}(t)) \otimes \nabla\partial_t u\left(t, \boldsymbol{x}_i - \boldsymbol{c}(t)\right) + \partial_t u\left(t, \boldsymbol{x}_i - \boldsymbol{c}(t)\right) \mathrm{P}^{\perp}_{\boldsymbol{x}_i - \boldsymbol{c}}\right] \zeta(\boldsymbol{x}_i). \tag{152}$$

Note that $\delta_{\boldsymbol{c}}\boldsymbol{\beta}_h(t, \boldsymbol{x})(\delta\boldsymbol{c})$ is still in the finite element space B_h, so we can easily take its gradient.

References

[1] F. Alouges, A. Desimone, and L. Heltai. Numerical strategies for stroke optimization of axisymmetric microswimmers. *Mathematical Models & Methods in Applied Sciences*, 21(2):361–387, Feb 2011.

[2] F. Alouges, A. DeSimone, and A. Lefebvre. Optimal strokes for low reynolds number swimmers: an example. *Journal of Nonlinear Science*, 18(3):277–302, 2008.

[3] A. Azari Nejat, A. Held, N. Trekel, and R. Seifried. A modified level set method for topology optimization of sparsely-filled and slender structures. *Structural and Multidisciplinary Optimization*, 65(3):85, Feb 2022.

[4] D. Boffi, F. Brezzi, and M. Fortin. *Mixed Finite Element Methods and Applications*, volume 44 of *Springer Series in Computational Mathematics*. Springer-Verlag, New York, NY, 2013.

[5] D. Boffi and L. Gastaldi. A fictitious domain approach with lagrange multiplier for fluid-structure interactions. *Numerische Mathematik*, 135(3):711–732, Mar 2017.

[6] D. Boffi, L. Gastaldi, and L. Heltai. *A Distributed Lagrange Formulation of the Finite Element Immersed Boundary Method for Fluids Interacting with Compressible Solids*, pages 1–21. Springer International Publishing, Cham, 2018.

[7] D. Braess. *Finite Elements: Theory, Fast Solvers, and Applications in Solid Mechanics*. Cambridge University Press, 2nd edition, 2001.

[8] E. Burman. Ghost penalty. *Comptes Rendus Mathematique*, 348(21):1217–1220, 2010.

[9] E. Burman, S. Claus, P. Hansbo, M. G. Larson, and A. Massing. Cutfem: Discretizing geometry and partial differential equations. *International Journal for Numerical Methods in Engineering*, 104(7):472–501, 2015.

[10] Burman, Erik and Hansbo, Peter. Fictitious domain methods using cut elements: III. a stabilized Nitsche method for stokes' problem. *ESAIM: M2AN*, 48(3):859–874, 2014.

[11] E. J. Campbell and P. Bagchi. A computational model of amoeboid cell swimming. *Physics of Fluids*, 29(10):101902, 10 2017.

[12] T. Chambrion and A. Munnier. Locomotion and control of a self-propelled shape-changing body in a fluid. *J. Nonlinear Sci.*, 21(3):325–385, 2011.

[13] G.-H. Cottet and E. Maitre. A semi-implicit level set method for multiphase flows and fluid–structure interaction problems. *Journal of Computational Physics*, 314:80–92, 2016.

[14] G.-H. Cottet, E. Maitre, and T. Milcent. *Level Set Methods for Fluid-Structure Interaction*. Applied Mathematical Sciences. Springer Cham, 1 edition, 2022.

[15] W. Croft, C. M. Elliott, G. Ladds, B. Stinner, C. Venkataraman, and C. Weston. Parameter identification problems in the modelling of cell motility. *Journal of Mathematical Biology*, 71(2):399–436, Sep 2014.

[16] M. C. Delfour and J.-P. Zolésio. *Shapes and Geometries: Analysis, Differential Calculus, and Optimization*, volume 4 of *Advances in Design and Control*. SIAM, 2nd edition, 2011.

[17] W. Dettmer and D. Perić. A computational framework for fluid–rigid body interaction: Finite element formulation and applications. *Computer Methods in Applied Mechanics and Engineering*, 195(13):1633–1666, 2006. A Tribute to Thomas J.R. Hughes on the Occasion of his 60th Birthday.

[18] R. Dziri and J.-P. Zolésio. *Shape Optimization and Optimal Design*, chapter Eulerian Derivative for Non-Cylindrical Functionals, pages 87–107. Lecture Notes in Pure and Applied Mathematics. Dekker, New York, 2001.

[19] K. M. Ehlers, A. D. Samuel, H. C. Berg, and R. Montgomery. Do cyanobacteria swim using traveling surface waves? *Proceedings of the National Academy of Sciences*, 93(16):8340–8343, 1996.

[20] Y. El Alaoui-Faris, J.-B. Pomet, S. Régnier, and L. Giraldi. Optimal actuation of flagellar magnetic microswimmers. *Phys. Rev. E*, 101:042604, Apr 2020.

[21] C. M. Elliott, B. Stinner, and C. Venkataraman. Modelling cell motility and chemotaxis with evolving surface finite elements. *Journal of The Royal Society Interface*, 9(76):3027–3044, 2012.

[22] D. Enright, R. P. Fedkiw, J. Ferziger, and I. Mitchell. A hybrid particle level set method for improved interface capturing. *Journal of Computational Physics*, 183:83–116, 2002.

[23] L. C. Evans. *Partial Differential Equations*. American Mathematical Society, Providence, Rhode Island, 1998.

[24] A. Fikl and D. J. Bodony. Adjoint-based interfacial control of viscous drops. *J. Fluid Mech.*, 911:Paper No. A39, 42, 2021.

[25] H. Garcke, K. F. Lam, and A. Signori. Sparse optimal control of a phase field tumor model with mechanical effects. *SIAM Journal on Control and Optimization*, 59(2):1555–1580, 2021.

[26] A. Goza, S. Liska, B. Morley, and T. Colonius. Accurate computation of surface stresses and forces with immersed boundary methods. *Journal of Computational Physics*, 321:860–873, 2016.

[27] B. E. Griffith and N. A. Patankar. Immersed methods for fluid–structure interaction. *Annual Review of Fluid Mechanics*, 52(Volume 52, 2020):421–448, 2020.

[28] P. Hansbo, M. G. Larson, and S. Zahedi. A cut finite element method for a stokes interface problem. *Applied Numerical Mathematics*, 85:90–114, 2014.

[29] M. Herrmann. A balanced force refined level set grid method for two-phase flows on unstructured flow solver grids. *Journal of Computational Physics*, 227(4):2674 – 2706, 2008.

[30] M. Herrmann and M. Gorokhovski. An outline of an les subgrid model for liquid/gas phase interface dynamics. In *Center for Turbulence Research*, volume Proceedings of the Summer Program, 2008.

[31] M. Hintermüller and A. Laurain. Optimal shape design subject to elliptic variational inequalities. *SIAM J. Control Optim.*, 49(3):1015–1047, 2011.

[32] A. Johansson, M. G. Larson, and A. Logg. High order cut finite element methods for the stokes problem. *Advanced Modeling and Simulation in Engineering Sciences*, 2(1):24, Sep 2015.

[33] H. Kasumba, K. Kunisch, and A. Laurain. A bilevel shape optimization problem for the exterior Bernoulli free boundary value problem. *Interfaces Free Bound.*, 16(4):459–487, 2014.

[34] E. Lauga. Life around the scallop theorem. *Soft Matter*, 7:3060–3065, 2011.

[35] A. Laurain. Distributed and boundary expressions of first and second order shape derivatives in nonsmooth domains. *Journal de Mathématiques Pures et Appliquées*, 134:328–368, 2020.

[36] A. Laurain and S. W. Walker. Droplet footprint control. *SIAM Journal on Control and Optimization*, 53(2):771–799, 2015.

[37] A. Laurain and S. W. Walker. Optimal control of volume-preserving mean curvature flow. *Journal of Computational Physics*, 438:110373, 2021.

[38] P. Lederer, C.-M. Pfeiler, C. Wintersteiger, and C. Lehrenfeld. Higher order unfitted fem for Stokes interface problems. *PAMM*, 16(1):7–10, 2016.

[39] C. Lehrenfeld, F. Heimann, J. Preuss, and H. von Wahl. ngsxfem: Add-on to NGSolve for geometrically unfitted finite element discretizations. *Journal of Open Source Software*, 6(64):3237, 2021.

[40] C. Lehrenfeld and M. Olshanskii. An Eulerian finite element method for PDEs in time-dependent domains. *ESAIM: Mathematical Modelling and Numerical Analysis*, 53(2):585–614, 2019.

[41] L. Li, S. J. Sherwin, and P. W. Bearman. A moving frame of reference algorithm for fluid-structure interaction of rotating and translating bodies. *International Journal For Numerical Methods In Fluids*, 38:187–206, 2002.

[42] Q. Li, E. Bou-Zeid, and W. Anderson. The impact and treatment of the gibbs phenomenon in immersed boundary method simulations of momentum and scalar transport. *Journal of Computational Physics*, 310:237–251, 2016.

[43] J. Lighthill. *Mathematical Biofluiddynamics*. SIAM, 1975.

[44] J. Lohéac and A. Munnier. Controllability of 3D low Reynolds number swimmers. *ESAIM Control Optim. Calc. Var.*, 20(1):236–268, 2014.

[45] J. Lohéac, J.-F. Scheid, and M. Tucsnak. Controllability and time optimal control for low Reynolds numbers swimmers. *Acta Appl. Math.*, 123:175–200, 2013.

[46] J. Lohéac and T. Takahashi. Controllability of low Reynolds numbers swimmers of ciliate type. *ESAIM Control Optim. Calc. Var.*, 26:Paper No. 31, 30, 2020.

[47] F. Losasso, F. Gibou, and R. Fedkiw. Simulating water and smoke with an octree data structure. In *ACM Trans. Graph. (SIGGRAPH Proc.)*, pages 457–462, Los Angeles, 2004.

[48] A. Massing, M. G. Larson, A. Logg, and M. E. Rognes. A stabilized Nitsche fictitious domain method for the Stokes problem. *J. Sci. Comput.*, 61(3):604–628, Dec. 2014.

[49] K. W. Morton and D. F. Mayers. *Numerical Solution of Partial Differential Equations*. Cambridge University Press, New York, NY, 1994.

[50] M. Moubachir and J.-P. Zolésio. *Moving Shape Analysis and Control: Applications to Fluid Structure Interactions*, volume 277 of *Pure and Applied Mathematics*. Chapman and Hall/CRC, 2006.

[51] A. Najafi and R. Golestanian. Simple swimmer at low reynolds number: Three linked spheres. *Phys. Rev. E*, 69:062901, Jun 2004.

[52] S. Osher and R. Fedkiw. *Level Set Methods and Dynamic Implicit Surfaces*. Springer-Verlag, New York, NY, 2003.

[53] N. A. Patankar and N. Sharma. A fast projection scheme for the direct numerical simulation of rigid particulate flows. *Communications in Numerical Methods in Engineering*, 21(8):419–432, 2005.

[54] O. Pironneau and D. F. Katz. Optimal swimming of flagellated microorganisms. *Journal of Fluid Mechanics*, 66(2):391–415, 1974.

[55] E. M. Purcell. Life at low Reynolds number. *American Journal of Physics*, 45(1):3–11, Jan 1977.

[56] J. San Martín, T. Takahashi, and M. Tucsnak. A control theoretic approach to the swimming of microscopic organisms. *Quart. Appl. Math.*, 65(3):405–424, 2007.

[57] J. Schöberl. C++11 implementation of finite elements in NGSolve. Technical Report ASC-2014-30, Institute for Analysis and Scientific Computing, September 2014.

[58] S. A. Sethian. *Level Set Methods and Fast Marching Methods, 2nd Edition*. Cambridge University Press, New York, NY, 1999.

[59] E. Setter, I. Bucher, and S. Haber. Low-reynolds-number swimmer utilizing surface traveling waves: Analytical and experimental study. *Phys. Rev. E*, 85:066304, Jun 2012.

[60] S. V. Shepel and S. Paolucci. Finite element level set formulations for modelling multiphase flows. In *ICCMSE '03: Proceedings of the international conference on Computational methods in sciences and engineering*, pages 593–597, River Edge, NJ, USA, 2003. World Scientific Publishing Co., Inc.

[61] J. Simons, L. Fauci, and R. Cortez. A fully three-dimensional model of the interaction of driven elastic filaments in a stokes flow with applications to sperm motility. *Journal of Biomechanics*, 48(9):1639–1651, 2015. Reproductive Biomechanics.

[62] G. D. Smith. *Numerical Solution of Partial Differential Equations, Third Edition*. Oxford University Press, Oxford, UK, 1985.

[63] J. Sokolowski and J.-P. Zolésio. *Introduction to Shape Optimization*. Springer Series in Computational Mathematics. Springer-Verlag, 1992.

[64] P. D. Spelt. A level-set approach for simulations of flows with multiple moving contact lines with hysteresis. *Journal of Computational Physics*, 207(2):389 – 404, 2005.

[65] H. A. Stone and A. D. T. Samuel. Propulsion of microorganisms by surface distortions. *Phys. Rev. Lett.*, 77:4102–4104, Nov 1996.

[66] Y. Sun and C. Beckermann. Diffuse interface modeling of two-phase flows based on averaging: mass and momentum equations. *Physica D*, 198:281, 2004.

[67] M. Sussman. A second order coupled level set and volume-of-fluid method for computing growth and collapse of vapor bubbles. *Journal of Computational Physics*, 187(1):110 – 136, 2003.

[68] M. Sussman and E. G. Puckett. A coupled level set and volume of fluid method for computing 3-d and axisymmetric incompressible two-phase flows. *Journal of Computational Physics*, 162:301, 2000.

[69] S. P. van der Pijl, A. Segal, C. Vuik, and P. Wesseling. A mass-conserving level-set method for modelling of multi-phase flows. *International Journal for Numerical Methods in Fluids*, 47:339–361, 2005.

[70] S. P. van der Pijl, A. Segal, C. Vuik, and P. Wesseling. Computing three-dimensional two-phase flows with a mass-conserving level set method. *Computing and Visualization in Science*, 11:221–235, 2008.

[71] N. P. van Dijk, K. Maute, M. Langelaar, and F. van Keulen. Level-set methods for structural topology optimization: a review. *Structural and Multidisciplinary Optimization*, 48(3):437–472, Sep 2013.

[72] A. Villa and L. Formaggia. Implicit tracking for multi-fluid simulations. *Journal of Computational Physics*, 229:5788–5802, 2010.

[73] H. von Wahl, T. Richter, and C. Lehrenfeld. An unfitted Eulerian finite element method for the time-dependent Stokes problem on moving domains. *IMA Journal of Numerical Analysis*, 42(3):2505–2544, 07 2021.

[74] S. W. Walker. *The Shapes of Things: A Practical Guide to Differential Geometry and the Shape Derivative*, volume 28 of *Advances in Design and Control*. SIAM, 1st edition, 2015.

[75] S. W. Walker and E. E. Keaveny. Analysis of shape optimization for magnetic microswimmers. *SIAM Journal on Control and Optimization*, 51(4):3093–3126, 2013.

[76] P. Yue, J. J. Feng, C. Liu, and J. Shen. A diffuse-interface method for simulating two-phase flows of complex fluids. *Journal of Fluid Mechanics*, 515:293, 2004.